University of Alberta

Library Release Form

Name of Author: Marek Welz

Title of Thesis: Blast Monitoring at Diavik Diamond Mines Inc. to Protect Fish Habitat

Degree: Master of Science

Year this Degree Granted: 2006

_____
Marek Welz
228-D CEB
University of Alberta,
Edmonton, Alberta
Canada T6G 2G7

University of Alberta

Blast Monitoring at Diavik Diamond Mines Inc. to Protect Fish Habitat

by

Marek Welz

A thesis submitted to the Faculty of Graduate Studies and Research in partial fulfillment of the requirements for the degree of Master of Science

in

Geophysics

Department of Physics

Edmonton, Alberta

Fall 2006

University of Alberta

Faculty of Graduate Studies and Research

The undersigned certified that they have read, and recommend to the Faculty of Graduate Studies and Research for acceptance, a thesis entitled **Blast Monitoring at Diavik Diamond Mines Inc. to Protect Fish Habitat** submitted by **Marek Welz** in partial fulfillment of the requirements for the degree of **Master of Science.**

_____
Dr. D. Schmitt (Supervisor)

_____
Dr. T.G. Joseph

_____
Dr. V. A. Kravchinsky

_____
Dr. W.M. Tonn

Date:

Dedication

To my mother.

Acknowledgements

I am indebted to Doug Schmitt; for his supervision, guidance and his hard work. Without him I would not have been able to complete this work. The work was collaboration with Sean Faulkner and Dr. Bill Tonn of the Department of Biological Sciences. I thank them for their expertise on fishes and for the support and many discussions about the project. This research was made possible through a research grant and in-kind support provided by Diavik Diamond Mines Inc. (DDMI). I would also like to thank the geophysics group and the support within it; Especially Len Tober for his technical expertise, and Dan Collis for his help in the initial deployment.

Vista 5.1 seismic processing software provided by Gedco of Calgary was used in processing of some of the data.

Abstract:

Diavik Diamond Mines Inc. is conducting open pit and underground mining of kimberlites within close proximity of a large freshwater lake that supports populations of fishes and other aquatic organisms. As the principal method of excavation is through blasting; the resulting blast wave is expected to expose incubating fish eggs to peak particle velocities (PPVs) greater than guidelines suggested by the Department of Fisheries and Oceans (DFO). Blasts were monitored using specialised 4 – component underwater sensors which measured the particle velocities and overpressures simultaneously. PPVs were related to mortality in fish eggs both in the lake and in a laboratory setting where blasting events were simulated. Standard blast monitoring techniques were used to analyse data and create scaled distance relations in order to predict the attenuation of PPVs. Results show that attenuation was greater than initially expected. Further analysis showed no changes in blasting effects as the pit deepened.

Table of Contents

Chapter 1) Introduction: 1

1.1) Objectives: 3

Chapter 2) Background 5

2.1) Basic Physical Principles of Seismic Waves 6

2.1.1) Basic Wave Propagation 7

2.1.2) Elastic Moduli 9

2.1.3) Wave Energy 17

2.1.4) Decay of Amplitude 19

i) Geometrical Spreading 19

ii) Intrinsic attenuation 21

iii) Attenuation at geologic boundaries 22

iv) Scattering Attenuation 23

v) Combination of effects 24

2.2) Introduction to Blast Monitoring 27

2.2.1) Peak Particle Velocity 30

2.2.2) Overpressure 32

2.2.3) Scaled Distance 33

2.3) Summary 36

Chapter 3) Diavik site overview 37

3.1) Geological Setting 38

3.2) Study site 41

3.3) Geophysical site characterisation 41
3.3.4) Refraction seismic survey 42
3.3.5) Passive seismic survey 44
3.4) Predicted Blast Zone 45
3.4.1) Peak Particle Velocity 46
3.4.2) Over Pressure 48
3.5) Summary 50
Chapter 4) Methodology; Field component 52
4.1) Site Selection 53
4.2) Sensor Placement 55
4.3) Equipment 56
4.4) Data Collection 57
4.5) Data Processing and analysis 61
Chapter 5) Field Component Results 62
5.1) Analysis 62
5.2) DDMI Prediction Function 63
5.3) South Dike (8902) 65
5.4) Reference Island (8903) 66
5.5) Tern Island (8904) 66
5.6) East Dike (8905) 66
5.7) Blast Zone 70
5.8) Changes in effects as the pit deepens 72
5.8.1) Changes in normalised PPV 74

5.8.2) Changes in the Scaled Distance function 76

Chapter 6) Laboratory Study 79

6.1) Methodology..... 80

6.2) Results 81

6.3) Pseudo energy..... 83

Chapter 7) Discussion..... 86

7.1) Field component 86

7.2) Changes in the blasting effects..... 90

Chapter 8) Conclusions..... 92

References..... 96

Appendices..... 99

Appendix 1: Response curves for the Underwater sensor 99

Appendix 2: Blast Mate blasting record 101

Appendix 3: Technical Specifications for the Instantel Minimate Plus Series III……...102

Appendix 4: Blasting Data..... 103

List of Tables

Table 1) Current Alberta seismic exploration regulation offsets, Schedule 2 of Alberta Government (2005). 29

List of Figures

Figure 1-1) Air photo showing the proposed pit (A154) location within the drained area near East Island on Lac de Gras. The A154N and A154S kimberlitic pipes are indicated in red. The inset map shows the location of DDMI in Canada's Northwest Territories. Courtesy, DDMI. 2

Figure 2-1) Poisson ratio plotted against the Vp/Vs ratio..... 13

Figure 2-2) The Vr/Vs ratio plotted against the Vp/Vs ratio. 14

Figure 2-3) Retrograde particle motion of a Rayleigh wave. Wave propagation direction along the surface is represented by the large horizontal arrow. At a given point the particles move 'backwards' around the ellipse as shown. 15

Figure 2-4) Illustration of the relative decay of a cylindrically spreading surface wave and a spherically spreading body wave with distance relative to the (arbitrary) reference distance of 0.1 m for a wave speed of 5000 m/s and a frequency of 100 Hz. Relative amplitudes report in dB^{10}. Numerical values represent quality factors included in the calculations. $Q = \infty$ means no attenuation. 26

Figure 2-5) Illustration of the definition of the PPV on a particle velocity versus time plot where the peak particle velocity is the maximum excursion from zero amplitude. 28

Figure 3-1) Simplified geology at Diavik. The blue background is Lac de Gras, DDMI's four kimberlie pipes (A154N, A154S, A418 and A21) are all situated within the waters of the lake very close to East Island where the operations are situated. (Modified from Stubley Geoscience, 1998)..... 39

Figure 3-2) Figure showing the location of the seismic line receiver array and the source. 42

Figure 3-3) Frequency spectrum of refraction seismic record. The record contains, seismically speaking, very high frequencies. 43
Figure 3-4) A shot from the refraction survey. Surface wave velocity is in the range of 1000 m/s. Data is displayed after ormsby filtering (10, 15, 600, 800) and RMS scaling. 43
Figure 3-5) The first arrival from the blasting event. A best fit line defines the velocity to be around 2600 m/s. 44
Figure 3-6) Frequency spectrum for the passively recorded blasting event. 45
Figure 3-7) Map of area showing proposed fish incubator sites (black squares). Circular contours represent distance from the centre of A154N/S, contours each 500-m and the red line indicates the DDMI predicted zone where PPVs would exceed DFO guideline levels. 47
Figure 4-1) Locations of the 4 sensors in relation to the dike, proposed pit and predicted Blast Zone (Red Line). Distance between scale marks is 1000 m of the UTM grid. DDMI sensors are deployed at various locations along the dike. Note that the Blast Zone takes into account the location of the next pit south and east of the original. 54
Figure 4-2) Placement of the 4-C sensor. The sensor is attached to the chain and also placed under rocks to ensure coupling. 56
Figure 4-3) A cutaway view of the OYO 4 Component sensor. The gimballed geophones can be seen and the hydrophone is situated at the left end of the sensor. 57
Figure 4-4) Typical waveform due to a blast as presented using the *Instantel Blast Ware*^{TM} software. The channels are overpressure (top), and the 3 geophone channels, longitudinal, vertical and transverse. The vertical scale is 10 mm/s for the PPV and 10 pa for the overpressure per division. Inset) Frequency spectrum for each of the geophone

channels; Y-axis Particle Velocity (mm/s) and, X-axis Frequency in Hz. Both Axes are log scale. 59

Figure 4-5) Blast record for a non blasting related event. As above, the channels are overpressure (top), and the 3 geophone channels, longitudinal, vertical and transverse. The vertical scale is 2 mm/s for the PPV and 10 pa for the overpressure per division. ... 60

Figure 4-6) A typical waveform due to electrical noise. As above, the channels are overpressure (top), and the 3 geophone channels, longitudinal, vertical and transverse. The vertical scale is 10 mm/s for the PPV and 10 pa for the overpressure per division. . 60

Figure 5-1) The DDMI prediction function (Equation 5-2) presented in red lines with the data collected by DDMI from August 27, 2002 to January 17, 2004. The black lines represent the prediction function derived from the plotted data (Equation 5-2)..... 64

Figure 5-2) Scaled Distance plot of the four U of A sensors compared to the DDMI data. The red lines represent the minimum, median and maximum PPV for a given scaled distance from the DDMI prediction function. 8902, 8903, 8904 & 8905 are South Dike, Reference Island, Tern Island and East Dike respectively. 64

Figure 5-3) Logarithmic plot of the measured particle velocity and scaled distance for the South Dike location. The lines indicate the minimum, median and maximum PPVs to be expected at the site (r-square .26). 67

Figure 5-4) Logarithmic plot of the measured particle velocity and scaled distance for the Reference Island location. The lines indicate the minimum, median and maximum PPVs to be expected at the site(r-square .09). 67

Figure 5-5) Logarithmic plot of the measured particle velocity and scaled distance for the Tern Island location. The lines indicate the minimum, median and maximum PPVs to be expected at the site(r-square .27). 68
Figure 5-6) Logarithmic plot of the measured particle velocity and scaled distance for the East Dike location. The lines indicate the minimum, median and maximum PPVs to be expected at the site(r-square .26). 68
Figure 5-7) Minimum, maximum and median predicted PPVs plotted along with actual recorded values for South Dike. The line indicates the DFO guideline value of 13 mm/s. 69
Figure 5-8) Minimum, maximum and median predicted PPVs plotted along with actual recorded values for Reference Island. Note that the vertical scale is much smaller in this case..... 69
Figure 5-9) Minimum, maximum and median predicted PPVs plotted along with actual recorded values for Tern Island. The line indicates the DFO guideline value of 13 mm/s. 69
Figure 5-10) Minimum, maximum and median predicted PPVs plotted along with actual recorded values for East Dike. The line indicates the DFO guideline value of 13 mm/s. 70
Figure 5-11) Logarithmic plot of the measured particle velocity and scaled distance for the East Dike, South Dike and Reference Island combined. The lines indicate the minimum, median and maximum PPVs to be expected (r-square .24). 71
Figure 5-12) PPV predictions for different charge weights and distances based on data from the 3 near dike sites. The dashed line represents 13 mm/s. The Predicted values are based on the upper bound of the function. 72

Figure 5-13) Blast elevations at DDMI since January 2003. Over time the elevations have decreased as the open pit operation increases in depth. 73
Figure 5-14) PPVs (mm/s) as measured by DDMI sensors since January 2003. 74
Figure 5-15) Normalised (DDMI) PPVs plotted against the date. 75
Figure 5-16) Normalised (DDMI) PPVs plotted against the blast elevation. 75
Figure 5-17) Normalised (DDMI) PPVs plotted against distance from blast. As the distance increases, the measured PPV decreases. 75
Figure 5-18) Normalised (DDMI) PPVs plotted against the blast weight. 76
Figure 5-19) Change in A & M over time. (DDMI data). The scalar variable, A, is on the left axis and M, the exponential variable is on the right axis. 77
Figure 5-20) Change in A & M as the depth increases (elevation decreases). (DDMI data). The scalar variable, A, is on the left axis and M, the exponential variable is on the right axis. 77
Figure 5-21) Change in A & M as the distance from the blast increases. (DDMI data). The scalar variable, A, is on the left axis and M, the exponential variable is on the right axis. 77
Figure 6-1) The weight-drop apparatus; a: steel pole, secured at top with straps (not shown); b: pin to release the weight apparatus; c: the weight set-up, including an aluminium sleeve and cast iron weights; d: holes drilled in the pole spaced 15 cm apart; e: 0.64 cm thick rubber mat; f: 0.64 cm thick steel base plate; g: 5 cm foam padding; h: 2.5 cm rubber mat, and i: fibreglass tank. 81
Figure 6-2) PPV = 138 mm/s Height = Standard Deviation (2.4) 82
Figure 6-3) PPV = 245 mm/s Height = Standard Deviation (3.0) 82

Figure 6-4) Blast records for a lab simulation event (a) and DDMI blasting event (b). The bottom panel shows the 3 component wave form and the top panel shows the pseudo energy calculated from the vector sum of the waveform. Note that the amplitude scales are the same for comparison sake but the time scales are different. The DDMI event is much longer than the lab event. 85

Figure 7-1) Comparison of scaled distance data over two periods shows that the distribution has stayed the same. The solid line indicates 13 mm/s. 90

List of Variables

PPV	Peak Particle Velocity, generally measured in mm/s
ω	Angular Frequency ($2\pi f$)
A	The displacement peak Amplitude
P	Pressure in Pascals
V_P/V_S	P & S wave velocities
ρ	Material density
E	Average over one wavelength of the total energy conveyed per unit wavefront
Z	acoustic impedance (ρV)
PV	Particle velocity
R / r	Radius
y, y', y''	Particle displacement, velocity and acceleration
Q	Quality factor
α	Attenuation coefficient
$SH_i(t)$	Time dependent particle velocity for one component of the waveform
W	Charge weight per delay
C	Seismic wave velocity
SD	Scaled distance (distance/(charge weight per delay)1/2
M_L	Richter Scale magnitude
t	Time (usually in seconds)
M	Scalar variable in the prediction function
A	Exponential variable in the prediction function

Chapter 1) *Introduction:*

Regulations are in place to limit negative effects that can be experienced due energy being released from blasting operations. In particular limits have been placed on the maximum Peak Particle Velocity (PPV) levels to prevent negative cultural or environmental effects. Prediction of maximum PPV is, therefore, important in determining the maximum size of an explosion that can be used without damaging anything at given distances.

Scaled distance relations that normalise for distance and blast weight per delay are employed in predicting PPVs at given distances. These relations are empirical and must be used carefully but can be very effective in PPV prediction once a reasonable data set is collected. At Diavik Diamond Mines Inc. (DDMI) a scaled distance relation provided by M. Davachi (Personal comm. DDMI, 1998a.) and calculations based on Department of Fisheries and Oceans (DFO) guidelines both suggested that PPVs in excess of the DFO mandated limit of 13mm/s would extend into Lac de Gras. Consequently, a *Fisheries Act* section 32 Authorization (SC98001) relating to this activity requires that DDMI monitor peak particle velocities and overpressures resulting from blasting activities in and around the predicted blast zone, to define the actual blast zone; effects of blasting on fish must also be determined. In particular, any incubating fish eggs within the blast zone could be susceptible to mortality or damage, especially since they would be exposed to the excessive velocities or pressures for 6-10 months. Because there is considerable uncertainty regarding the cumulative effects of repeated guideline-exceeding forces on over-wintering, developing eggs in Arctic lakes, and because the use of explosives in or near arctic Canadian fisheries waters will likely increase in the future, it is important to

conduct a study into effects on fish and especially fish eggs, both with respect to the A154 pit (Figure 1-1.) but also to assess more generally the relationship between the current guidelines and effects under arctic field conditions.

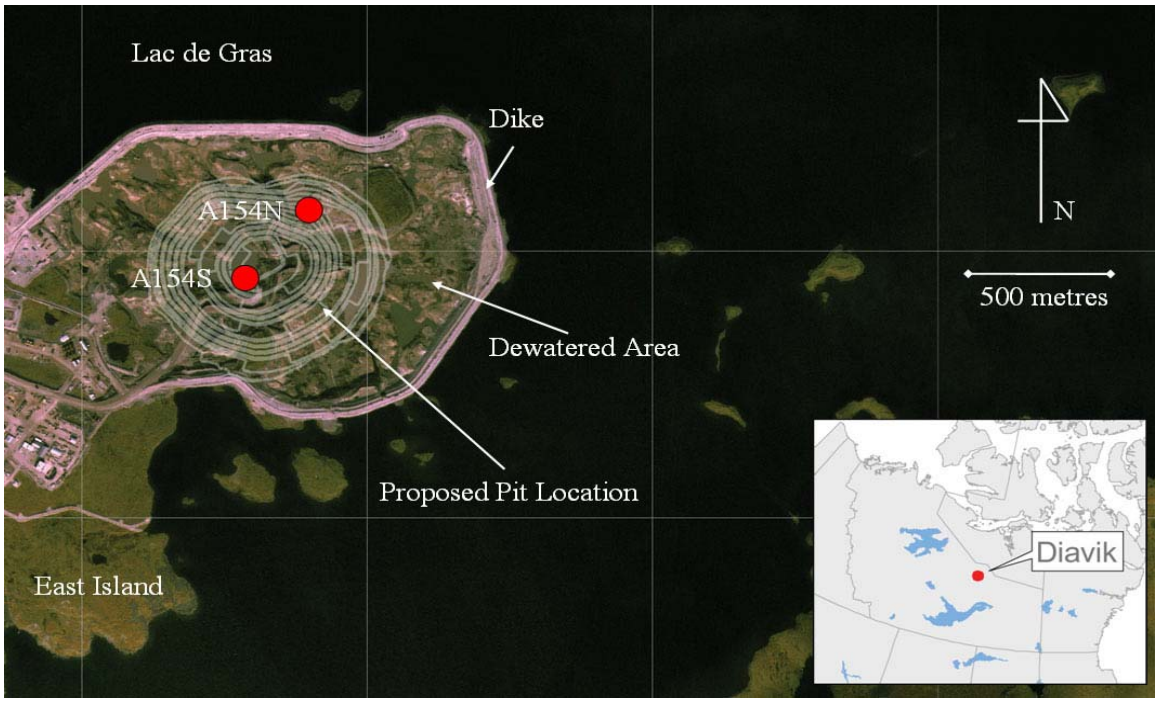

Figure 1-1) Air photo showing the proposed pit (A154) location within the drained area near East Island on Lac de Gras. The A154N and A154S kimberlitic pipes are indicated in red. The inset map shows the location of DDMI in Canada's Northwest Territories. Courtesy, DDMI.

This project is divided into two main components, a field study and a laboratory study. The first component of the field study was monitoring and recording the effects of blasting events on lake trout eggs that were placed beside the sensor. The second portion of the field study, is to monitor as many blasting events as possible to assess the changes in effects on the lake substrate as the pit deepens.

Less than 10 blasting events at DDMI caused PPVs greater than the DFO mandated 13 mm/s at sensor locations in the lake. During the period when the studied fish eggs

were in the lake only 3 events actually exceeded the guideline. The biological study noted that no fish egg mortality could be attributed to the blasting at DDMI.

As a result of these findings, and in keeping with objectives 4 and 5 (listed below), a lab study was developed where eggs were exposed to PPVs much greater than any guidelines to try and determine a PPV that may actually increase mortality of fish eggs.

Of interest also is that guidelines for blasting all look at the maximum particle velocity while ignoring many other components of a blast wave. Frequency, acceleration and duration of an event are also important factors that may determine mortality of incubating fish eggs.

This work will focus on the geophysical aspect of the project. Results from the field project are presented as well as the results from an in lab blast simulation experiment. Results from the biological component will be presented only briefly and not discussed. For more information on the biological component the reader is referred to work by Faulkner et al. (2006) and Faulkner (2006).

This report is divided into two main parts; the field component and the lab component of the studies.

1.1) Objectives:

The objectives of the overall project based on the initial proposal submitted to DDMI, and consistent with DFO authorisation, are as follows:

1) Determine the spatial extent of the "blast zone" beyond the dike of the A154 pit and determine the attenuation of peak particle velocity and over-pressures away from the centreline of the dike; as per DFO requests this will require monitoring of as many blasts as possible both inside and outside of the predicted blast zone. Further,

measurements will assess differences between particle motion velocities and pressures during the year with and without lake ice.

2) Monitor areas outside of the dike, regularly during the spawning season and less intensely during routine inspections during other times, for the presence of dead or moribund fish. Dead fish will be examined to assess the degree of trauma to internal organs;

3) Determine if mortality of lake trout eggs is increased within the blast zone, relative to a reference site and if it is, determine to what degree hatching success is reduced;

4) If egg mortality is increased, determine the relationship of mortality to peak particle velocity and/or over-pressure, allowing delineation or calculation of a "realized" blast zone;

5) Assess if enhanced egg mortality and reduced hatching is due to limited exposure during early development or the result of extensive exposure throughout the incubation period; and

6) Assess if geophysical and biological effects of blasting attenuate over time as the pit deepens.

Objective 1 was covered by the 'in lake monitoring programme' where the PPVs of most blasts that take place at DDMI were measured. Objectives 2 through 5 are directly related to the biological component of the project and will not be discussed intensively here. Objective 6 is the last phase of the studies and it is related to the deepening of the pit.

Chapter 2) *Background*

Blast monitoring is a standard practice anywhere that blasting is taking place. Protection of both cultural objects and the environment are of concern to blasters. Monitoring of blasts allows blasters to keep the level of the blast and its associated blast wave within safe levels such that damage to the surrounds is kept to nominal levels. This chapter will review some of the background associated with the basic principles of blasting, blast monitoring, and the physics behind blast (seismic) wave propagation and attenuation.

A recent study of regulations on blast-induced vibrations (Schneider, 2001) found a large discrepancy between regions on the maximum allowed levels of shaking, commonly known as peak particle velocity. Where regulations exist, ground vibration is limited to a peak particle velocity (PPV) anywhere between 5 mm/s and 50 mm/s. The only Canada wide regulation limits vibration in fish habitat to 13 mm/s. To ensure compliance, blast monitoring is a common practice. The energy can also enter a water column and the resulting pressure wave, commonly referred to as overpressure, can be harmful to aquatic animals such as fish.

Studying the blasts and measuring the resulting Peak Particle Velocities (PPVs) at given distances for given charge weights per delay allows for a statistical analysis from which an empirical relation is produced for future prediction of PPVs. Guidelines which are based on measurement of Peak Particle Velocity on land and Over Pressure in the water column are in place for protection of everything from buildings to aquatic life. With some prior site knowledge, a simplified “back of the envelope” calculation can be made to help blasters stay well within the localised guidelines and quickly determine the

maximum safe blast weights as will be discussed in detail in later chapters. Knowing the densities of materials and their acoustic properties, we can model the PPVs and overpressures in order to determine their potential effect, as is discussed in detail in later chapters.

When energy is released in sudden, catastrophic events such as earthquakes or due to large detonations of explosives, seismic energy propagates outwards from the source equally in all directions and the distance a detectable seismic wave travels depends on the nature of the medium that carries it. A variety of factors, such as seismic absorption and scattering due to variations in density and elasticity, influence a seismic wave's propagation and hence its intensity at a given distance from the activating source. For example, in an ideal, non-attenuating substrate, the intensity decays in inverse proportion to the square of the distance from the source. At geologic boundaries, further energy is lost from the forward propagating wave as only some energy passes through the boundary while the rest reflects back. The reflection is dependent on the density contrast between the two media and the angle of incidence. Here an overview of the progressive reduction in the amplitude of a seismic signal as it travels farther from the point of origin is provided in order to allow for the understanding and interpretation of the observations.

2.1) Basic Physical Principles of Seismic Waves

Seismic waves are transient disturbances propagating on the surface and in the subsurface and created by any impact or failure on the surface or within the earth. The term, seismic wave, however, is too generic and here, the types of waves, and their behaviour, are described below.

A blast wave is composed of both body and surface waves. The propagation, or wave, velocity is the speed at which the wave travels. As the wave-front propagates its intensity declines due to seismic attenuation. The observed amplitudes, which are of concern here in blast monitoring, will depend on factors such as the density and elasticity of the material, the distance from the source to the receiver, scattering from heterogeneities, and attenuative properties. Each of these aspects are briefly reviewed.

2.1.1) Basic Wave Propagation

When seismic waves propagate, they carry energy through the ground or along the surface. In the context of blast monitoring, it is crucial to understand what this means. A general 'elastic' wave, which includes sound and seismic waves, is essentially a transient disruption of the material that travels at a speed *c*. That is, as the wave passes a given point in the earth, the 'particle' at that point undergoes motion; and from basic physics we know that we can look at this in terms of the particle's displacement, its speed, or its acceleration. If the particle is in a material continuum, it will also be subject to pressure or stress. Usually these motions are considered to be 'harmonic' meaning that the particle motions are described by simple sinusoidal function with a given frequency. In one dimension '*x*', we can define the particle displacement u_x, the particle velocity u_x' and the particle acceleration u_x'' of wave propagating along the x axis with x-directed displacement through this harmonic function and its derivatives with respect to time.

$$u_x = A\cos(\omega t - kx) \quad \textbf{(2-1)}$$

$$u_x' = -\omega A\sin(\omega t - kx) \quad \textbf{(2-2)}$$

and

$$\ddot{u}_x'' = -\omega^2 A\cos(\omega t - kx) \quad \textbf{(2-3)}$$

where $\omega = 2\pi f$ is the angular frequency, A is the displacement peak amplitude, $k = \omega/c$ is the wave number, t is time and x is the location. It needs to be noted that the particle velocity is the velocity at which the particles move when the seismic wave passes and not the velocity of the wave front propagation. As will be necessary in later discussions in this chapter, it should also be kept in mind that there will actually be three components of particle motion with $\vec{u}(\vec{x},t) = u_x(\vec{x},t)\hat{i} + u_y(\vec{x},t)\hat{j} + u_z(\vec{x},t)\hat{k}$ where $\left[\hat{i},\hat{j},\hat{k}\right]$ is the set of directional unit vectors parallel to the reference co-ordinate system *[x,y,z]* axes with position in 3D space given by the vector $\vec{x} = x\hat{i} + y\hat{j} + z\hat{k}$. Similarly, the amplitude needs to generally be described by a constant vector $\vec{A} = A_x\hat{i} + A_y\hat{j} + A_z\hat{k}$ although much of the discussion below will reduce this to a scalar for the sake of simplicity. The formulae describing the particle motion in the y and z directions are similar to those for Eqns. 2.1 – 2.3 immediately above.

Consequently, a wave can be characterised by its particle displacement, its particle velocity, or its particle acceleration. A given receiver will measure only one of these. For example, highly sensitive seismometers that sense the arrival of low frequency seismic waves produced by distant earthquakes register submicron particle displacements. Geophones are typically sensitive to frequencies used in seismic exploration, and also in many blast monitoring applications over the band from about 10 Hz to 300 Hz and at their simplest rely on the motion of a permanent magnet through a wire coil. The current produced in such a coil consequently depends on the speed at which the magnet moves through the coil, according to Faraday's Law; and the output of the geophone relates directly to the particle velocity. Accelerometers are used in

situations where strong ground motions are expected and are used to assist in determination of earthquake hazards; the values from these strong motion instruments are often given as a ratio with respect to the earth's gravitational acceleration.

As will be seen later, the instruments deployed here in blast monitoring typically involve geophones primarily due to their simplicity and robustness. The jargon used in the engineering blast monitoring community is that the particle velocity, which is a function of time, is represented as 'PV'. Further, most regulatory guidelines are given in terms of 'peak particle velocity' (PPV) with units of in/sec in the United States and mm/s in the rest of the world. Schneider (2001) provides a relatively recent review of existing blasting regulations in different jurisdictions worldwide.

A hydrophone is the second type of transducer that is used in this thesis to record the propagation of wave energy. Hydrophones are sensitive to the pressure of a passing sound wave in water and as noted in the first chapter there are also guidelines on allowable 'overpressures'.

2.1.2) Elastic Moduli

However, in order to link these pressures to stresses in a solid material, it is necessary to first briefly define the elastic moduli, which for purposes of this study will be confined to:

1. **The bulk modulus K** = $-\partial P/(\partial V/V)$ with units of N/m^2 (Pascals) which is a measure of the change in pressure (or more precisely the normal stress) induced in a material due to a change in volume of the material. All solids and fluids have a bulk modulus and can support a pressure.

2. **The shear modulus $\mu = \tau/\gamma$** in units also of Pascals with the shear stress τ and shear strain γ. The shear stress can be envisaged as the ratio of the stress pulling horizontally within a surface to the area of the surface. The shear strain may, for small deformations, be defined as the resulting decrease in the angle between two fibres that prior to deformation were at right angles to one another. The shear modulus essentially describes the change in the shape of an object due to deformation. Only solids may have a shear modulus; fluids cannot support a shear stress. Indeed, this lack of ability to support shear stress is one of the defining characteristics of fluids.

The Poisson's Ratio $\nu = -\varepsilon_z/\varepsilon_x$ which is the ratio between the z-directed strain ε_z to the x-directed strain ε_x induced by applying a uniaxial z-directed stress to a bar of the material. Various physical restraints require $-1 \leq \nu \leq 0.5$ however, most earth materials typically[1] will fall within $0.1 \leq \nu \leq 0.4$.

The elasticity of an isotropic material (i.e. one which has the same physical properties regardless of the direction from which it is observed) is completely described by only two elastic constants. K and μ are not the only ones that are defined; two others are the Lamé parameters λ and μ, introduced mostly due to the mathematical simplifications they allow. The second μ is the same shear modulus. The first $\lambda = K - 2\mu/3$ does not have a simple physical definition but in the absence of a shear modulus μ for a fluid collapses to K. With the use of the elastic constitutive Hooke's law may be written succinctly as:

[1] A negative Poisson's ratio means that the width of an object will shrink when it is compressed along its length, such materials do exist but are usually only artificially produced for specific purposes.

$$\sigma_{ij} = \lambda\theta\delta_{ij} + 2\mu\varepsilon_{ij} \quad \textbf{(2-4)}$$

Where $\theta = (\varepsilon_{11} + \varepsilon_{22} + \varepsilon_{33})$ is the volumetric strain, δ_{ij} is the Kronecker's delta (δ_{ij} = 1 when i = j and $\delta_{ij} = 0$ when $i \neq j$), and ε_{ij} is the strain defined by:

$$\varepsilon_{ij} = \frac{1}{2}\left(\frac{\partial u_i}{\partial x_j} + \frac{\partial u_j}{\partial x_i}\right) \quad \textbf{(2-5)}$$

As noted, a wave is a propagating disturbance that results in both changes in volume, shape, and stress. For a perfectly elastic medium (i.e. one in which there is no intrinsic loss of energy due to wave absorption) one may derive a vector wave equation by considering: 1) Hooke's Law constitutive relationships between stresses, the elastic moduli, and strains, 2) Newton's second law F = ma that relates the acceleration of a small element in the material due to unbalanced forces on either side of it as the wave passes. Again, the details of the derivation of this equation can be considerable and are provided in many texts (e.g. Stein and Wysession, 2003) but the equation takes the form:

$$(\lambda + \mu)\vec{\nabla}\left(\vec{\nabla} \bullet \vec{u}(\vec{x},t)\right) + \mu\vec{\nabla}^2\vec{u}(\vec{x},t) = \rho\frac{\partial^2\vec{u}(\vec{x},t)}{\partial t^2} \quad \textbf{(2-6)}$$

where overhead arrows signify a vector operation of quantity, $\vec{\nabla}$, $\vec{\nabla}\bullet$, and $\vec{\nabla}^2$ are the vector gradient, divergence, and Laplacian operators, respectively, and ρ is the mass density. The solutions to the wave equation take a harmonic form:

$$\vec{u}(\vec{x},t) = \vec{A}e^{i\left(\omega t - \vec{k}\vec{x}\right)} \quad \textbf{(2-7)}$$

where $\vec{k}$ is the vector wavenumber. While this all looks very imposing, the final results upon examination of the solutions is relatively simple for an isotropic elastic medium. In general, two 'body' waves will exist: a compressional or P-wave[2] with wave velocity:

$$V_P = \sqrt{\frac{K + \frac{4}{3}\mu}{\rho}} = \sqrt{\frac{\lambda + 2\mu}{\rho}} \qquad \textbf{(2-8)}$$

And with particle displacements parallel to the direction that the wave is propagating, and a slower shear or S-wave[3] propagating at

$$V_S = \sqrt{\frac{\mu}{\rho}} \qquad \textbf{(2-9)}$$

One final comment here is that $V_P > V_S$ always and the theoretical limits for an elastic medium are enforced by;

3. Poisson's ratio is also tied to the V_P/V_S ratio via:

$$\nu = \frac{1}{2}\frac{\left(V_P/V_S\right)^2 - 2}{\left(V_P/V_S\right)^2 - 1} \qquad \textbf{(2-10)}$$

A part of the range of which is plotted in Figure 2-1 for illustration.

---

[2] The P-wave is also known in other disciplines as the longitudinal wave to signify the relation between the particle motion and wave propagation direction. Compressional refers to one aspect of the material behaviour as the wave passes the volume of the material dilates and contracts. The origin of 'P' wave is from seismology and likely refers to the fact that this wave has the higher velocity and as such arrives first and is therefore 'primary'.

[3] This wave is also known in other disciplines as a transverse wave. The designation of 'S' is also not known but likely arises from its 'secondary' arrival or from its shear nature.

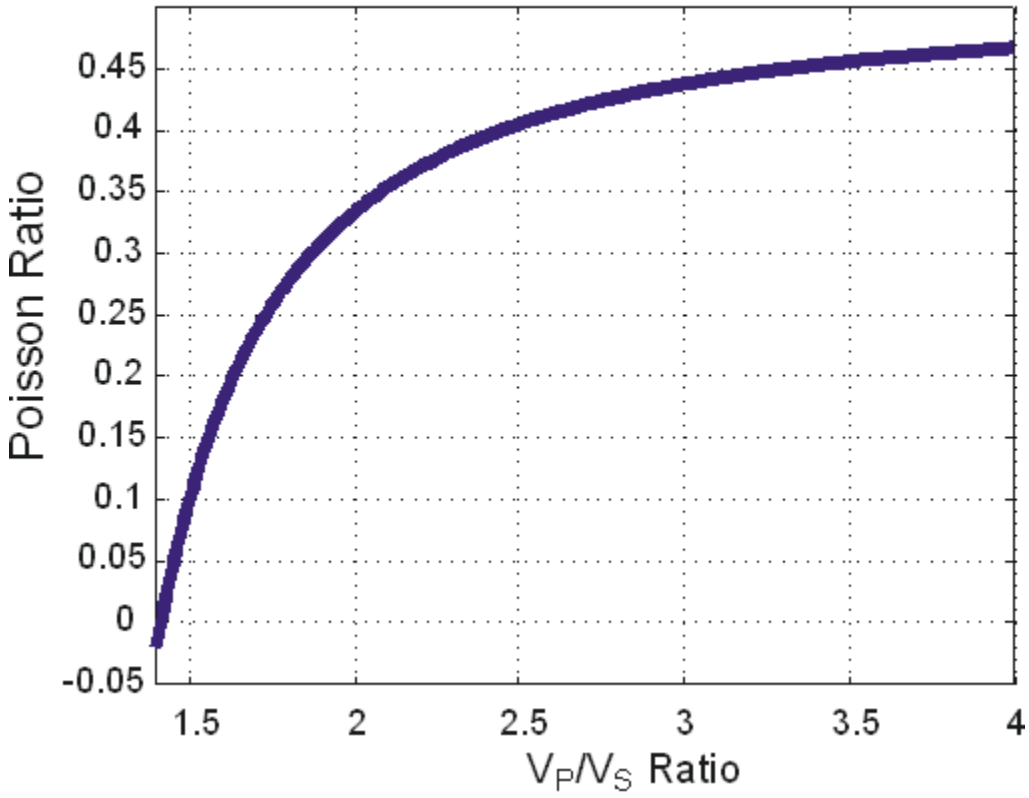

Figure 2-1) Poisson ratio plotted against the Vp/Vs ratio.

Body waves propagate through a three dimensional medium; in the current context they will appear as the P-wave, the S-wave, and the air-blast wave. However, these are not the only seismic waves and, indeed, are often not the ones of most concern in surface vibration monitoring. The strongest ground motions, in earthquake and exploration seismology and in blast vibration monitoring are generally Rayleigh[4] surface waves. Rayleigh waves dominate at large distances for blasting or construction vibrations. (Dowding, 1985). These seismic waves exist whenever there is a 'free' surface, such as at

[4] These waves were first described by William Strutt, third Baron Rayleigh (1842-1919) who wrote prolifically on many topics and particularly on the propagation of sound waves. He received the Nobel Prize in Physics in 1904.

the contact between the solid earth and the atmosphere, the influence of the latter can usually be ignored. The speed of propagation of these waves V_R also depends on the elastic physical properties of the half-space upon which they travel, and they must be found from the zero that satisfies the requirement $0 < V_R < V_S$:

$$\left(2-\frac{V_R^2}{V_P^2}\right)^2 + 4\left(\frac{V_R^2}{V_S^2}-1\right)^{1/2}\left(\frac{V_R^2}{V_P^2}-1\right)^{1/2} = 0 \qquad \textbf{(2-11)}$$

The relationship between V_R and the V_P/V_S ratio, also given as a ratio of V_R/V_S, is plotted in Figure 2-2, which shows that V_R is about 90% of V_S.

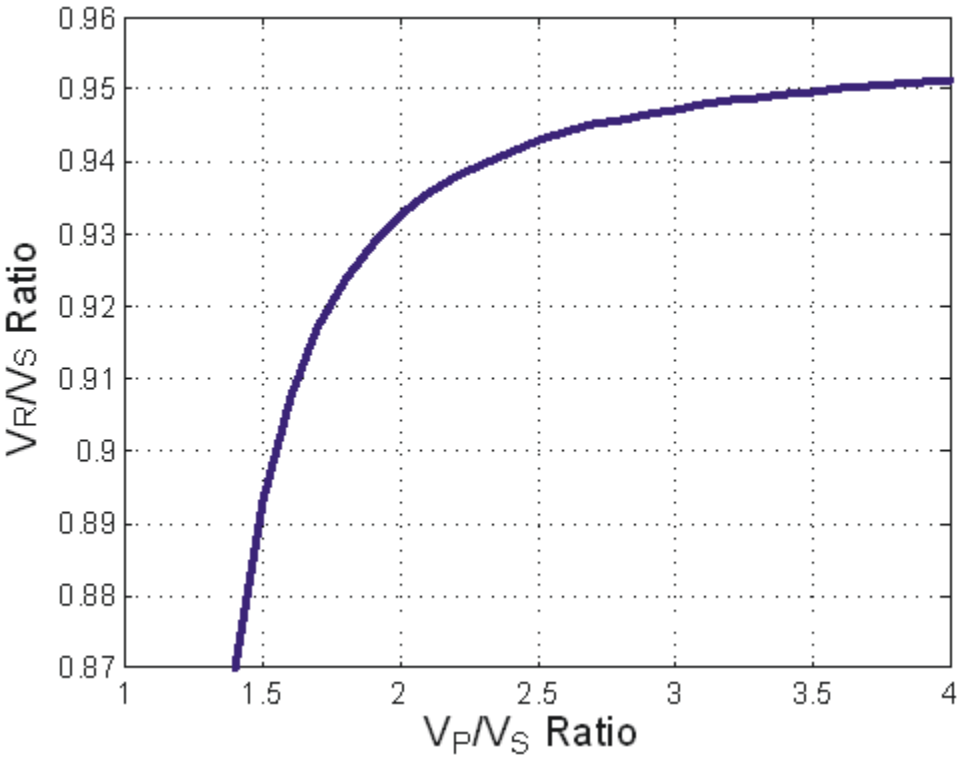

Figure 2-2) The Vr/Vs ratio plotted against the Vp/Vs ratio.

The Rayleigh wave particle motions are substantially more complex than those for the linearly polarised P- and S-waves and they are dependent on a variety of factors of which the depth is the most important. Again, surface waves are trapped by and decay

exponentially away from the surface. Finding these particle displacements is laborious and here an example of the formulae for the two components of particle displacement at the surface for a Poisson solid (i.e. one with ν = 0.25) for a Rayleigh wave propagating in the positive x-direction will be

$$\begin{aligned} u_x(x,t) &= 0.42Ak_x \sin(\omega t - k_x x) \\ u_z(x,t) &= 0.62Ak_x \cos(\omega t - k_x x) \end{aligned} \qquad \textbf{(2-12)}$$

These formulae define an elliptical 'retrograde' particle path which means that the shape of the path is elliptical but that the trajectory as it rises along the path is reverse to the wave propagation direction as indicated in Figure 2-3.

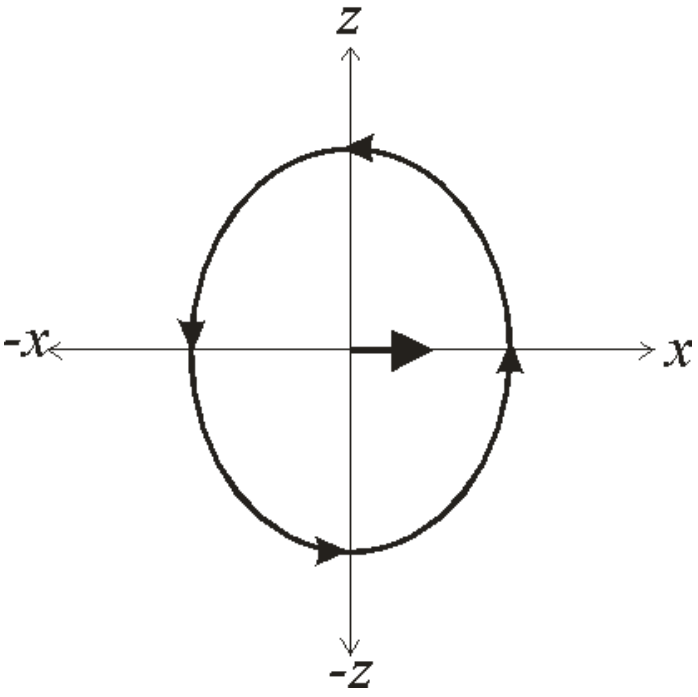

Figure 2-3) Retrograde particle motion of a Rayleigh wave. Wave propagation direction along the surface is represented by the large horizontal arrow. At a given point the particles move 'backwards' around the ellipse as shown.

This elliptical motion is similar to that experienced by a small boat on the water and which causes sea sickness, although these 'gravity' waves on water have the opposite, prograde motion.

The current discussion only touches some of the basics of surface wave propagation. The real earth is much more complex than the simple half-space considered above. For example, another surface wave called the Love[5] wave is produced by the interference of horizontally polarized shear wave reverberations within a low velocity layer over a half-space. Love waves are by their very nature 'dispersive' meaning that the speed of their propagation depends not only on both the variations in the shear wave speeds between the layer and the underlying half-space but particularly on the frequency. This results in spreading of the wave form pulse with distance from the source.

The behaviour of the Rayleigh wave, too, becomes more complex even with such a trivial addition to the geological structure. There are two new aspects to this. First, the Rayleigh wave also becomes dispersive with its velocity now dependent on the frequency and, second, there are additional interfering Rayeigh wave modes produced by the interference of reverberating P- and S-waves. While such complexities complicate analysis of Rayleigh waves, they do add considerable information that can be profitably used in delineating the subsurface structure (e.g. Beaty and Schmitt, 2003). While these are useful points to consider, however, they are beyond the current scope of this contribution which focuses mostly on the monitoring aspects of blast vibrations from a rather basic level. That does not mean that such complications should not be included to further refine blast monitoring technology in the future.

---

[5] The Love wave was first predicted theoretically by and is named after A.E.H. Love (1863-1940) who worked extensively in the theory of elasticity and wave propagation.

2.1.3) Wave Energy

In blast vibration monitoring it is important to understand what influences the observed amplitudes and this first requires some idea of the energy carried by a harmonic[6] wave which is, without derivation (see Stein and Wysession (2003), pg 35 & pg 61), given by

$$E = \frac{A_o^2 \omega^2 \rho}{2} \qquad \textbf{(2-13)}$$

where E is the average over one wavelength of the total energy conveyed per unit wavefront (in units that reduce to J/m^3 and as such is analogous to an energy density), ρ is the density of the material, ω is the angular frequency and A_o is the peak particle displacement amplitude. Simple examination of the last equation shows that the energy is proportional to the squares of both the peak amplitude and the frequency. The magnitude of the vector energy flux F is the rate at which the wave transfers the energy past a given point and is found by multiplying by the wave velocity, hence for the P-wave the flux F is

$$F = \frac{\omega^2 A_o^2 \rho V_P}{2} = \frac{\omega^2 A_o^2 Z}{2} \qquad \textbf{(2-14)}$$

Where $Z = \rho V_p$ is the acoustic impedance of the material. Z is a measure of the resistance to motion of the mateiral by the passing wave. Note that dimensionally F has units of kg/s^3 which is dimensionally the same as the intensity: the power per unit area in Watts/m^2; this is the term that is more normally used in introductory physics texts when sound wave energy is discussed.

---

[6] Harmonic means monofrequency, i.e. a cosine or sine wave.

The last two equations really only consider propagation of the wave within a single medium with uniform properties. They are more instructive when the case of constant energy flux is compared between two media with impedances $Z_1 > Z_2$ which upon examination of the last equation shows that the peak amplitude in the first medium A_1 must be less than that in the second medium A_2. That is, a dense and high wave speed material is displaced less than a lighter and low wave speed material by a passing wave of the same intensity.

The last two equations allow relation of the wave energy to the particle displacement, and hence to particle velocities. One other aspect of the current study, however, is the measurement of pressure variations within the water column due to blasting. The pressure P, or more precisely the variation of pressure from the equilibrium atmospheric in air or hydrostatic in water, of the wave is coupled to the particle motions. Later with regards to blast monitoring this will be called the 'over-pressure'. As mentioned above, in fluids only a P-wave is transmitted and as is well known such 'sound' or 'acoustic' waves have a particle displacement in the direction of the wave propagation and are related to other characteristics of the wave propagation within:

$$P = \rho V_P \omega A_o = Z\omega A_o = ZA'_o = \frac{A''_o Z}{\omega} = \frac{F}{A'_o} = \sqrt{FZ} \qquad \textbf{(2-15)}$$

where A_o, A'_o, and A''_o are the peak particle displacements, particle velocities ('PV' above), and particle accelerations due to the passing wave, respectively.

2.1.4) Decay of Amplitude

Understanding the factors that influence the observed amplitudes is critical in the interpretation of blast vibration records. Energy loss, or decrease in the amplitude, occurs as the waves pass through media. Seismic waves lose energy through absorption, reflection and refraction at interfaces, through mode conversion and through spherical divergence, or spreading of the wave. The primary factors crucial to decay of the seismic signal are geometrical wavefront spreading, intrinsic attenuation, and scattering attenuation. More details on this may be found in Grech (M.Sc. thesis, 1998). Perplexingly, the blast vibration literature has focussed primarily on highly empirical and statistical descriptions without much in the way of a critical examination of the underlying physics of the problem, a deficiency recently discussed by Blair (2004). This is likely because, as will be hinted at below, the decay of surface waves is relatively complicated. Below, I re-examine briefly some of the important aspects that will influence the decay of amplitudes from the seismic source[7].

i) Geometrical Spreading

The above discussion has focussed on the propagation of monofrequency 'plane waves': an idealized theoretical construct that simplifies mathematical descriptions of wave propagation. As the name suggests, a plane wave front is flat and two-dimensional; this can be useful if one is in the 'far-field' of a seismic source where the wavefront is for practical purposes flat as, for example, studies of 'teleseisms' in global seismology.

---

[7] A seismic source is considered to be a controlled source used in exploration. The source may be an explosive, a hammer or a seismic vibrator.

This assumption is not adequate in the current context of blast vibration and over-pressure monitoring where the source can be within tens of metres of the recording sensor. The simplest approximation is for body waves propagating from a hypothetical 'point' source in a three-dimensional continuum. In such a case the wave energy moves out in all directions radially from the source with the energy of the wave uniformly distributed over the surface of a sphere. Of course, the radius R of the sphere increases linearly with time at a rate proportional to the wave speed. Correspondingly, the surface area of this expanding sphere increases in proportion to R^2, and since energy is conserved on the wavefront the intensity must decrease in proportion to $1/R^2$. Consequently, the observed amplitudes, regardless of whether they are for particle displacements, velocities, or accelerations, will decay proportion to $1/R$.

The situation differs somewhat for surface waves that propagate over a two-dimensional surface. A circular surface wave front also expands out along the surface proportionally to the wave speed but the energy is now distributed along the circular locus and hence the local intensity at a point on the wavefront decays less rapdily at $1/R$ dependence. Similarly, the amplitudes have a $1/\sqrt{R}$ dependence. This slow decay of amplitude is the major reason why surface waves are so strong relative to either P or S waves. In summary, the amplitude decay is proportional to $1/r$ for a body wave and $1/\sqrt{r}$ for a surface wave; and in practice Rayleigh waves will dominate typically within only a distance of 2 wavelengths from the source (Lai et al., 2002).

In general, the rate of decay of the particle velocity due to the divergence of the wave front can be described by

$$\dot{y}_1 = \dot{y}_2 \left(\frac{R_1}{R_2} \right)^n \qquad \textbf{(2-16)}$$

where $\dot{y}_1$ and $\dot{y}_2$ are peak particle velocities at radii R_1 and R_2, n is 1 for a body wave except at surface where n is 2 and, for a Rayleigh wave, n is 1/2.

Dispersion, which is particularly important in the propagation of surface waves, has another effect that is related to the geometry of the situation. As noted above, the duration of a dispersive seismic pulse lengthens with propagation distance. This means that the energy of the pulse is spread out over a longer time; the longer the pulse travels the smaller the instantaneous intensity and hence the instantaneous amplitudes will be. While this may be obvious to a seismologist, this factor does not appear to be considered in the design of the somewhat arbitrary predictive empirical formulae for blast vibrations as will be discussed later, although engineers should not be faulted as this remains an area of active scientific study. This is particularly true in the near surface geophysical community where there have been more recent attempts to examine the truer geometrical decay of Rayleigh waves using cylindrical waves described with Bessel functions instead of by plane waves (Zywicki and Rix, 2005). This recent work shows that the square root decay provides an estimate of the minimum decay experienced by the Rayleigh wave.

ii) Intrinsic attenuation

The energy contained by the wave and its amplitude attenuate as they pass through media. The physical properties of the media dictate the rate of attenuation. All materials will absorb seismic energy to some degree, and because this absorption is irreversible it is often also referred to as internal friction. There are a variety of mechanisms that have been proposed for this absorption that in include thermally dependent motion of defects

in crystals and grain boundary sliding (applicable in the deeper crust and mantle and in metals), frictional sliding on mineral grains (in weakly consolidated rocks), and differences between the motion of the saturating fluids and the solid mineral frame due to the wave passing.

The attenuation results in the progressive dissipation of energy as the wave travels also contributing to the loss of amplitude. That is, one form of energy is converted into another as the wave travels. In this case, example, seismic waves are partially converted to heat as they pass through rock.

iii) Attenuation at geologic boundaries

At physical boundaries, or geological interfaces energy is lost as only some of the wave is passed into the next medium while the rest is reflected. The percentage of reflection is dependant on the density contrast between the media. Absorption, or material damping is the energy lost due to friction. With each cycle (wavelength) the blast wave loses a small amount of energy to overcome friction. It is defined by

$$\dot{y}_2 = \dot{y}_1 e^{-\alpha(R_2 - R_1)} \qquad \textbf{(2-17)}$$

where α is the attenuation coefficient which is given in units of m^{-1}.

The attenuation co-efficient is frequency dependent for a given material and one way to overcome this limitation is with the quality factor Q is the ratio between the total energy stored by the wave to the energy lost per radian (or equivalently 2π times the total energy stored by the wave to the energy lost per cycle). So, the less energy lost per cycle the greater the value of Q. Q is related to α via:

$$Q(\omega_o) = \frac{\omega_o}{2\alpha V_o}\left[1 - \frac{\alpha^2 V_o^2}{\omega_o^2}\right] \cong \frac{\omega_o}{2\alpha V_o} = \frac{\pi f}{\alpha V_o} \qquad \textbf{(2-18)}$$

with the right-most approximation essentially active under the assumption that Q remains constant. Hence, because Q is usually assumed to remain constant or nearly so it more conveniently describes the attenuation than *a*. For the sake of comparison, typical values of Q are $>10^6$ for fused quartz glass, $\sim 10^5$ for aluminium metal, ~ 50 for P-waves and ~30 for S-waves in acrylic glass (e.g. Plexiglas™), ~ 200 or more for typical metamorphic rocks, ~ 40 or more for sedimentary rocks, and as low as ~15 for bitumen saturated sands.

iv) Scattering Attenuation

A third type of amplitude decay is caused by the 'scattering' of the seismic wave by elastic heterogeneities such as pores, fractures, and any other features of the geology that result and spatial variations of the wave speeds and densities. In scattering attenuation no energy is dissipatively lost by conversion to heat as for intrinsic attenuation above, but instead portions of the energy are partitioned between the forward travelling 'ballistic' wave pulse that propagates from the source to the receiver and the 'scattered' energy that moves off in different directions. The simplest form of this scattering is the division of the energy of a pulse by simple reflection and transmission at a geological boundary. The effect of this is that the energy remaining in the forward moving ballistic pulse, and hence its amplitude relative to the total energy in the system, is diminished every time such a boundary is encountered.

Scattering attenuation is a large, complex, and still intensively studied topic. Scattering of light is experienced everyday, however, and this provides some frame of reference for discussion of the topic. For example, the sky is blue because of the

Rayleigh[8] scattering of the sun's light by the small molecules in the air. The degree of scattering is proportional to $1/\Lambda^4$ where Λ is the wavelength; therefore, the bluer and smaller wavelength fractions of the white sunlight are preferentially scattered back to us to make the sky blue. When one looks more directly at the Sun, however, the light surrounding it does not appear to have any colour, this is because of Mie[9] scattering from larger particulates, which is not so frequency dependent. Seismic waves are similarly subject to these kinds of scattering.

It is difficult to separate the effects of Rayleigh and Mie scattering from the intrinsic scattering discussed earlier. A practical outcome of this is that these effects may be incorporated into an experimental determination of Q.

v) Combination of effects

Combining equations 2-4 & 2-5 we can define the attenuation of the amplitude from y_1 to $\dot{y}_2$ as the wave produced by a point source propagates out from radial distance R_1 to R_2 can be generally be described by:

$$\dot{y}_2 = \dot{y}_1 \left(\frac{R_2}{R_1} \right)^n e^{-\alpha(R_2 - R_1)} \qquad \textbf{(2-19)}$$

where again n = 1 for body waves and n = ½ for surface waves. Again, however, it must be noted that this equation is based on rather simple assumptions and workers are still actively working on more physically meaningful solutions to this complex problem of

---

[8] Again, first considered by the same Lord Rayleigh discussed above. In Rayleigh scattering the wavelengths are much larger than the scattering particles which in the case of the blue sky are mostly N_2 molecules.

[9] Mie theory is named after G. Mie (1868-1957) who first developed the theory of the scattering of an electromagnetic wave (e.g. light) by a dielectric (insulating) sphere in 1908. In Mie scattering the wavelengths are roughly comparable to the particulate size.

Rayleigh waves (e.g. Lai and Rix, 2002; Zywicki and Rix, 2005). In order to gain a better understanding of this equation, the decay of amplitude with distance from the source to the receiver is plotted in Fig 2-4 below. This case uses some parameters that will be realistic for the blast monitoring case studied with V_P = 5000 m/s and f = 100 Hz. Assuming a uniform reference intensity with value of unity at a reference distance of 10 cm from the center of the radiating sphere (for body waves) or cylinder (for surface waves) the loss of amplitude is calculated for three cases of Q = ∞, 100, and 10 for the surface wave for comparision[10]. This shows the substantially larger difference in the geomtric decay between surface and body waves; for the same initial amplitude at the reference distance here of 10 cm, there is a 40 dB (100 times) difference in their amplitudes at 1 km offset. This further highlights the relative importance of surface waves in controlling the maximum amplitudes.

[10] Fig.2-4 is plotted in terms of units of dB (decibels) versus distance which is an accepted standard measure of relative amplitude, this is named in honor of the inventor of the telehone, Alexander G. Bell. Because of the square relationship between amplitude and intensity, the relative value plotted is $20\log_{10}(y/y_{ref})$. Consequently, a signal that has decreased by 10 dB is $10^{0.5}$ = 3.16 times smaller amplitude, 20 dB is 10 times lower, 30 dB is 31.6 times lower, etc. It must be remebered that the usage here is in terms of particle amplitude, whether it be displacement, velocity, or acceleration. This is similar to, but differs somewhat, from the dB scale most readers will be familiar with from knowledge of sound intensity with a well defined reference intensity.

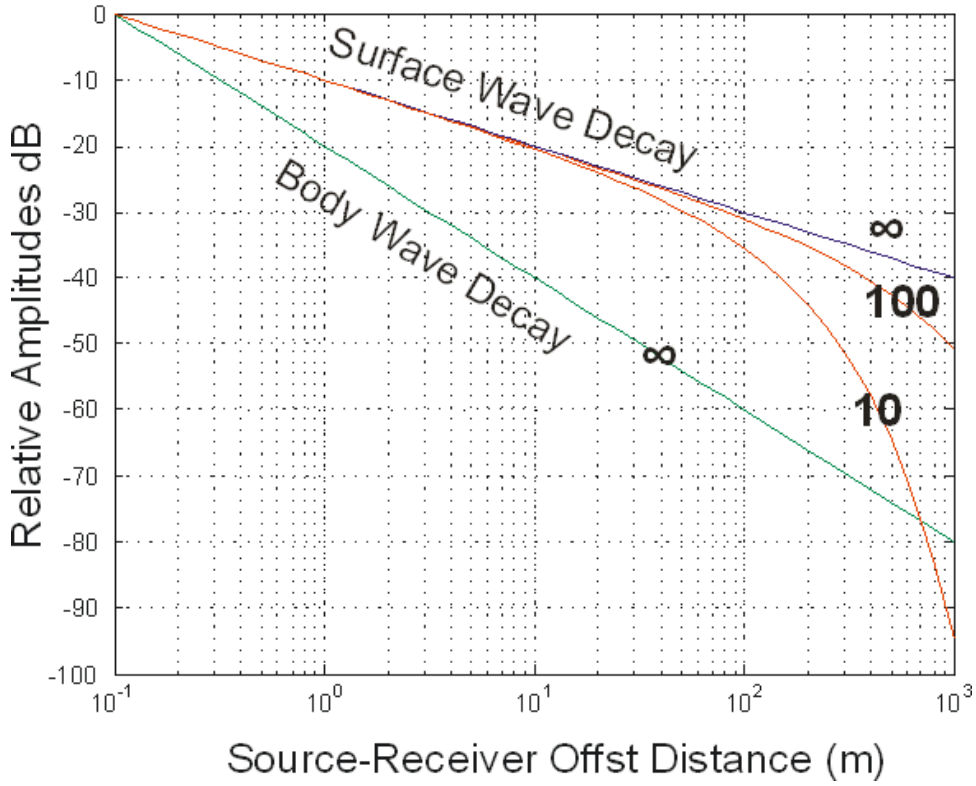

Figure 2-4) Illustration of the relative decay of a cylindrically spreading surface wave and a spherically spreading body wave with distance relative to the (arbitrary) reference distance of 0.1 m for a wave speed of 5000 m/s and a frequency of 100 Hz. Relative amplitudes report in dB[10]. Numerical values represent quality factors included in the calculations. $Q = \infty$ means no attenuation.

An important question to ask is what is the actual displacement that might be expected from an explosion? The total amount of energy released by the explosive material itself can be taken to depend linearly on the amount of explosive used and is usually calculated relatively easily from knowledge of the chemistry. For example, Trinitrotoluene TNT ($C_6H_2(NO_2)_3CH_3$) releases approximately 616 kJ/mol or 2175 J/g. However, what is just as or more important than the amount of energy released are other factors such as the 'detonation velocity' which for TNT is nearly 7000 m/s[11]. Even this is a gross simplification, as the detonation velocity will depend on other factors such as the

[11] Surprisingly, gasoline releases much more energy but is not as explosive (but still dangerous) and only has a flame advance speed of 0.34 m/s in air.

size of the hole, the type of explosive, the peak pressure produced, the shape of the charge, and the strength of the rock surrounding the explosive.

The ultimate energy of the explosive is converted directly to heat, to fracturing, crushing, and moving the rock, and to seismic energy. The fraction of this available explosive energy that actually goes into producing seismic waves (vibrations) is very difficult to determine. Hinzen (1998) carried out a number of simple tests in a hardrock (gneiss) mine that showed the seismic efficiency (i.e. the percentage of energy radiated as seismic waves to the chemical energy of the explosive) to range from 2% to 25% depending on the geometry of the source. However, this applies more to near field body waves than to the more typical surface situation where the Rayleigh waves will be important.

In any case, despite all these complications, the amount of energy in seismic waves depends on the total amount of explosive detonated. This is usually given as the *'blast weight per delay'* which is the total amount of explosive detonated at '*the same time'* with the same time usually defined within an 8 ms interval.

2.2) Introduction to Blast Monitoring

In field practice, effects on the environment are measured as the *peak particle velocity* (PPV) for ground shaking and *over-pressure* for energy transferred into the water column. As noted in the previous section, PPV will be measured by the maximum value of the *magnitude* of the vector particle velocity as will be described below; for illustration however the PPV value is shown in Fig 2-4.

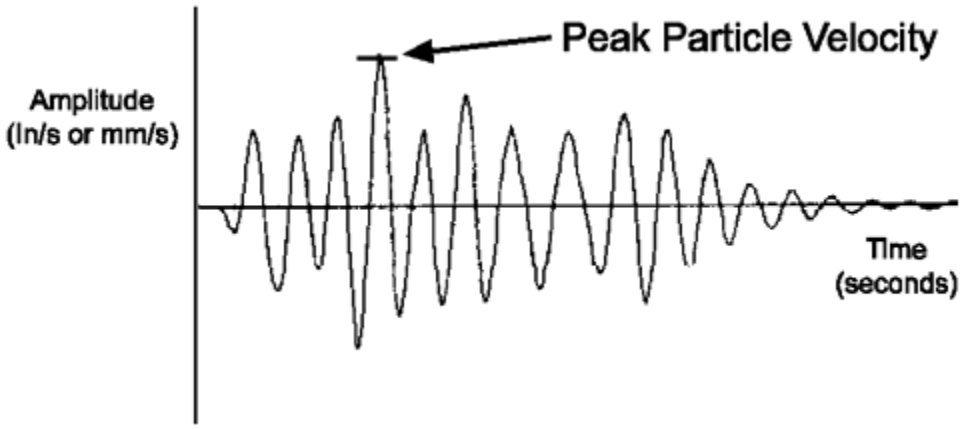

Figure 2-5) Illustration of the definition of the PPV on a particle velocity versus time plot where the peak particle velocity is the maximum excursion from zero amplitude.

Different levels of each are deemed acceptable for different industries and different parts of the world (e.g. Schneider, 2001) but there appears to be little in the way of consistency in the way many of these regulations have been developed, measured, or applied. Grogan and McAnuff (2005) recently provided a short review of the blasting and vibration regulatory environment in Canada from the perspective of mining and construction; they found that that most provinces have no set regulations. Ontario and Nova Scotia require routine monitoring if the PPV levels exceed 12.5 mm/s while Manitoba sets this level at 12 mm/s. In Alberta and British Columbia, mine inspectors evaluate each case on an individual basis and the limits become part of the permit. In contrast, Alberta, British Columbia, and Saskatchewan all have restrictions on seismic exploration. These are not described by PPV but are given in terms of the distance that the seismic source, which can also be a seismic vibrator instead of explosives, must be from a particular feature such as a pipeline. For the sake of comparison, the current Alberta government (2005) regulations are reproduced in Table 1. The basis of these

regulations is not known but it is likely that they originated from a series of studies in the late 1970's on the influence of seismic blasting on water wells (Goble, 1980)

Table 1) Current Alberta seismic exploration regulation offsets, Schedule 2 of Alberta Government (2005).

Structure	Explosive		Non-Explosive Dist. (m)	Test Hole Dist. (m)
	Charge Weight (kg)	Dist. (m)		
A. Residence, barn, cemetery, a building or structure with a concrete base, irrigation headworks, dam, water well	2 or less	64	50	64
	Greater than 2, not greater than 4	90		
	Greater than 4, not greater than 6	110		
	Greater than 6, not greater than 8	128		
	Greater than 8, not greater than 10	142		
	Greater than 10, not greater than 12	156		
	Greater than 12, not greater than 20	200		
	Greater than 20, not greater than 40,	284		
	Greater than 40, not greater than 100	450		
B. High pressure pipeline (measured) From the centre line of the pipeline, oil or gas well	2 or less	32	15	32
	Greater than 2, not greater than 4	45		
	Greater than 4, not greater than 6	55		
	Greater than 6, not greater than 8	64		
	Greater than 8, not greater than 10	70		
	Greater than 10, not greater than 12	78		
	Greater than 12, not greater than 20	100		
	Greater than 20, not greater than 40	142		
	Greater than 40, not greater than 100	225		
C. Driveway, gateway, survey monument, buried telephone or telecommunications line	All	2	2	2
D. Low-pressure distribution line (measured from the centre line of the pipeline)	All	3	3	3

E. Irrigation canal more than 4 metres wide	All	10	10	10
F. Buried water pipeline	All	10	10	10

The only Canadian wide regulations are enforced by the Department of Fisheries and Oceans (DFO). Wright & Hopky (1998) state that maximum allowable PPV in fish habitat is 13 mm/s and maximum allowable pressure in the water column is 100 kPa (approximately 1 atmosphere of overpressure). DFO provides sample calculations for calculations of the PPV and water pressure based on the charge weight and the distance between the source and the receiver (Eqns. 2-22 to 2-25).

Much literature is devoted to blast monitoring for prediction of damage to cultural items. Effects on aquatic life from on land blasting is only discussed by regulating bodies such as the DFO. Monitoring of blasts at construction, mining or any other sites where activities induce ground vibration is common practice.

Blasts are monitored to measure and predict the effects on cultural and natural objects, for example; fish habitat or man-made structures such as dikes. Ideally, the monitoring and prediction will keep effects of the blasting below damaging levels.

2.2.1) Peak Particle Velocity

The Peak Particle Velocity is the maximum particle velocity attained when the seismic wave passes a measurement point on the earth (Figure 2-5). In most of the world its values are generally noted in metric units of mm/s or cm/s. As noted above, it should be remembered that this is the velocity at which the particles are moving and not the speed at which the wave front is moving. The actual wave front velocity is of no importance to this project as we are only interested in the energy of the wave front and its

attenuation. In Canada, as per DFO regulations, the maximum allowable shaking in the substrate is 13 mm/s. Shaking beyond this level is considered to be potentially harmful to incubating fish eggs.

Particle velocity is measured using three orthogonally placed geophones usually oriented with respect to the vertical and horizontal. The observed PPV is calculated from the responses of the three geophones $SH_1(t)$, $SH_2(t)$, and SV(t) that respectively represent the time dependent particle velocities for the two horizontal and one vertical components. Referring back to Eq. 2-7, these explicitly would look like:

$$\vec{u}'(\vec{x},t) = \vec{A}\omega e^{i\left(\omega t - \vec{k}\vec{x}\right)} = \omega e^{i\left(\omega t - \vec{k}\vec{x}\right)}\left(A_x\hat{i} + A_y\hat{j} + A_z\hat{k}\right) = \left(SH_1(t)\hat{i} + SH_2(t)\hat{j} + SV(t)\hat{k}\right) \quad \textbf{(2-20)}$$

These may be taken as components of the particle velocity vector with magnitude with time PV(t) given by:

$$PV(t) = \sqrt{SH1(t)^2 + SH2(t)^2 + SV(t)^2} \quad \textbf{(2-21)}$$

with PPV equal to the maximum value of *PV(t)* over the time window of interest. This is a simple attribute extracted from the data and it is worth noting that while this is a useful measure it does not incorporate any information with regards to the direction of maximum shaking, its duration, or its acceleration. It is also important to note that this definition is often not consistent within the engineering literature or even within existing regulations from place to place; often, only the vertical component SV is used, or in other cases, the peak-to-peak value may be used.

To predict the peak particle velocities, DFO provides a simplified calculation where the minimum safe distance from the blast is calculated based on the maximum charge weight to limit the PPV to 13 mm/s or less.

$$R = \sqrt{W} * 15.09 \quad \textbf{(2-22)}$$

where R is the distance from the blast location in metres and W is the charge weight per delay, in kilograms, of the blast.

The PPVs can be modelled once several blasts have been monitored based on statistical methodology where $R/\sqrt{W}$ is considered to be the scaled distance.

2.2.2) Overpressure

In the blast vibration monitoring lexicon, overpressure is defined as a pressure deficit/excess created by the seismic pressure wave in the water column and is measured in kiloPascals (kPa)[12] using what is known as a hydrophone. In Canada, as per DFO regulations, a pressure change over 100 kPa is considered to be harmful to aquatic life.

To approximate a minimum offset for a given charge weight a series of calculations need to be made as per DFO. Firstly, the transfer of pressure from the substrate to the water column is calculated, the pressure in the substrate is found using a maximum value of 100 kPa in the water column (Equations 2-23 & 2-24).

$$P_w = \frac{2(Z_w / Z_r)P_r}{1 + (Z_w / Z_r)} \quad \textbf{(2-23)}$$

$$Z_w / Z_r = \frac{D_w C_w}{D_r C_r} \quad \textbf{(2-24)}$$

here P_w is the pressure (kPa) in the water column, Pr is the pressure in the substrate and Z_w and Z_r are the acoustic impedances of water and the substrate respectively, D_w and D_r are the densities (g/cm3), C_w and C_r are the compressional wave velocities. Then the PPV due to pressure is calculated

[12] For reference, one standard atmosphere of pressure is 101.325 kPa.

$$PPV = \frac{2P}{\rho \times V} \tag{2-25}$$

where P is the pressure in the substrate, ρ is substrate density and V is seismic wave velocity in the substrate. Knowing the PPV at the substrate interface, the safe distances and charge weights can be solved for as outlined in the previous section.

Of course, as with the PPV, once some data are in place a statistically based empirical formula is used for future blast level predictions.

2.2.3) Scaled Distance

As may be gleaned from the discussions above, while at its base the physics of the problem of wave decay seems fairly straightforward, there are many complications related to the source blasting configuration; the seismic efficiency, the effective material properties at the receiver site, and the dispersive nature of Rayleigh waves to name a few, that make predicting vibration levels problematic. As a result, more empirical routes are taken.

This problem has been addressed for many decades in the earthquake seismology community who initially developed criteria to place some quantitative meausure on the size of earthquakes. The most famous example of this is the logarithmic *Richter Magnitude Scale*, which, despite its misappropriation in the media, applies to the specific case of consistent measurements of amplitude using a specific Wood-Anderson seismometer over the Caltech array in Southern California. As such this is more properly called a Local Scale and it explicitly takes the form:

$$M_L = \log_{10}\left(A(mm)\right) + 3\log_{10}\left(8\Delta t\right) - 2.92 \tag{2-26}$$

where A(mm) is the peak particle displacement of the shear wave produced by the earthquake and recorded on the Wood-Anderson seismometer and Δt is the S-P arrival time difference which is essentially a rough measure of how far the earthquake was from the seismometer vault. $M_L = 0$ was set for a 1 μm particle displacement for a 100 km distant earthquake. So, while this may not be an elegant solution it does have buried in it information with regards to the energy of the earthquake (via the amplitude) and the distance of the earthquake (via Δt). A similar scale exists for surface waves, which may be the only phase observed, at teleseismic distances.

The blast vibration community has the inverse problem to earthquake seismologists in that they want to predict the vibration levels generated in blasting and they usualy use an empirical *scaled distance* approach. Normalisation of the blast weight per delay and the distance from the blast zone to the sensor is known as *Scaled Distance.* Scaled distance plotted against the PPV for each blast is used to create an empirical relationship which can be used to predict blast effects at given distances for given charge weights. Blast monitoring and predicting effects of blasting are of great importance to any operation where blasting is used. An empirical relation is based on measuring blast induced vibrations at different distances from the blasts for different charge weights. Essentially, these formulae attempt to account for the decay of the seismic energy with distance and the differing amounts of energy released during the blast. The former depends on factors discussed in detail above such as geometrical spreading of the seismic waves which results in lower intensity and other factors such as attenuation of the seismic waves within the rock mass. The latter relates energy released to the mass of explosive employed.

The blast weight per delay and distance from the blast to the sensor are first normalised and then plotted against the recorded PPV. The scaled distance SD is:

$$SD = D/W^{r} \quad \textbf{(2-27)}$$

Where D = distance, W = charge weight per delay and in practice the exponent is typically assigned either r = ½ (Square root) or 1/3 (Cube root). The exponential factor of 1/2 < r < 1/3 are empirical limits given in the literature. The derivation of these exponents is not exactly clear in the literature. Dowding (1985) refers to earlier work technical reports; but the actual development does not seem straightforward. Apparently, these were derived not so much with some physical insight into the problem but from an application of dimensional analysis. From a physical basis, the exponent r = ½ might be somewhat justified in that the weight of explosive detonated at any one time should be directly proportional to the amount of energy released. As the equations above show, the square of the amplitude of a wave is directly proportional to its energy density; or alternatively the square root of energy density is proportional to the particle motion amplitude. This plot is an exponential function where the PPV decreases as the scaled distance increases. A 'best fit' straight line via linear regression is determined after taking the logarithm of both axes. This best fit line is in the form Y = Mx + B and its slope and intercept are used in the prediction function

$$\ln(PPV) = M \times \ln(SD) + \ln(A) \quad \textbf{(2-28)}$$

where A = Y intercept giving a prediction formula for the decay of the wave with scaled distance:

$$PPV = A(SD)^{M} \quad \textbf{(2-29)}$$

This best fit line to Eqn. 2-28 provides the coefficients for predicting the mean PPV value. Statistical confidence limits give upper and lower bounds within which 95% of the data fall. The upper bound is generally then used to predict safe distances from a blast. Dowding (1985), again referring back to earlier technical reports, suggests that at short scaled distances M ~ -2.8 while at greater scaled distances M ~ -1.6. Of course, one problem with this is that it is difficult to actually predict what the displacements might be at the beginning of a given project as these will be, to a large degree, site dependent. It is only after some blasts have been made that one is able to begin to generate an appropriate predictive curve.

2.3) Summary

This chapter has shown that the motion of seismic waves through any media is very complicated. The effects of these waves at distances from the source are highly dependant on many variables. Nonetheless, blasters employ empirically derived techniques to predict shaking and to minimise the effects. At Diavik Diamond Mines Inc. a blast monitoring programme is employed to study the effects of blasting on fish habitat.

Chapter 3) *Diavik site overview*

The Diavik Diamond Mine Inc. (DDMI) mine site is located on a 20 km^2 island in Canada's Northwest Territories at 64º 30' N latitude, 110 º 20' W longitude some 300 kilometres north-east of the capital city of Yellowknife (Figure 3-1). Diavik Diamond Mines Inc. (DDMI) is a world class diamond deposit with an estimated 29.8 million tonnes of kimberlite ore averaging 3.9 carats per tonne (Diavik Fact Book, 2005) of high grade diamonds. DDMI began production in January of 2003.

Diamonds are found almost exclusively within kimberlitic *pipes*: remnants of volcanoes of which the magma originates deep within the crustal cratons. While many kimberlite pipes have been discovered world wide, only a small percentage of kimberlites are economically diamondiferous. DDMI has discovered four of these pipes to date at Lac de Gras. Even though this is rich kimberlite ore, many tonnes of material must be extracted to produce even a small amount of diamonds. The kimberlite and the host granitoid rock is sufficiently strong that explosives must be used to break it up so that it may be moved and processed. It is the blasting associated with this comminution of ore and associated country rocks that is of concern because of the potential impact on the environment of Lac de Gras.

The motivation for this study is, of course, to monitor the vibrations in support of a larger project to study the blast effects on fish habitat within Lac de Gras itself. The lake is 60 kilometres long and on average 16 kilometres wide. Average depth is 12 metres with a maximum depth of 56 metres. The shoreline measures 740 kilometres. Water temperature ranges from 0°C to 4°C in winter and 4°C to 18°C in summer (DDMI).

This chapter contains more specific background information on the site of the study including a brief overview of the geology and the mine.

3.1) Geological Setting

Geologically speaking, Lac de Gras and DDMI's mining operations are located in the Archean[1] central *Slave Province* within the *Canadian Shield.* The Slave Craton broadly consists of a variety of metamorphosed granitoids, turbidites, and greenstone belts with ages which have been dated by lead isotope techniques to be approximately 2.6 Ga, a starting point for further investigations of this is Davis et al. (2003). In fact, the world's oldest remaining rock, the 4.03 Ga Acasta gneiss, lies only a few hundred kilometres to the west of Lac de Gras. The lithosphere, or the more rigid plate-like uppermost part of the earth, is believed to be thicker and colder than in younger geological provinces; this colder regime may allow for both the survival of the diamonds as they are transported relatively rapidly from great depths of ~ 200 km or more and bring the diamond stability field closer to the earth's surface. It is interesting to note that the diamonds themselves are old, likely ~ 3.3 Ga, and hence have been 'stored' beneath deep cold lithosphere until they were transported to the surface in igneous eruptions. In contrast, the kimberlite 'ore' material that brought the diamonds to the surface at Lac de Gras erupted recently during the Eocene[2] about 55 Ma.

According to publicly available geologic descriptions of the site provided by DDMI (Bryan and Bonner, 2004), the country bedrock consists of typical 2.6 Ga greywacke-

[1] The Archean Eon covers the earliest development of the earth's crust and atmosphere as 'recorded' in the rock record.
[2] The current boundaries of the Eocene are set at 54.8 Ma to 33.7 Ma.

mudstone metaturbites, tonalite-quartz diorites, and granites through which the kimberlite deposits intruded. These Archean 'basement' rocks are also intruded by a series of Proterozoic[3] diabase dyke families. In short, aside from cross-cutting dykes, all of the country rock is highly metamorphosed and are considered 'hard-rocks' or 'crystalline' rock. Such rocks will be typified by low or vanishing porosities, by P-wave velocities of about 6 km/s, and S-wave velocities of about 3.5 km/s. These velocities should only be taken as rough estimates as the wave speeds will depend on many factors such as density, mineralogy, and texture. Schmitt et al. (2003) provides a recent compilation of the velocities found in such hard rock.

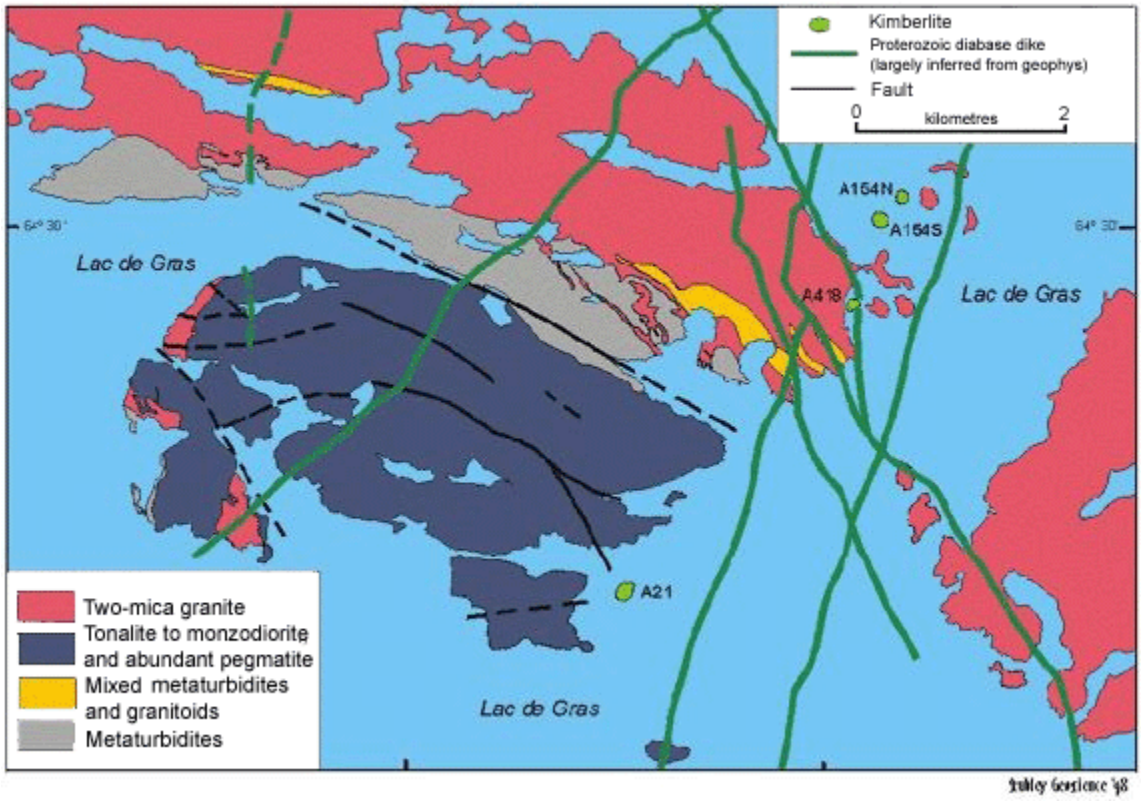

Figure 3-1) Simplified geology at Diavik. The blue background is Lac de Gras, DDMI's four kimberlie pipes (A154N, A154S, A418 and A21) are all situated within the waters of the lake very close to East Island where the operations are situated. (Modified from Stubley Geoscience, 1998)

[3] The Proterozoic eon saw the rise of the first multi-cellular life forms and currently has the boundaries from 2.5 Ga to 543 Ma.

The surface materials at Diavik, however, differ substantially from the crystalline bedrock. These materials are primarily glacial tills[4] left about 8.5 ka by the retreat of the laurentide ice sheet of the last 'Tioga' phase of the Wisconsin glaciation[5]. These materials cover most of the area but they are not that thick. In the portion of the lake that was dewatered for mining purposes the till ranged in thickness from 1 m to 3 m. On the dry surface there is only a discontinuous layer of mixed boulders and clay-rich till material about 30 cm thick. In the author's on-site experience, however, many spots bare metamorphic rock is exposed right to the surface.

As the mining operations are located in close proximity of a lake and its fish habitat, extra care must be taken in order to ensure that exploitation activities have a minimum impact on the fish habitat. As the preferred method of excavation of the diamondiferous kimberlite pipes is explosive blasting creating a chemical reaction which produces a high pressure and high temperature gas (Lucca, F.J. 2003). The high pressure and associated energy not only breaks the targeted rock mass apart but also dissipates into the surrounding rock.

In order to ensure the fish habitat is adequately protected the Department of Fisheries and Oceans (DFO) has provided simplified formulae, as outlined in chapter 2, in order to predict the maximum charge weights and minimum distances that would allow for minimum impact on the fish habitat

As part of its commitment to minimise impact of exploitation activities on the fishes, DDMI did its own calculations for safe standards. These calculations predict a larger

---

[4] Till generally refers to any mixed rock-clay mixture that is directly of glacial origin.
[5] The Winconsin glaciation is the name for the last major advance of the North American continental glaciers. This consisted of three phases of glaciation: the Tahoe (which peaked ~ 70 ka), the Tenaya (less well defined), and the Tioga (which peaked about 20 ka and retreated about 12 ka to 8.5 ka).

blast zone (blast zone is defined as the area within which it is expected to get PPVs greater than the allowable 'safe' value) than that predicted by the DFO formulae. In turn the predicted levels for over pressure in the water column are all substantially lower than the allowed limit which can be shown using several different approaches.

3.2) Study site

To date four diamondiferous kimberlite pipes have been identified in this area. All of these pipes are under the waters of the lake likely because the ultramafic kimberlite rock weathers rapidly under surface conditions and was preferentially eroded out by the glaciations relative to the surrounding metamorphic rock. To access the kimberlites, DDMI undertook an immense, award winning, engineering project to build dikes around the known kimberlite locations. Dewatering of the 154 South and 154 North pit area (Figure 1-1) was completed in 2002. During dewatering, all fish were removed and transferred into the open lake waters.

Mining is initially being conducted as an open pit operation up to a depth of about 400 metres at which point it will be changed to an underground operation. The first monitored excavation blast occurred on August 27 of 2002.

3.3) Geophysical site characterisation

To aid in characterisation of the rock properties at DDMI two types of seismic surveys were conducted; one passively recorded a mining blast in the pit while the second was a standard refraction survey using a hammer as a source.

Figure 3-2) Figure showing the location of the seismic line receiver array and the source.

Both of these surveys were completed using the same geophone layout with the 20 receivers at a 2-m spacing were placed north-east of the pit (Figure 3-2).

3.3.1) Refraction seismic survey

The refraction survey was done using a hammer and plate as a source and the twenty geophones as receivers. Five shot points were used spaced at approximately 5 m. Maximum offset was at 0.5 m. The sampling rate was 4000 samples per second (f_n = 2000Hz*)*; a half second record was collected from 10 stacks. The frequency content is very high (Figure 3-3) which is consistent with the tight spacing and dense rock type.

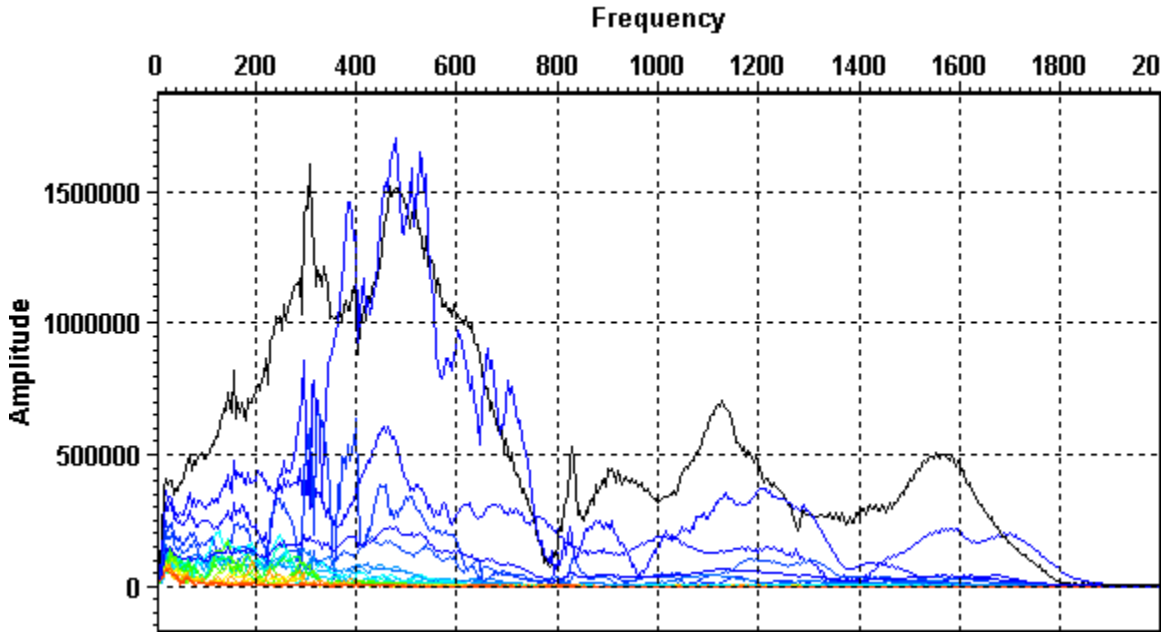

Figure 3-3) Frequency spectrum of refraction seismic record. The record contains, seismically speaking, very high frequencies.

Analysis of the data is difficult. Offset was insufficient to be able to see a refracted wave and the high velocity combined with tight spacing made discrimination of wave types impossible. Only an estimate of the surface wave is made to be in the range of 1000 m/s (Figure 3-4).

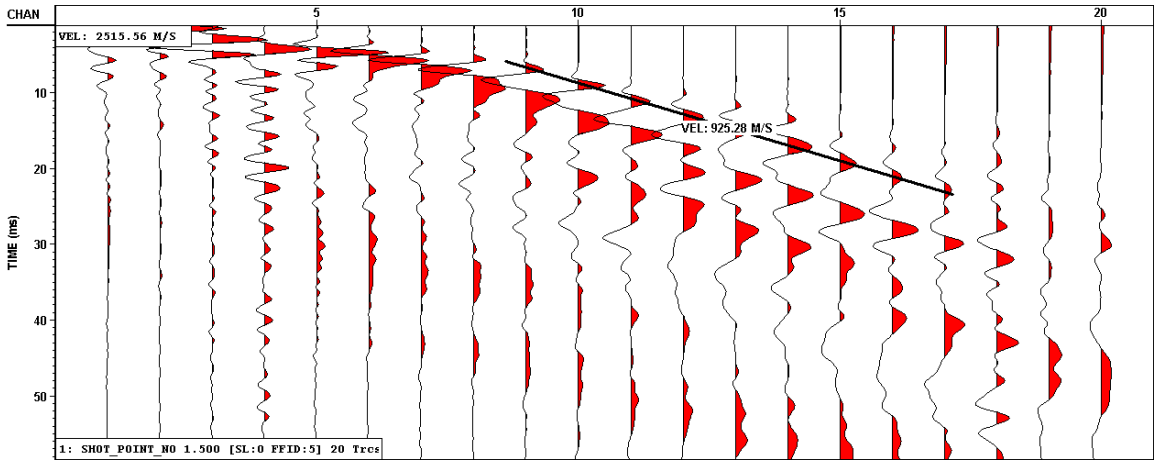

Figure 3-4) A shot from the refraction survey. Surface wave velocity is in the range of 1000 m/s. Data is displayed after ormsby filtering (10, 15, 600, 800) and RMS scaling.

3.3.2) Passive seismic survey

Two blasts were recorded but only one of the blasts was important enough to be recorded in the DDMI data, as such, blast related data such as its location and weight is only known for the February 12, 2004 blast. The seismic record was collected by manually triggering the software to produce a 65 second trace sampled at 250 samples per second. Still, at this sampling rate it was difficult to accurately resolve the first break.

An intermediate sized blast, 660 kg per delay centred about 1000 m from the seismic array, was detonated and recorded by the geophone array. Since the exact timing of the blast is not known we can only study the difference in time as the blast wave reaches each geophone. Using the time difference between arrivals and the distance between the geophone and the centre of the blast pattern we can estimate a rayleigh wave velocity of around 2600 m/s (Figure 3-5). The frequency spectrum is much more in line with standard seismic frequencies (Figure 3-6).

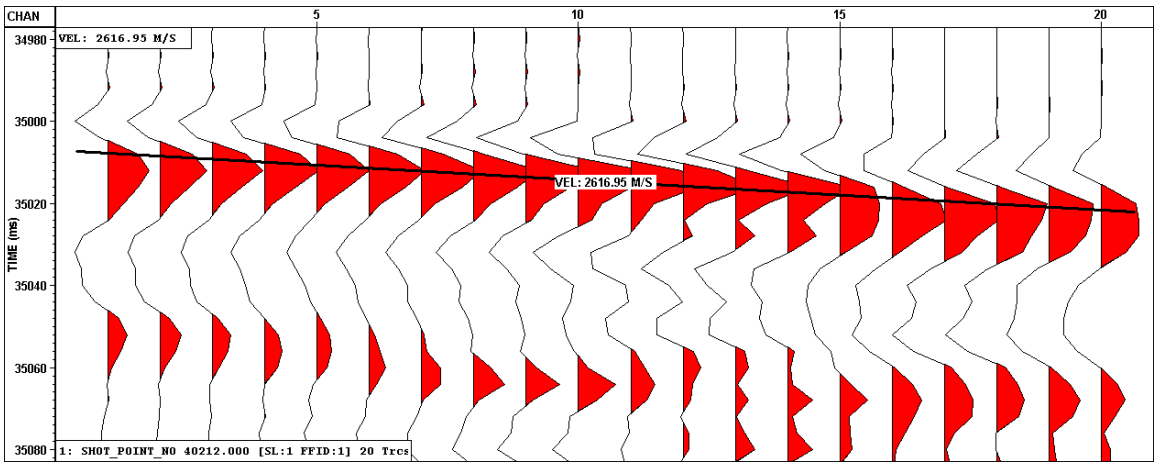

Figure 3-5) The first arrival from the blasting event. A best fit line defines the velocity to be around 2600 m/s.

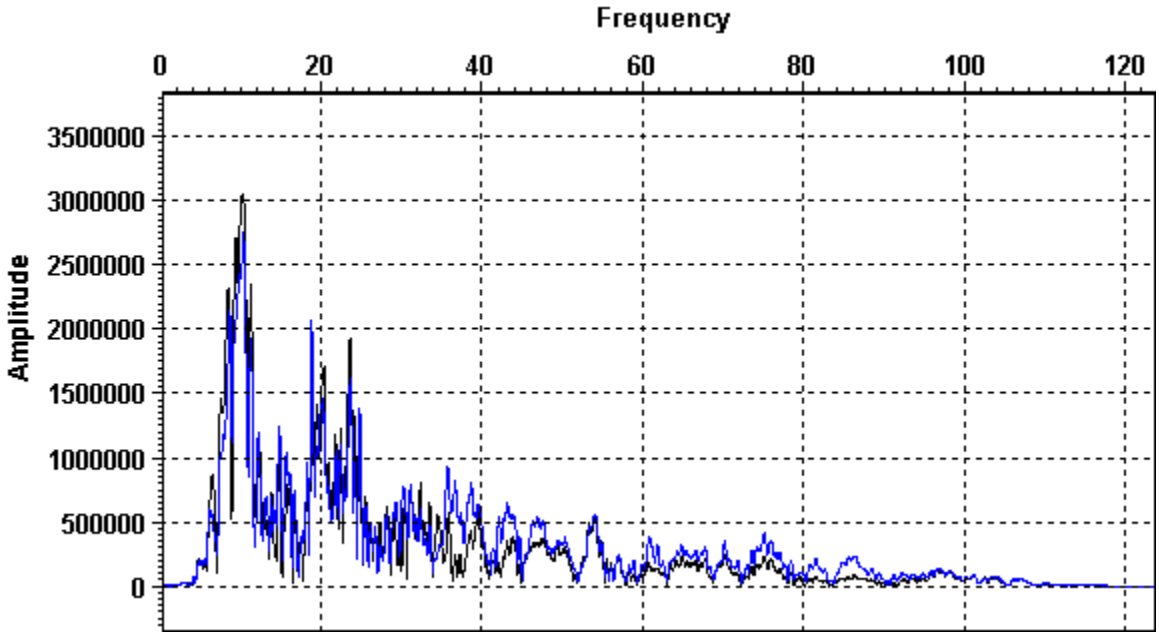

Figure 3-6) Frequency spectrum for the passively recorded blasting event.

3.4) Predicted Blast Zone

DDMI (1998a.) outlines the potential for damage to both aquatic life and the dike structure due to blasting associated with the mining operations. Sample calculations were made to estimate the intensity and strengths of the blast wave at the dike wall and also in the substrate of the lake and into the water column.

According to DFO guidelines (Wright, and Hopky, 1998), a maximum of 13 mm/s peak particle velocity in fish habitat or 100 kPa in the water column is permitted. It is unknown how these criteria were exactly derived and they, particularly for the case of the particle velocity, are believed to be conservative estimates. However, it should be noted that 100 kPa is nearly 1 atmosphere of pressure.

Assuming minimum distances from the outside of the dike and the blast weights that would be used some simple predictions can be made for peak particle velocity in the

substrate and also the transfer of energy into the water column, measured as overpressure. The Department of Fisheries and Oceans also provides simple calculations for prediction of the PPV and over pressure. Furthermore, other calculations can be made to predict the transfer of energy into the water column.

To calculate estimates of the effects of overpressure and PPV outside of the dike walls DDMI made several assumptions (DDMI, 1998a) that included a typical explosive weight per delay of 1140 Kg, a closest distance between a blast and the outer edge of the dike wall of 310m, and the density of the till and dike material are 1.92 g/cm^3 and 2.04 g/m^3, respectively.

3.4.1) Peak Particle Velocity

DDMI calculated that PPVs could exceed 13 mm/s up to 400 m beyond the dike wall and into the lake. The DFO formula gives a less conservative estimate of only 200 metres beyond the dike. Even within the DFO blast zone, however, numerous fish spawning habitats are found.

Using a generalised empirical formula provided by M. Davachi (personal communication) DDMI, 1998a) DDMI predicted a blast zone (Figure 3-7) that would extend into Lac de Gras.

This formula is of the same type that is generated from a scaled distance plot as shown in Equation 2-9.

$$PPV = 1727\left(R/\sqrt{W}\right)^{-1.6} \quad \textbf{(3.1)}$$

Using known blast weight (W) we are able to solve for the distance (R) by setting the PPV at 13 mm/s. The minimum safe distance based on this very conservative formula is 717.04 m.

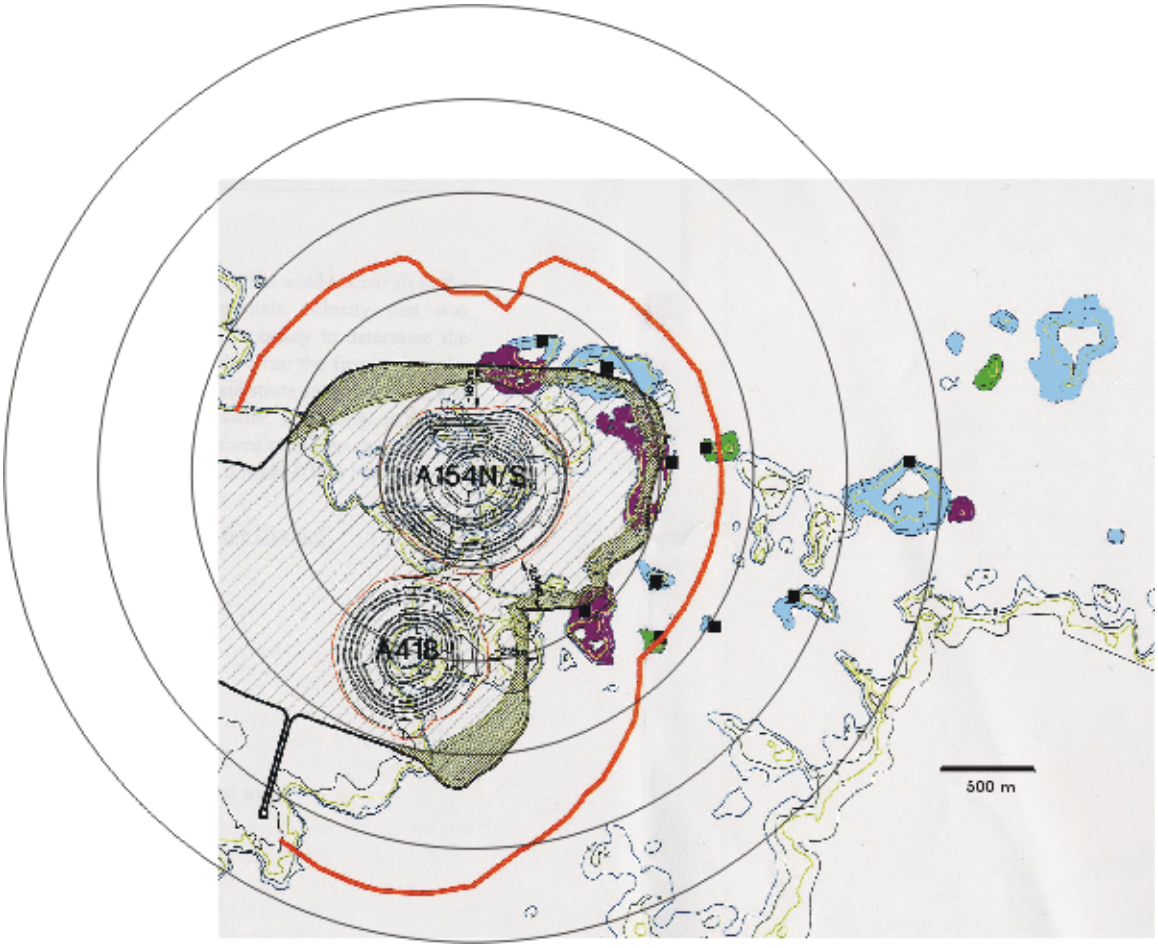

Figure 3-7) Map of area showing proposed fish incubator sites (black squares). Circular contours represent distance from the centre of A154N/S, contours each 500-m and the red line indicates the DDMI predicted zone where PPVs would exceed DFO guideline levels.

Based on a typical charge weight of 1140 Kg the minimum safe distance to keep the PPVs at or under the mandated 13 mm/s, calculated using the simplified DFO formula (equation 2-22), is 509.5 m.

Both formulae predict a zone where PPVs will exceed 13 mm/s will extend beyond the dike wall and into the lake substrate, and therefore, into fish habitat:

DFO; 510 metres from the blast centre or up to 200 metres into the lake.

DDMI; 717 metres from the blast centre or up to 407 metres into the lake.

3.4.2) Over Pressure

The over pressure, or *Instantaneous Pressure Change* in the lake waters due to blasting on land can be calculated based on DFO formulae discussed in chapter 2. Firstly we predict the peak particle velocity (eqn. 3-2). Assuming a minimum distance of 310 m to the outer edge of the dike and an average charge weight of 1140 kg we calculate a maximum particle velocity of 4.97 cm/s at the edge of the substrate. The pressure in the substrate is then calculated by solving for P_r (kPa) from equation 2-6.

$$P_r = PPV * D_r C_r / 2 \quad \textbf{(3.2)}$$

PPV is the predicted Peak Particle Velocity (mm/s) and D_r is the density of the substrate (2.04 kg/m^3) and C_r is the compressional wave velocity in saturated soil (146.3 m/s). Then from equation 2-4 the pressure transferred into the water column is found to be 74.2 kPa.

Using DDMI guideline calculations we can determine the minimum offset needed to limit the pressure transferred into the substrate to 100 kPa. Assuming a charge weight of 1140 kg, a substrate velocity of 5,000 – 6,000 m/s and a water velocity of 1,453 m/s we can calculate the minimum safe distance.

Knowing the densities of the substrate and the water we can use equation 2-4 to calculate that, the amount of pressure that gets transferred from the substrate into the water column is only 14%. A pressure of 714 kPa in the substrate would transfer 100 kPa into the water column. To achieve this pressure a particle velocity of between 116.7 and 142.8 mm/s (depending on the substrate velocity) is needed (from equation 2-6). Based on the PPV we can calculate the distance using equation 2 – 8 to solve for *R*. The minimum safe distance for keeping the induced over pressure transferred into the water

column by an 1140 kg blast is 113.9 m for a substrate velocity of 5,000 m/s to 129.3 m for a substrate velocity of 6,000 m/s.

Another calculation can be made to address the transfer of seismic energy across an interface. Two equations for transfer and reflection of energy (Telford et al 1990) are shown. The transmitted (E_t) and reflection (E_r) of energy for a P-wave normally incident on the interface between the rock and the water, initially propagating in the rock substrate, and transmitting as a P-wave into the water are given by:

$$\frac{E_r}{E_i} = \left(\frac{Z_2 - Z_1}{Z_2 + Z_1} \right)^2 \quad \textbf{(3.3)}$$

$$\frac{E_t}{E_i} = \frac{4 Z_1 Z_2}{(Z_2 + Z_1)^2} \quad \textbf{(3.4)}$$

where the acoustic impedance Z is the product of the material density and compressional wave (P-wave) velocity and E_i is the original energy of the wave. Assuming the same values for density and P-wave velocities as above, we can show that less than 40% of the energy is transferred into the water column. The problem becomes much more complicated if one accounts for variations in the angle of incidence of the seismic wave with respect to the rock-water interface (i.e. the lake bottom). Examination of the results of more detailed calculations (e.g. Stein and Wysession, 2003) show that generally the maximum transmission occurs at normal incidence and hence the above equations provide the maximum values of transmission. Of course, usually the angle of incidence of these body waves will be less as the lake bottom will be at some angle with respect to the incoming wavefront.

As an exercise, it is useful to see some relationships between overpressures in the water and particle motions in the rock. Eqn. 3-4 could also be written in terms of the particle motions with

$$A_t = A_i \frac{2Z_1}{(Z_2 + Z_1)} \tag{3.5}$$

where, A_t and A_i are the transmitted and incident particle displacements. Examination of Eqn, 2.2 will show that the amplitudes can just as easily be given in terms of the particle velocities which are measured. Consider the case with the physical properties for the rock of V_p = 6000 m/s and ρ = 2700 kg/m^3 and with lake water with V_p = 1450 m/s and ρ = 1000 kg/m^3 which yields A_t/A_i = 1.84. For the sake of argument, consider a high amplitude incident P-wave in the rock with Ai = 10 mm/s; this gives At = 18.4 mm/s which equates to an overpressure in the water of $P = Z_2 A_t$ = 26.6 kPa. Note, that this is for a body wave and a value of 10 mm/s for the P-wave propagation is a very strong pulse. As noted earlier, however, the main particle motion of the passing wave is due to propagation of the Rayleigh waves which provide substantially lower coupling of wave particle motion to pressure in the water. Consequently, this rather simple analysis suggests that the overpressures in the water produced by blasting in the hard rock will be minimal. One should not, however, use these simple estimates to determine overpressures in the water for a water borne explosion, which is a completely different problem.

3.5) Summary

Using three different approaches we can show the transfer of energy into the water column is minimal and that the DFO mandated guideline of 100 kPa is not attainable

based on typical explosive sizes and distances from the lake. On the other hand several different approaches show that PPVs in excess of 13 mm/s may potentially reach well beyond the dike and into the lake substrate. DDMI suggests that harmful PPVs can extend up to 407 metres into the lake while DFO calculations suggests up to 200 metres into the lake. As such, DDMI teamed up with the University of Alberta departments of Biological Sciences and the Institute for Geophysical Research to monitor blasting and study the blast effects on fish habitat within Lac de Gras

Analysis of the seismic data gives some insight to the seismic properties of the host rock. The passive data suggests a Rayleigh wave velocity of about 2600 m/s and the refraction survey indicates a surface wave velocity of about 1000 m/s.

Chapter 4) *Methodology; Field component*

The objectives of the overall field study are to 1) determine if blasting causes increased mortality among incubating lake trout eggs and 2) to determine if blasting effects on fish habitat at Lac de Gras change as the pit deepens. The work in this thesis focuses primarily on the technical aspects of recording and predicting the blast levels to complement the parallel work of (Faulkner, 2006). In this chapter, I outline the development of a specialised system that allowed the simultaneous measurement of both particle velocities and overpressures at the same point in the lake. This development relied on some recent innovations with sea floor detectors developed for time lapse seismic monitoring on the ocean bottom.

To quantify the effects due to blasting, Blast Mate® recorders produced by Instantel, of Ottawa Ontario, are used to record the movement in the ground and also the pressure changes in the air. Conventionally, each unit is connected to a 3 component geophone and a microphone. DDMI generally deploys 4 of these units on or within the dike. Using a special 4 component sea type sensor that replaces the microphone with a hydrophone to measure water pressure, the U of A team was able to monitor the same blasts as they are felt within the lake substrate. Three sites within the predicted blast zone and one well outside were chosen for blast monitoring.

During the first component of the field study, incubators holding fish eggs were placed alongside of the sensors. Mortality in the fish eggs was counted and compared to monitored and predicted PPVs.

The second component of the field study encompasses all blast monitoring data collected at DDMI for analysis to determine the changes in blasting effects as the pit deepens.

4.1) Site Selection

Four sites were selected for sensor placement (Figure 4-1), based on the quality of the lake bed for fish habitat and the distance from the pit. Informally they are known for their location and recorder serial number as South Dike (8902), Reference Island (8903), Tern Island (8904) and East Dike (8905).

Lake trout move onto rocky shallows inshore or on shoals in mid-August prior to spawning. Spawning habitat suitability is generally based on depth (2.5-7 m but next to deeper water), substrate size (4-30 cm, but up to 1 m) and shape (angular), interstitial space (20 cm – 1 m deep), and being located away from depositional effects (Scott and Crossman 1973, Gunn 1995, Marsden et al. 1995a, DDMI 1997b). These eggs then incubate over winter and hatch 8-10 months later (May to July in Lac de Gras). It is over this long incubation period they are exposed to the ambient environmental conditions, and to disturbances such as blasting.

The first three sites are all situated near the dike and within the DDMI predicted blast zone while the Reference Island site is selected to provide baseline measurements (Figure 4-1.). The reference site is chosen for its distance from the blasting operations where 3 km is considered to be far enough away that shaking and PPV values are negligible. The East and South dike sites were selected at strategic locations along the dike to allow for ease of access. A fourth site at Reference Island, about 1 km offset, was selected to

provide a baseline measurement where it is believed that blasting will have none, or negligible, effects.

Figure 4-1) Locations of the 4 sensors in relation to the dike, proposed pit and predicted Blast Zone (Red Line). Distance between scale marks is 1000 m of the UTM grid. DDMI sensors are deployed at various locations along the dike. Note that the Blast Zone takes into account the location of the next pit south and east of the original.

The East Dike and South Dike locations are easily accessible directly on the dike while the 2 other sensors are accessible only by boat during the summer and by snowmobile when the lake is frozen. During winter freeze-up and spring thaw or during extreme weather conditions these two sensors cannot be safely reached. As such, the data set from the latter sensors are not as complete as that of the other two.

4.2) Sensor Placement

Sensors were placed in the four selected sites on September 9th of 2003. All of the sensors were placed at a depth of 3 to 5 metres together with the fish incubators. This depth was chosen in order to avoid as much as possible the lake ice during winter. Detailed descriptions of these incubators may be found in Faulkner et al. (2006) but, briefly, these consisted of 50 cylindrical 'cells' produced by drilling holes through a 12.5 cm x 25 cm x 1 cm Plexiglas sheet.

Eggs were placed into each of the cells and then sealed using a fine mesh that was intended to keep the developing embryos safe from predation and escape. Twenty incubators were placed at each site. Ten incubators were collected from each site after 20 days, related to the anticipated fish development.

Divers secured the chains, the incubators and the sensors to the boulder strewn lake bottom. The sensors were attached to a chain along with the incubators and also wedged under rocks to ensure coupling with the substrate (Figure 4-2). The sensors were then connected to the on-land recording devices by a 100 m. cable allowing for access from dry land. On land, the recording units were protected by a standard insulated cooler and kept warm using rice filled bags that were heated prior to deployment.

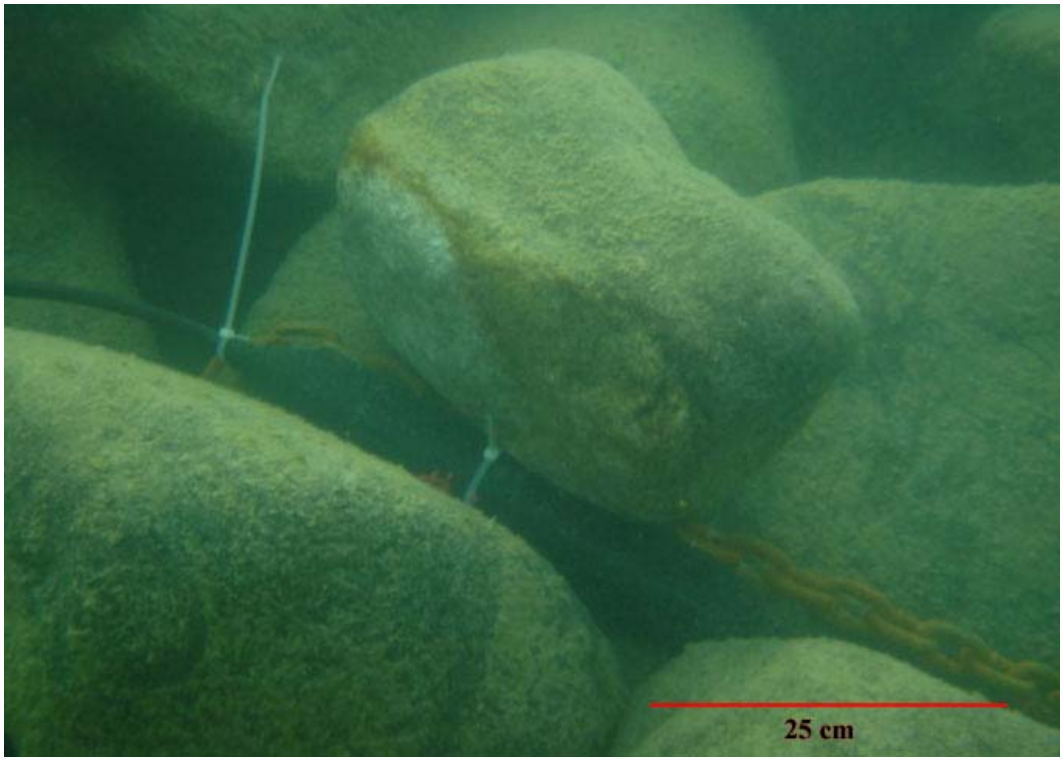

Figure 4-2) Placement of the 4-C sensor. The sensor is attached to the chain and also placed under rocks to ensure coupling.

4.3) Equipment

An *OYO Sea Array 4*™ 4-component underwater geophone was used to measure the ground vibrations and over pressure, attached to an *Instantel Minimate Plus*™ recording unit. Data processing was done using the *BlastWare Series III* Software (Release 4.37) and other standard software packages.

The 4-components on this specialised underwater package consist of 3 orthogonal 10 Hz. geophones that provide the PPV measurement of the motion of the solid substrate and a single 10 Hz hydrophone that provides a measure of the pressure within the overlying water column (Figure 4-3). This package is only recently commercially available as such detectors are now used on a routine basis for deep water studies in the North Sea where the combination of the 4 different components adds greatly to data

quality. The 3 orthogonally oriented geophones are mounted on gimbals that ensure that two are always horizontal and the third is vertical. Availability of this unit greatly simplified the present field tests. The detectors were matched and calibrated with the recording units by personnel at Instantel prior to field deployment.

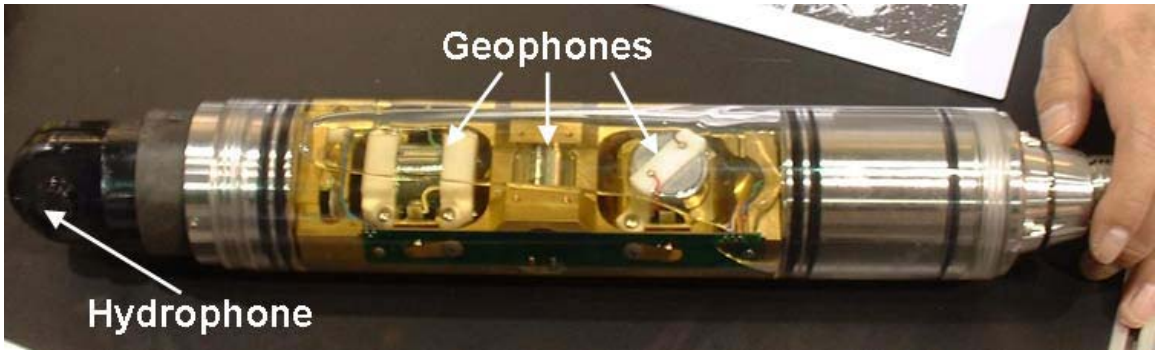

Figure 4-3) A cutaway view of the OYO 4 Component sensor. The gimballed geophones can be seen and the hydrophone is situated at the left end of the sensor.

The Minimate sensors acquired for this project had an expanded memory capacity allowing for 1200, 1 second records at a sampling rate of 1024 samples per second. Sampling rates available to us were 1024, 2048 and 4096 samples per second. The units continuously record leaving a .25 second buffer in the memory. When a preset trigger level is achieved, the unit will record for a desired amount of time plus up to .25 second pre-trigger waveform.

4.4) Data Collection

Prior to each blast, whenever outside conditions and safety considerations allowed, DDMI personnel would connect the blast mates to the sensors to record both the PPV and the overpressure due to the blast wave. Travel to two of the four study sites was hampered by extreme weather conditions, freeze up, and spring thaw, resulting in

incomplete data collection for these sites. During the period of September 9, 2003 and July 27, 2004, 97 blasts were conducted but of the possible 388 records only 194 were recorded. The remaining events were not recorded due to 1) extreme weather conditions when travel to sites was not possible, 2) the recording unit was not properly connected or 3) the blast was not large enough to trigger (i.e. commence recording) by the recording units.

Three of the sensors are set to trigger on either of the geophone channels at 1.5 mm/s while the Reference Island site sensor (see Figure 4-1.) is set at the minimum threshold of .51 mm/s. Often the units were left out for longer periods up to 2 days and recorded many non blast related events due to the low trigger level. The units continuously record and hence are able to store a 'buffer' of pre-trigger time data for up to .25 seconds. The memory on the units allows for a continuous record for only 1 to 13 seconds. Technical specifications are provided in Appendix 1. All units were set to pre-trigger by 0.2 seconds and to record for 10 seconds. Generally, the blast induced vibration lasted less than 5 seconds. The extended memory capacity of the unit allowed for recording of up to 30 of these 10 second events. The highest possible sampling rate of 4096 samples per second was chosen; this corresponds to a Nyquist (i.e. peak resolvable frequency) of about 2 kHz which was well above the frequency content of the blast signals as shown in Chapter 3.

After blasting the recording units were collected and the data were downloaded to a PC and sent to the U of A for analysis. The data were routinely scrutinized by University of Alberta personnel to determine if recorded events can be attributed to the actual blasting (Fig. 4-4) or due to mistriggers from non-blast related events (Figure 4-5) or electrical noise (Figure 4-6). The desired blast related events display a very distinctive

waveform from other non-events. A further difference was that the non-blast events would rarely trigger all of the instruments. A time correlation between blast and record time removed any final doubt as to the source of the signal. Each record includes Peak Particle Velocity for each channel (geophone and hydrophone) and its corresponding frequency, the time of the peak in relation to the trigger, the peak acceleration and the peak displacement. A plot of all of the waveforms for the 10 second recording period is presented along with a plot of Velocity vs. Frequency. Also the largest peak vector sum is calculated over the entire event. A typical blast record produced by the Instantel software is presented in Fig. 4-4, however all the original digital data were obtained to allow for additional analyses.

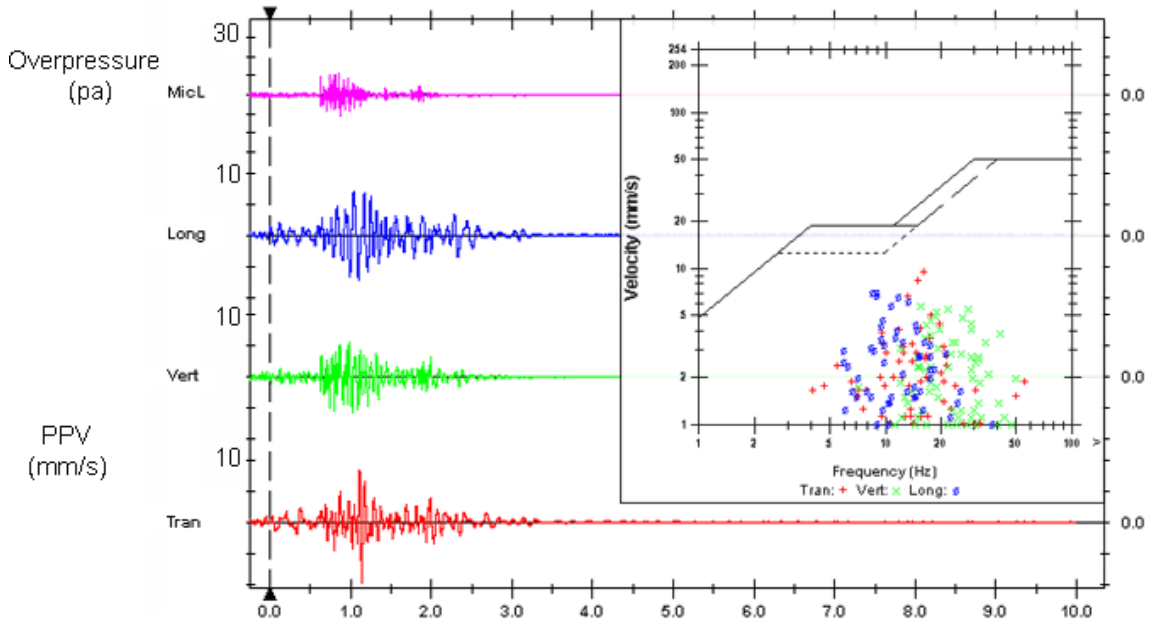

Figure 4-4) Typical waveform due to a blast as presented using the *Instantel Blast Ware*^{TM} software. The channels are overpressure (top), and the 3 geophone channels, longitudinal, vertical and transverse. The vertical scale is 10 mm/s for the PPV and 10 pa for the overpressure per division. **Inset)** Frequency spectrum for each of the geophone channels; Y-axis Particle Velocity (mm/s) and, X-axis Frequency in Hz. Both Axes are log scale.

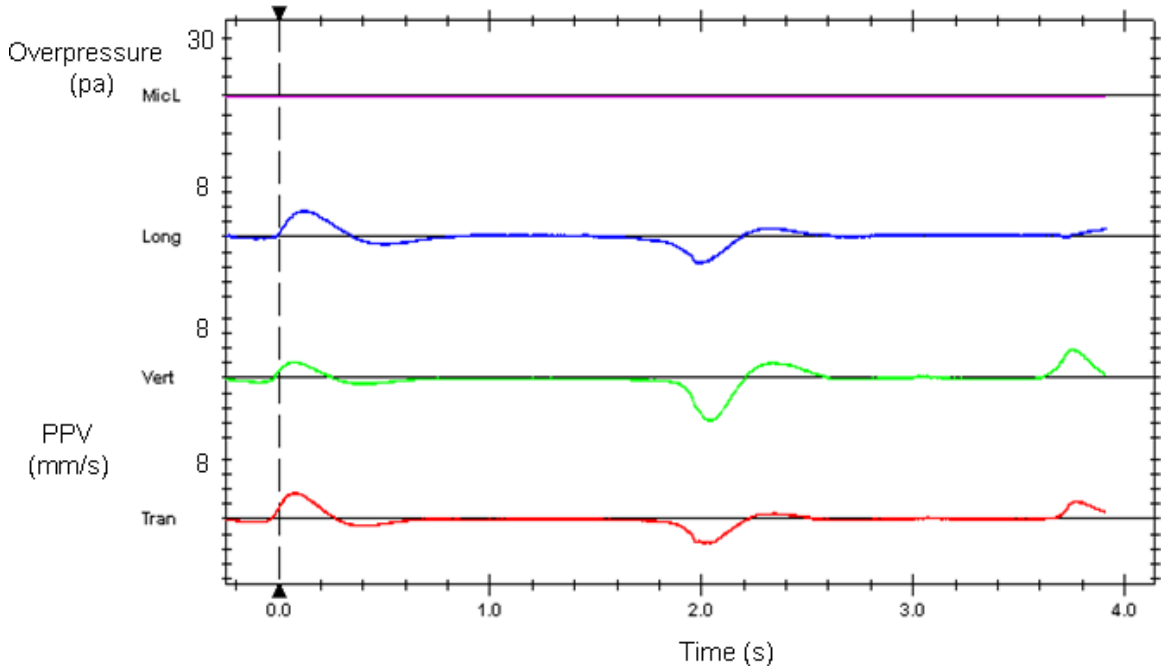

Figure 4-5) Blast record for a non blasting related event. As above, the channels are overpressure (top), and the 3 geophone channels, longitudinal, vertical and transverse. The vertical scale is 2 mm/s for the PPV and 10 pa for the overpressure per division.

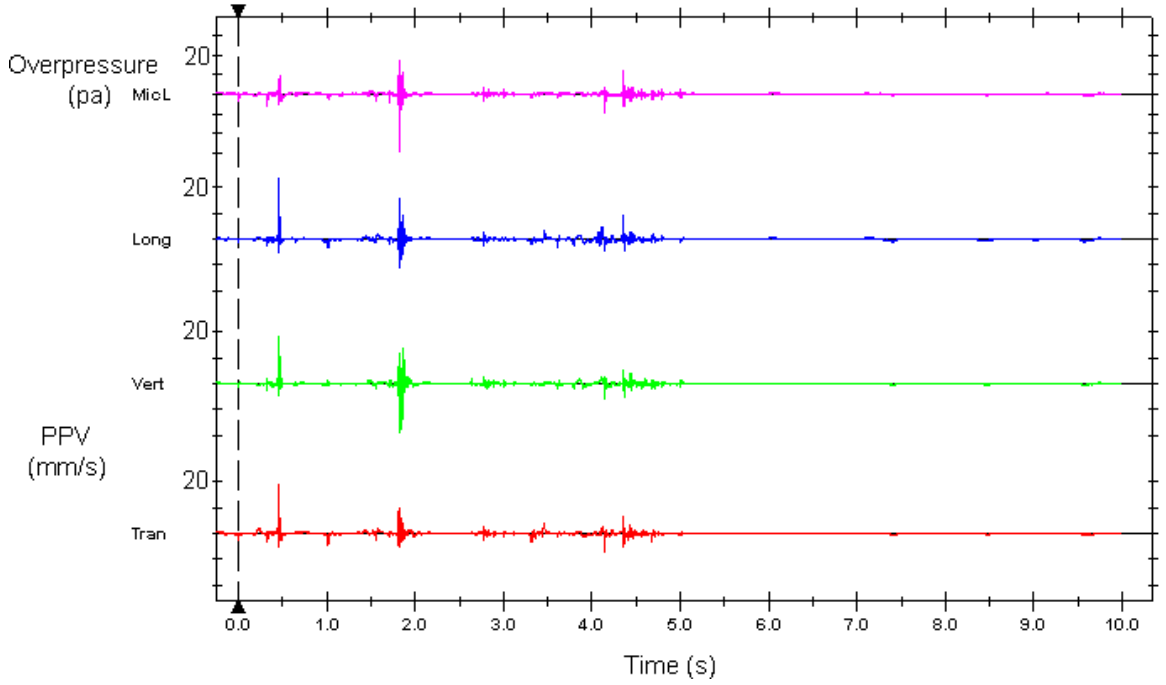

Figure 4-6) A typical waveform due to electrical noise. As above, the channels are overpressure (top), and the 3 geophone channels, longitudinal, vertical and transverse. The vertical scale is 10 mm/s for the PPV and 10 pa for the overpressure per division.

4.5) Data Processing and analysis

To allow for analysis of the data, collected as the Amplitude of the Particle Velocity over Time, the corresponding blast data (i.e. blast weight per delay and location) is needed. Knowing the scaled distance and the PPV standard blast monitoring techniques are used to predict safe blasting levels. Scaled distances were calculated for all available U of A data. Logarithmic plots were created for each site using the PPV in mm/s as provided directly by the *Instantel Blast Ware*^{TM} software and as checked independently by our own calculations.

The data can be further analysed as in the second part of the study by comparing changes in the components of the PPV prediction function.

Chapter 5) *Field Component Results*

The objective of the field study was to determine what, if any, were the effects on the incubating fish eggs and to relate these effects to mortality among the eggs. To achieve this, Faulkner et al. (2006) assessed the mortality in fish eggs to relate it to the vibration exposure at each site. The blast data was then analysed to produce a PPV prediction function for each site and to redefine the blast zone.

The second objective of the field component was to monitor changes in blasting effects as the pit deepens and to assess if geophysical and biological effects of blasting attenuate over time as the pit deepens.

5.1) Analysis

During the period of September 9, 2003 through July 27 2004, 107 blasts were (Data is presented in Appendix 4) conducted; of the total 428 possible recordings (107 for each of the four sites) only 184 were recorded. Of these 184 events 8 were found to have exceeded the Department of Fisheries and Oceans (DFO) guideline of 13 mm/s Peak Particle Velocity (PPV) at three of the four study sites. The largest recorded event was 28.5 mm/s. The prediction function suggests that up to 72 blasts during this time may have exceeded guidelines and reached up to a maximum PPV of 28.8 mm/s.

To complete their study, Faulkner et al. (2006) required a PPV value for each blast at each incubator in order that appropriate vibration and overpressure exposure levels could be determined. As there were gaps in the data set, shaking levels for each blast that was not recorded were predicted using one of two empirical prediction functions. One method involved utilising the prediction function derived by DDMI using their earlier collected

data and prediction function. The second involved analysis and creation of our own empirical prediction function from the observations covering the period while incubators were in the lake.

Transmission of the blast energy into the water column from the rock substrate was not consistently measured, however, it is considered to be of little effect, see Chapter 3, and in fact the largest measured pressure was only 11 Pa, a value that was barely detectable, and as such only results from ground vibration are discussed in the remainder of the thesis as overpressure does not appear to be of concern.

5.2) DDMI Prediction Function

The DDMI blast monitoring program has developed a scaled distance plot from their collected data at the site. These data likely were collected early in the blasting programme as they do not fit analysis done by us.

$$PPV = 700 \times SD^{-1.6} (mm/s) \quad \textbf{(5-1)}$$

The upper and lower bounds are defined as 2 x and 0.5 x the PPV. It is interesting to note that the maximum predicted PPV scalar multiplier is 1400 (i.e. max PPV = 1400x$SD^{-1.6}$) while the initial prediction (Chapter 3.) used a value of 1700.

For our own analysis of the data collected by DDMI from August 27, 2002 to January 17, 2004, we find, through regression analysis, the following function:

$$PPV = 510 \times SD^{-1.5} (mm/s) \quad \textbf{(5-2)}$$

Using the same methodology as that at DDMI and Ekati, the lower and upper bounds are 2 x and 0.5 x the PPV.

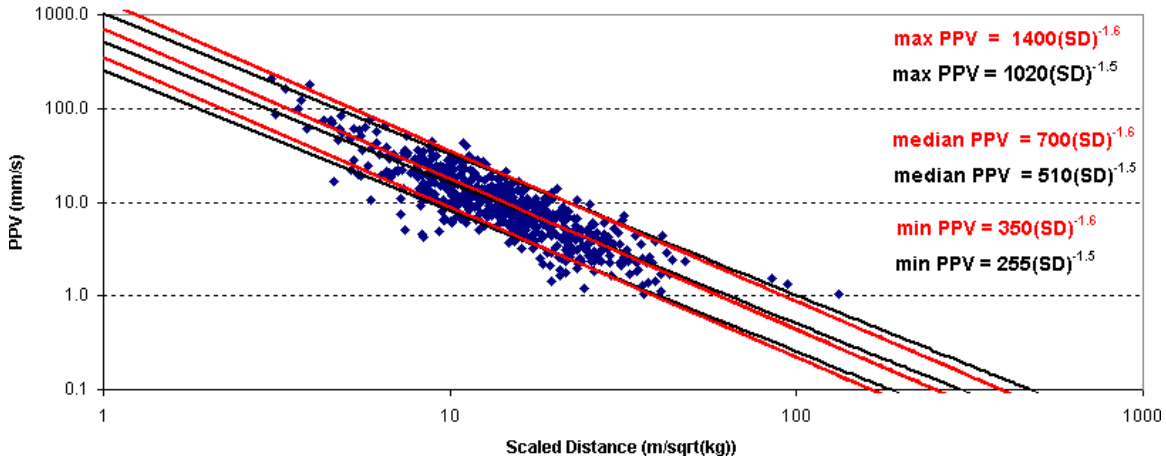

Figure 5-1) The DDMI prediction function (Equation 5-2) presented in red lines with the data collected by DDMI from August 27, 2002 to January 17, 2004. The black lines represent the prediction function derived from the plotted data (Equation 5-2).

The DDMI prediction function (Figure 5-1) has a good fit with the data but it can be seen that many more events fall below the lower bound than fall above the upper bound.

To best use these functions to predict PPVs, it is important to place sensors within the area in question. The DDMI sensors are typically placed in 3 different types of locations; the dike crest, the toe berm and also within the dike which are expected to have a different elastic behaviour from the original solid rock substrate.

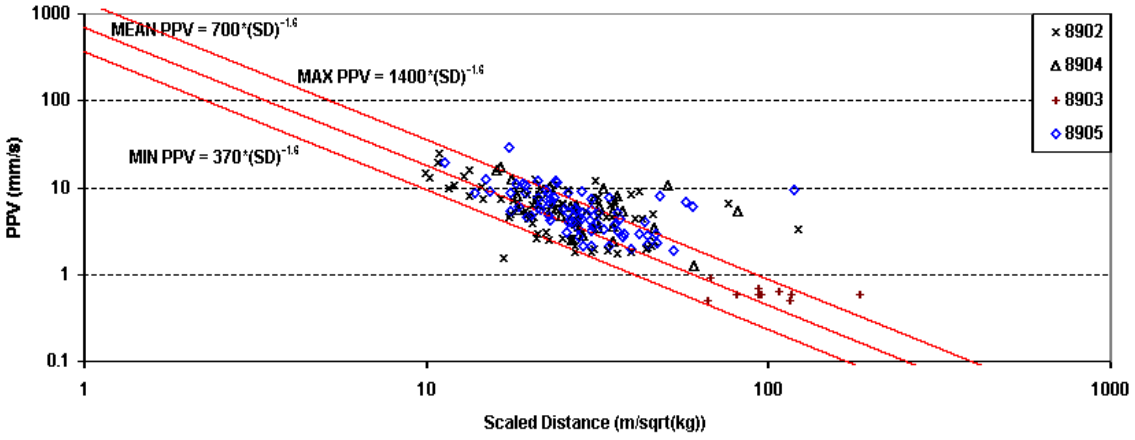

Figure 5-2) Scaled Distance plot of the four U of A sensors compared to the DDMI data. The red lines represent the minimum, median and maximum PPV for a given scaled distance from the DDMI prediction function. 8902, 8903, 8904 & 8905 are South Dike, Reference Island, Tern Island and East Dike respectively.

The U of A sensors, are instead, placed within the waters of Lac de Gras on lake substrate and a better PPV prediction function can be had from data collected there. Data plotted from our four sensors and compared to the DDMI prediction function (Figure 5-2) show poor correlation; they are not well contained within the bounds and display a different slope.

Consequently a linear regression analysis was done on our data and the best fit line and confidence limits were found for each of the four sensors' data sets and then the PPV was predicted for each blast at each location. Finally a blast zone where the PPV may exceed 13 mm/s was derived using data from the 3 sites situated near the dike.

Each of the sensors is presented separately with data from the three sensors combined to derive an updated blast zone. As a result a more useful predictive function can be established enabling Faulkner et al to have a range of PPV values that can be used for their analysis.

5.3) South Dike (8902)

The South Dike sensor was located just outside of the dike wall (Figure 4-1). The distance from the sensor to the minimum, mean and maximum distance to the blast locations is 335 m, 744 m and 1059 m respectively. Of the 78 events recorded at the South Dike location, 4 exceeded 13 mm/s. Using the prediction function (5-3) no events are predicted to exceed the guideline while using the upper bound, up to 28 events could exceed 13 mm/s.

$$PPV = (SD^{-0.732}) \times 53 \text{ (mm/s)} \quad \textbf{(5-3)}$$

5.4) Reference Island (8903)

The Reference Island sensor was located well outside of the dike wall (Figure 4-1) at an average distance of 3014 m. from blast location. Minimum and maximum distances are 2570 m and 3350 m respectively. Of the 10 events recorded at the Reference Island location, none exceeded the guidelines and in fact, most events did not even trigger the recording unit. Using the prediction function (5-4), no events can exceed the guidelines.

Based on the regression analysis we can predict the PPVs experienced for all blasts.

$$PPV = (SD^{-0.732}) \times 1.3 \text{ (mm/s)} \quad \textbf{(5-4)}$$

5.5) Tern Island (8904)

The Tern Island sensor was located on an island situated about 100 m away from the dike wall (Figure 4-1) at an average distance of 940 m from blast location. Minimum and maximum distances are 540 m and 1240 m respectively. Of the 31 events recorded at the tern Island site, 2 exceeded 13 mm/s. Of the total 107 events it is predicted that none exceed guidelines (5-5) using the best fit line while up to 24 events could exceed 13 mm/s using the upper bound to predict the PPVs.

$$PPV = (SD^{-0.81}) \times 88 \text{ (mm/s)} \quad \textbf{(5-5)}$$

5.6) East Dike (8905)

The East Dike sensor was located just outside of the dike wall (Figure 4-1) at an average distance of 875 m from blast location. Minimum and maximum distances are 425 m and 1185 m respectively. Of the 75 events recorded at the East Dike location, 2 exceeded 13 mm/s including the highest recorded value of 28.5. Of the total 107 events it

is estimated that none exceeded guidelines using the best fit line while up to 20 events could exceed 13 mm/s using the upper bound to predict the PPVs.

Based on the regression analysis we can predict the PPVs experienced for all blasts.

$$PPV = (SD^{-0.75}) \times 65 \ (mm/s) \qquad \textbf{(5-6)}$$

The data is presented here graphically, firstly we have the four regression functions and then we show the plot of predicted PPVs for each site.

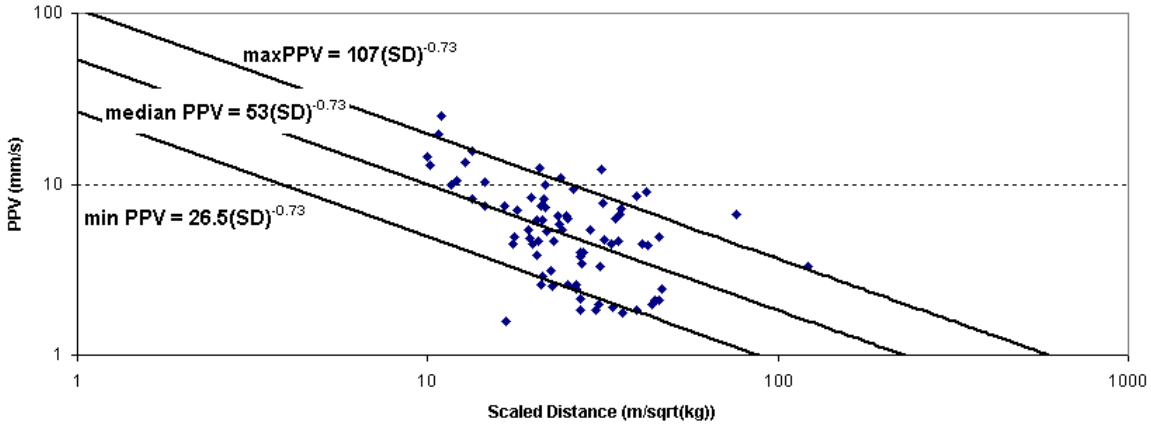

Figure 5-3) Logarithmic plot of the measured particle velocity and scaled distance for the **South Dike** location. The lines indicate the minimum, median and maximum PPVs to be expected at the site (r-square .26).

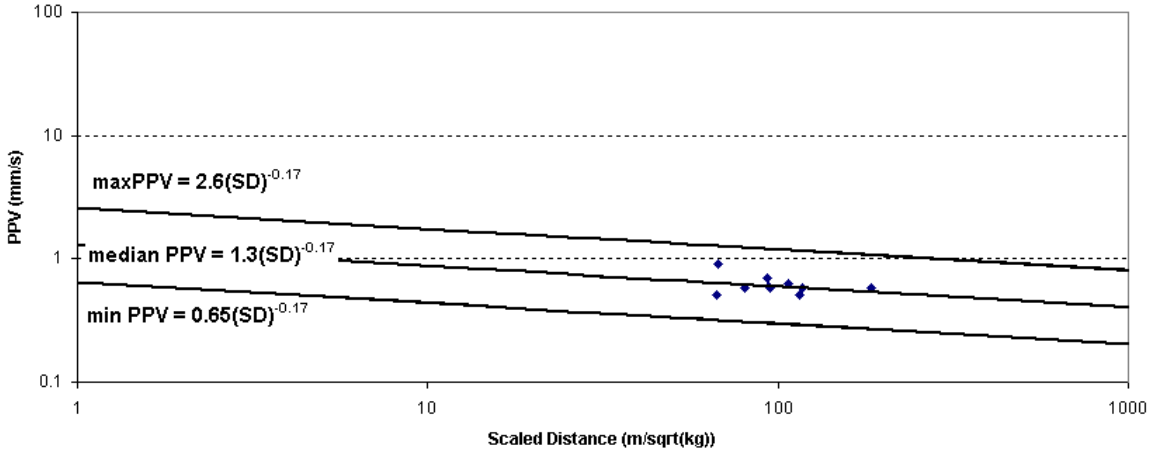

Figure 5-4) Logarithmic plot of the measured particle velocity and scaled distance for the **Reference Island** location. The lines indicate the minimum, median and maximum PPVs to be expected at the site(r-square .09).

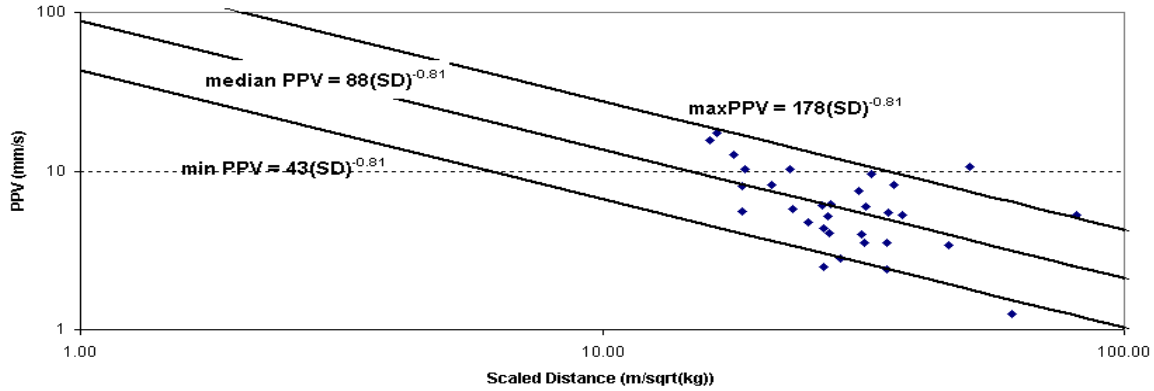

Figure 5-5) Logarithmic plot of the measured particle velocity and scaled distance for the **Tern Island** location. The lines indicate the minimum, median and maximum PPVs to be expected at the site(r-square .27).

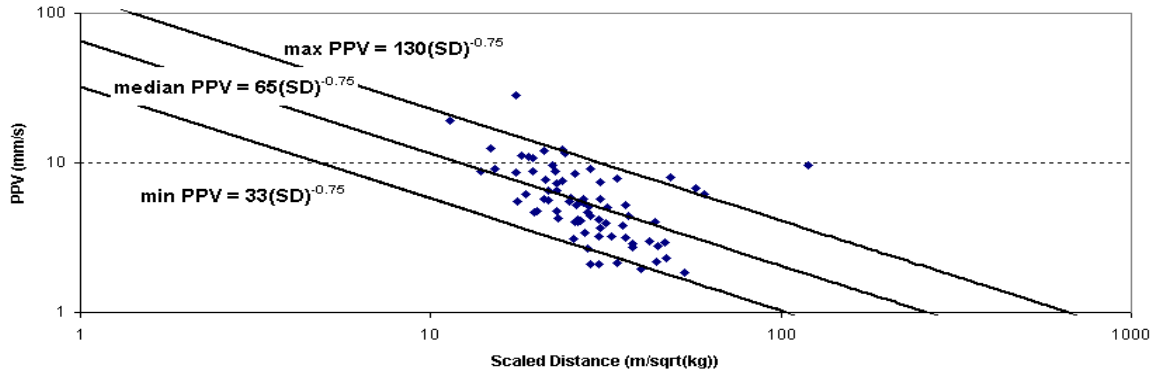

Figure 5-6) Logarithmic plot of the measured particle velocity and scaled distance for the **East Dike** location. The lines indicate the minimum, median and maximum PPVs to be expected at the site(r-square .26).

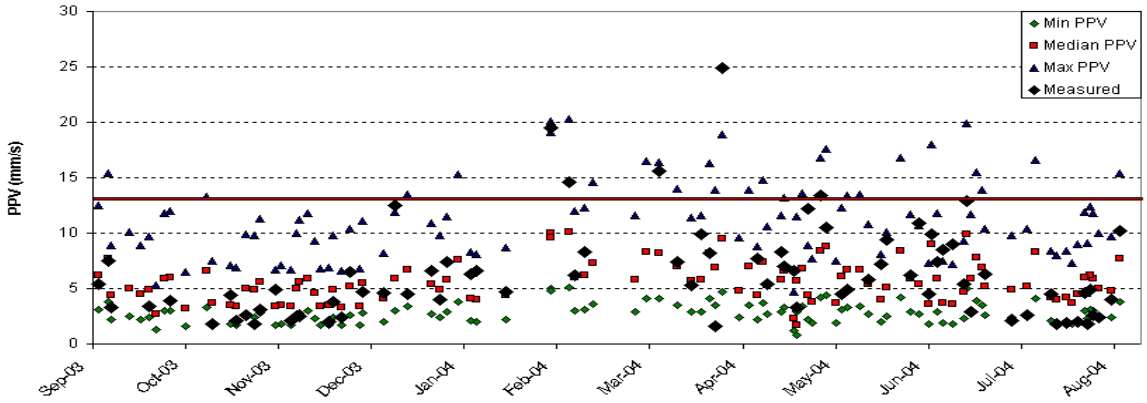

Figure 5-7) Minimum, maximum and median predicted PPVs plotted along with actual recorded values for **South Dike**. The line indicates the DFO guideline value of 13 mm/s.

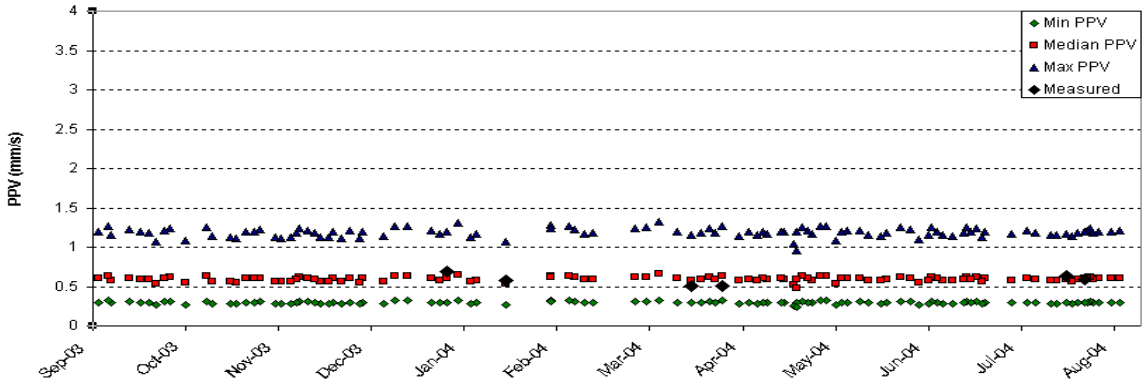

Figure 5-8) Minimum, maximum and median predicted PPVs plotted along with actual recorded values for Reference Island. Note that the vertical scale is much smaller in this case.

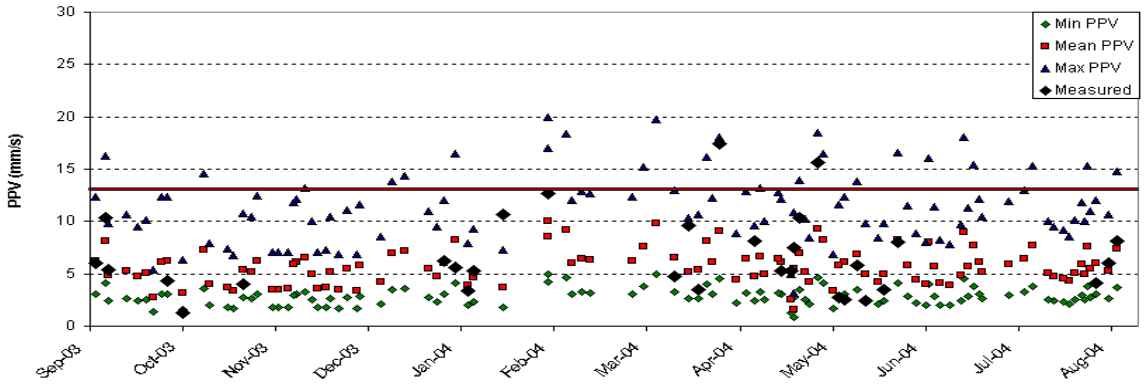

Figure 5-9) Minimum, maximum and median predicted PPVs plotted along with actual recorded values for **Tern Island**. The line indicates the DFO guideline value of 13 mm/s.

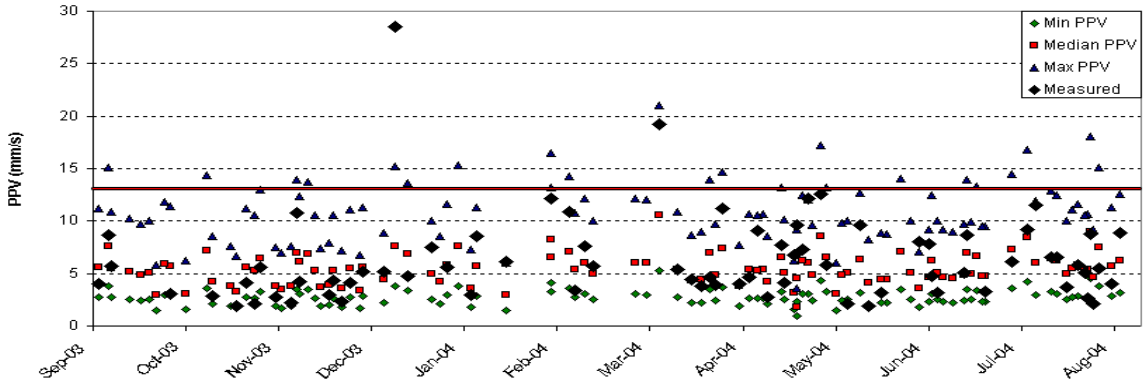

Figure 5-10) Minimum, maximum and median predicted PPVs plotted along with actual recorded values for **East Dike**. The line indicates the DFO guideline value of 13 mm/s.

5.7) Blast Zone

DDMI defined their blast zone and suggested that it could reach as much as 407 m beyond the dike wall while the DFO calculations suggest that it could reach as far as 200 m. Using the DDMI data and the charge weight of 1140 kg, using our regression methodology (Eq. 5-2) minimum safe distance would be 619 m from the blast (309 m into the lake). The best measure, however, of blasting effects in the substrate is to analyse data that were collected there. We can combine the data from the 3 sensors that were situated near the dike wall. The East dike, south dike and tern island data sets are exposed to similar PPV readings and are situated at similar distances from the blasting area..

Based on the regression analysis (Figure 5-11), of the 3 data sets, we can predict the PPVs for all blasts.

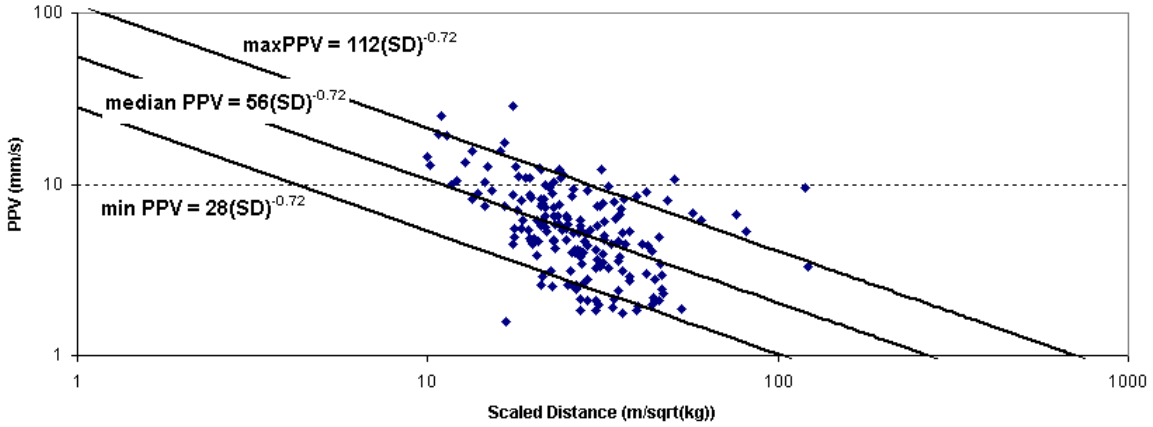

Figure 5-11) Logarithmic plot of the measured particle velocity and scaled distance for the East Dike, South Dike and Reference Island combined. The lines indicate the minimum, median and maximum PPVs to be expected (r-square .24).

.

$$PPV = (SD^{-0.72}) \times 56 \text{ (mm/s)} \quad \textbf{(5-7)}$$

Once again, assuming a blast weight of 1140 kg, the minimum safe distance would be 672 m meaning that 13 mm/s could be exceeded up to 362 m into the lake.

Blast weights used at DDMI, however, range from 71 kg to 3000 kg with mean and median values at 1012 kg and 985 kg respectively. Assuming maximum predicted PPV and 3000 kg weight, 13 mm/s can be attained in the ground for as far 1090 m (780 m beyond the dike wall).

Distances are calculated for a range of charge weights (Figure 5-12) from equation 5-7 to predict both the median and maximum distances before PPVs drop to the DFO guideline of 13 mm/s.

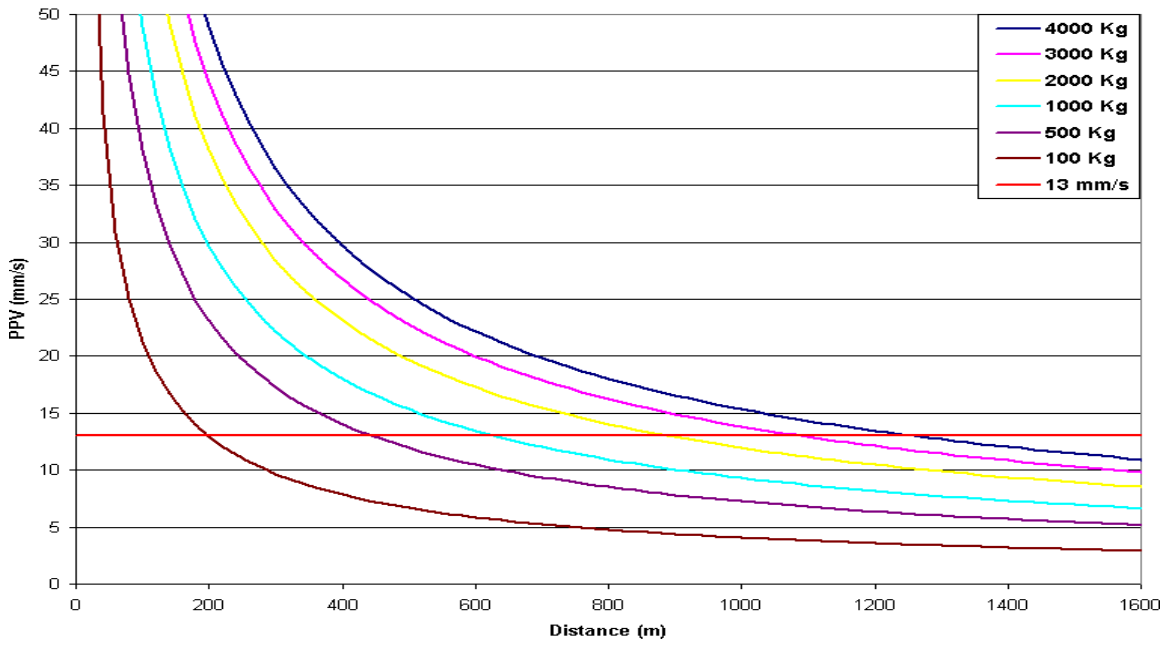

Figure 5-12) PPV predictions for different charge weights and distances based on data from the 3 near dike sites. The dashed line represents 13 mm/s. The Predicted values are based on the upper bound of the function.

We are able to predict PPVs for events that were not recorded to complete the data needed for the study by Faulkner et al. This is done from data collected by the U of A team. This data set is then used to redefine the blast zone where PPVs may exceed 13 mm/s based on charge weights used in the mining operations.

5.8) Changes in effects as the pit deepens

From the beginning of the mining operation until June 2005 the open pit has deepened by 90 metres. Analysis of the blast data collected by DDMI and of our own data is done to assess if geophysical and biological effects of blasting attenuate over time as the pit deepens.

Two methods were employed to track changes: a) a normalised PPV is calculated by normalising the Scaled Distance to see trends in the measured PPV over time, and, b).

Scaled Distance plots are calculated for 2 month intervals to see the changes in the prediction function variables A and M.

Since the 27th of August, 2002 when production and blasting began at DDMI 1243 blasts were recorded through June 29, 2005. 1116 of these blasts have grid co-ordinates and, hence, elevations. The elevations (Figure 5-13) range between 328 and 420 metres. The elevations of the blasts tend to decrease as the pit deepens, but as is seen, some blasting is still being done at higher benches. The figure also shows the tendency to blast on benches at every 10 metres.

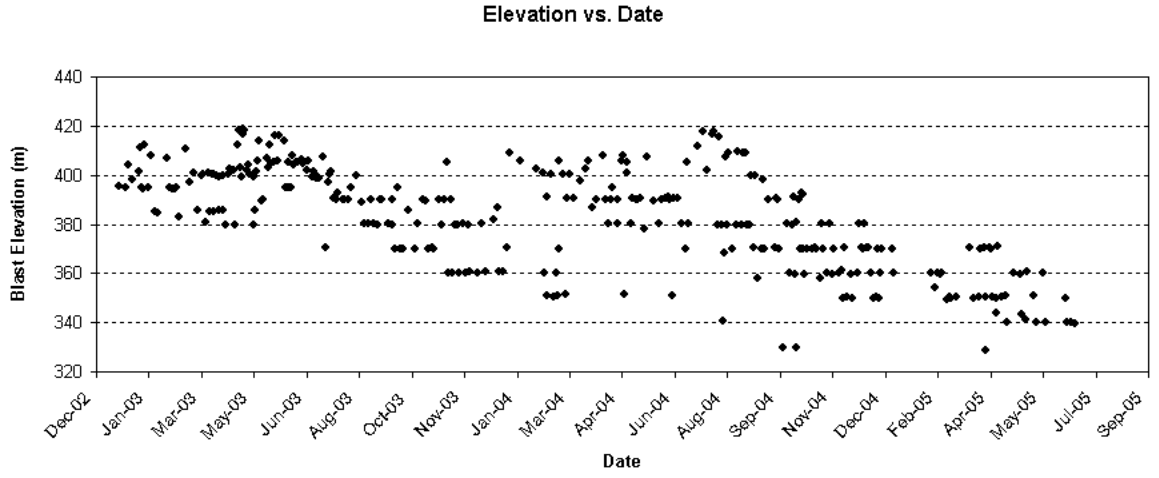

Figure 5-13) Blast elevations at DDMI since January 2003. Over time the elevations have decreased as the open pit operation increases in depth.

Analysis of the recorded PPVs over time (Figure 5-14) shows that, while extremely high PPVs are not frequent there are extremes in both May 2003, and March 2004. Further analysis shows that these data points are due to blasts being very close to sensors, (100 m. or less). A normalisation for the scaled distance should remove the extremes. Nonetheless, no trend is apparent.

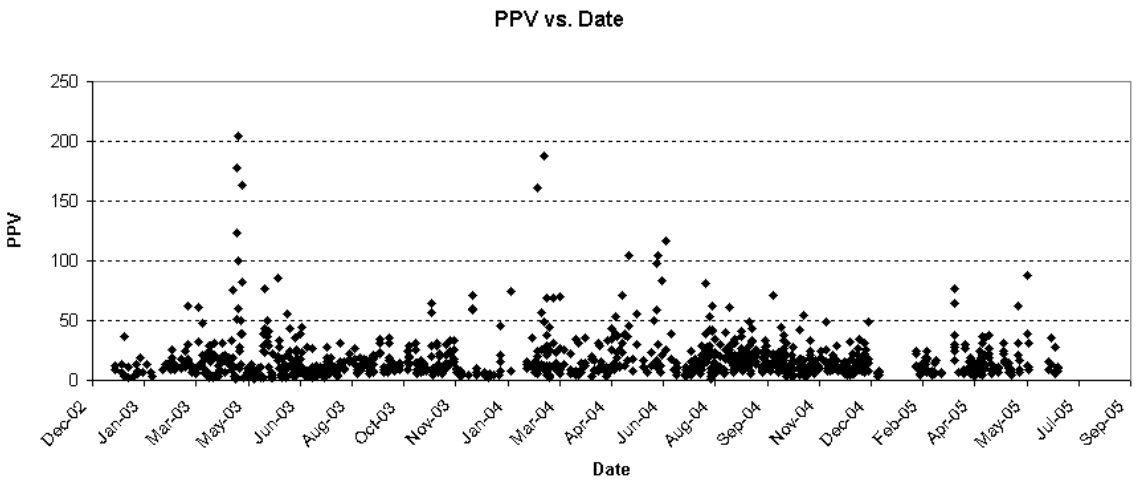

Figure 5-14) PPVs (mm/s) as measured by DDMI sensors since January 2003.

5.8.1) Changes in normalised PPV

From the recorded blasts, the minimum, maximum and mean values of the scaled distances are 1.9, 74.2 and 11.9 respectively. The mean value of 11.9 is chosen to be used as a normalisation factor to calculate a normalised PPV

$$PPV_n = PPV * \frac{SD}{11.9} \quad \textbf{(5-8)}$$

where PPV_n is the normalised peak particle velocity and SD is the scaled distance. The normalised PPV values can be compared against date, elevation, distance and the blast weight.

Once the normalised value is plotted against date no discernible trend is seen (Figure 5-15). Comparing PPV_n to the blast elevation also shows no trend (Figure 5-16). Comparing PPV_n to the blast weight or to the distance is trickier as they are both components of the scaled distance which is the normalisation factor. As distance to the blast increases, PPV_n decreases exponentially, in a similar manner to that of the Scaled Distance plot (Figure 5-17).

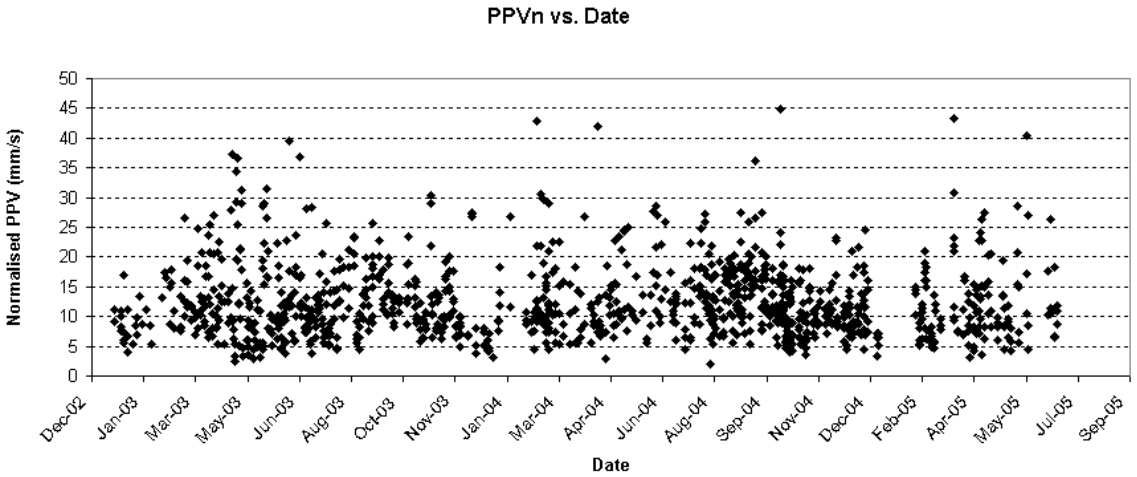

Figure 5-15) Normalised (DDMI) PPVs plotted against the date.

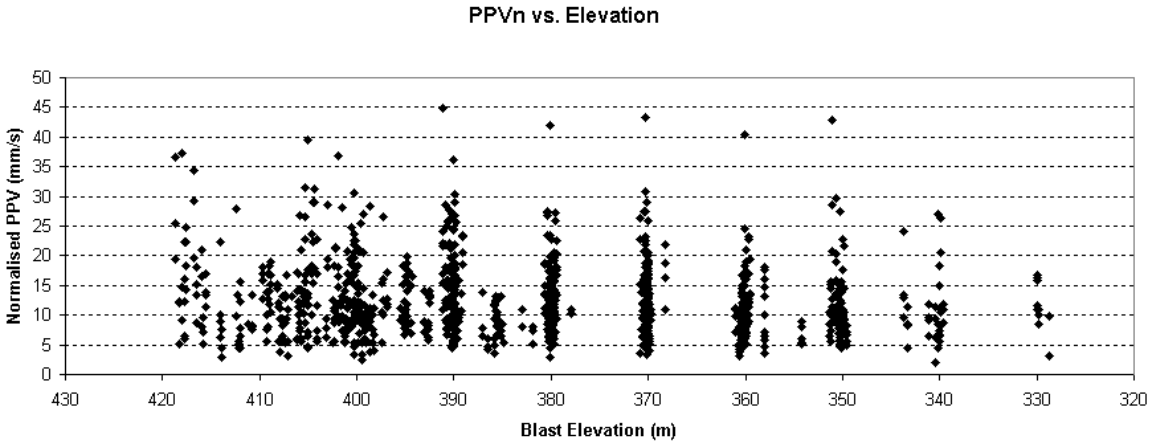

Figure 5-16) Normalised (DDMI) PPVs plotted against the blast elevation.

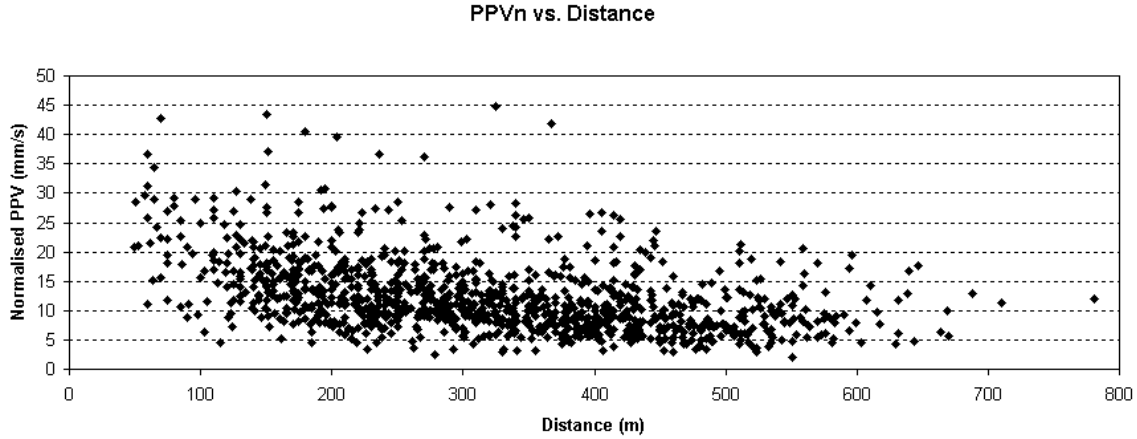

Figure 5-17) Normalised (DDMI) PPVs plotted against distance from blast. As the distance increases, the measured PPV decreases.

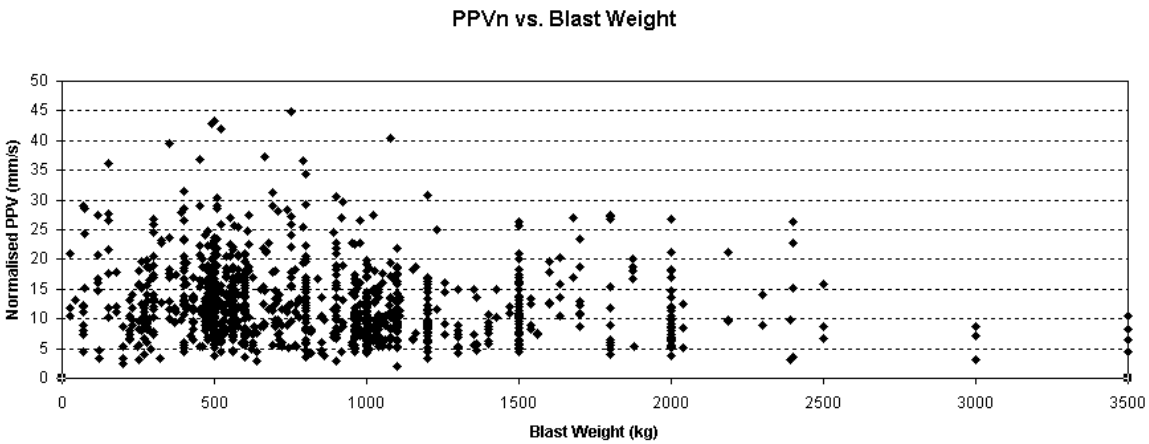

Figure 5-18) Normalised (DDMI) PPVs plotted against the blast weight.

Comparing PPV_n and the blast weight, no real trend is seen (Figure 5-18). The normalisation factor accounts for changes in the blast weight.

5.8.2) Changes in the Scaled Distance function

An alternative analysis of changes over time is to see how the Scaled Distance function evolves over time and with change in pit depth and distance from the blast. For the DDMI data, Scaled Distance functions are created for small time, depth and distance intervals for comparison.

In the empirical PPV prediction function (Eqn. 2-29) A & M are the scalar and exponential variables. These variables are analysed and presented (Figures 5-19 to 5-21).

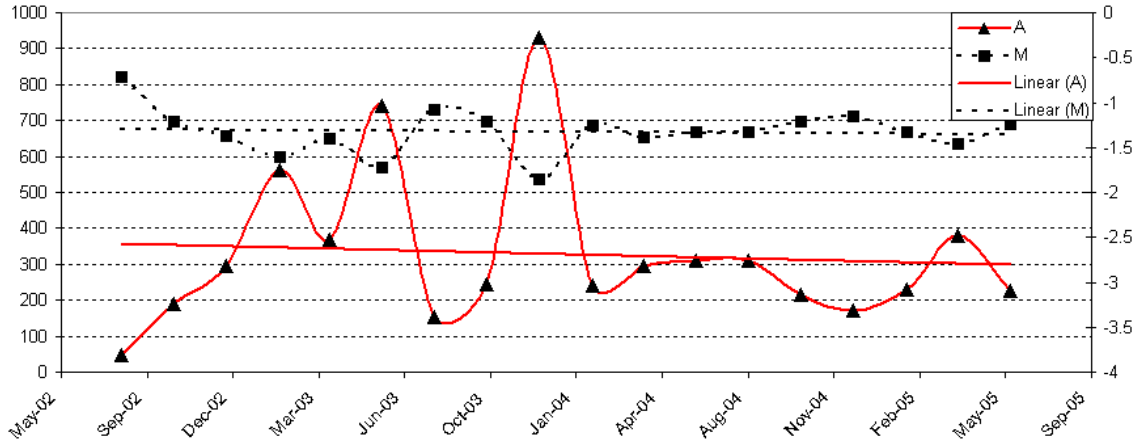

Figure 5-19) Change in A & M over time. (DDMI data). The scalar variable, A, is on the left axis and M, the exponential variable is on the right axis.

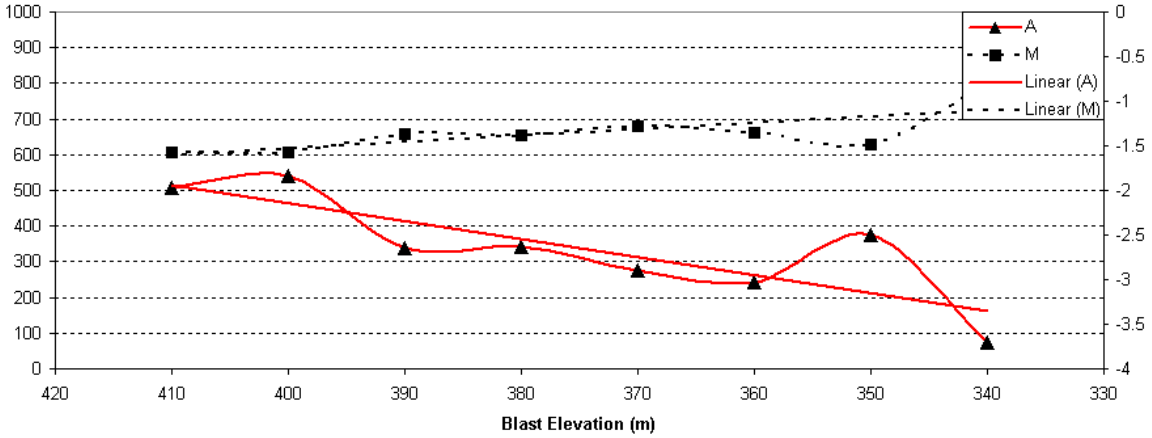

Figure 5-20) Change in A & M as the depth increases (elevation decreases). (DDMI data). The scalar variable, A, is on the left axis and M, the exponential variable is on the right axis.

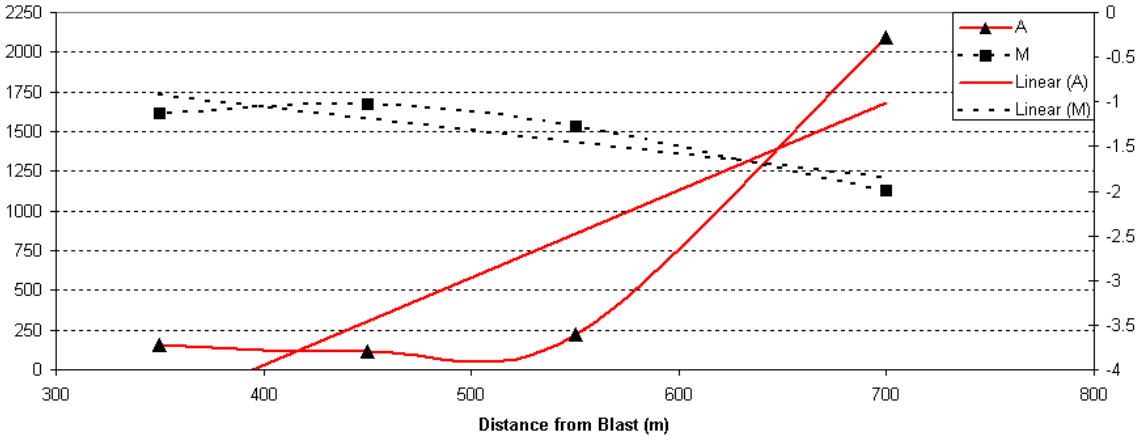

Figure 5-21) Change in A & M as the distance from the blast increases. (DDMI data). The scalar variable, A, is on the left axis and M, the exponential variable is on the right axis.

It is interesting to note that the trends of the two variables are opposite suggesting that they balance each other out. As is earlier noted, changes over time are not a good measure of changes with increase in depth. In fact, over time neither *A*, nor *M* change much (Figure 5-19). As the depth of the pit increases, *A* decreases and *M* increases (Figure 5-20). The opposite is found as the distance from the blast increases (Figure 5-21). The question here is; are the changes in *A* balancing out the changes in *M* within error bars or are there actual changes in the SD functions as either distance, or depth into pit, change?

Chapter 6) *Laboratory Study*

Although the maximum allowable PPV limit for protecting spawning beds is a precise albeit somewhat arbitrary number, previous attempts to relate physical effects of blasting to mortality of incubating eggs has failed to show any increases in mortality. Our work (Faulkner et al. (in press), Faulkner thesis) found no evidence for elevated mortality of lake trout eggs from the blasting exposures at DDMI's operations at Lac de Gras as described in detail in the previous chapter, despite exposures more than double the PPV guideline (28.5 mm/s). However, the field setting did not allow for proper control regarding the number, timing, and sizes of blasts to allow researchers to properly determine the critical PPV levels at which survival of fish eggs decrease. The objective of the laboratory study was to emulate field blasting conditions and their effects on fish and to find a PPV level where an increased mortality is seen.

A laboratory experiment was designed where incubating Rainbow Trout eggs could be exposed to particle motions as great as 250 mm/s. Blast events were simulated in a tank and measured by identical equipment to that described in chapter 3. PPV, acceleration, frequency and duration of blast event are all criteria that were noted and improved whenever possible to better simulate Diavik-like conditions. To allow for direct comparison of blasting effects between lab and field events, a normalised 'pseudo energy' waveform attribute was calculated.

Three sets of laboratory experiments were conducted and as is common in experimental developments, each consecutive experiment was an improvement on the previous. New technical developments allowed the final round in September of 2005 to

be much more repeatable with a small error on the PPV reduced to only ~1.5%. This allowed the final experiment to be conducted without the sensor in the tank thus allowing for more room in the tank. In fact, the eggs were placed in a gravel bed to better simulate the field conditions. Only the results from the third, and final, study were used (Faulkner et al. 2006) and only these results will be reported here. In this interdisciplinary effort, Faulkner et al. (2006) was primarily responsible for detailing the statistical results of the vibration exposure tests while this report provides the details of the experiments. Consequently, while the predominant part of this study was biological in nature, the development and calibration of the instrumentation and the analyses of the blast and laboratory data were carried out primarily by the author.

6.1) Methodology

A weight drop experiment was designed whereby fish eggs were exposed to a controlled vibration exposure that partially simulated a blasting event. The experimental apparatus consisted of a 2 m X 1 m X 0.635 cm metal plate used as the supporting substrate. A 2 m high pole (Figure 7-1) attached to this plate guided dropped weights released from known heights h. Ignoring the effects of friction of the weight and of air resistance, the potential energy E_p provided by the dropped weight with mass M was linearly proportional to the height h according to $E_p = Mgh$. The impact of the weight on the plate sent a simulated blast wave through the plate and the small tank where the fish eggs were placed.

To measure and record the effects of the simulated blast, the same Oyo 4-C sensor used in the field tests was placed inside the tank and its responses recorded during each tests. As with the field experiment, the *Instantel Minimate Plus*™ was automatically

triggered by the event. Five second records were kept with a pre-trigger of 0.25 seconds. Work was done to ensure that the 5 heights used would repeatedly produce a known a shaking measured in PPVs. To allow for more room in the tank, the sensor was removed for the experiment and the calibrated heights were used to reproduce a given PPV.

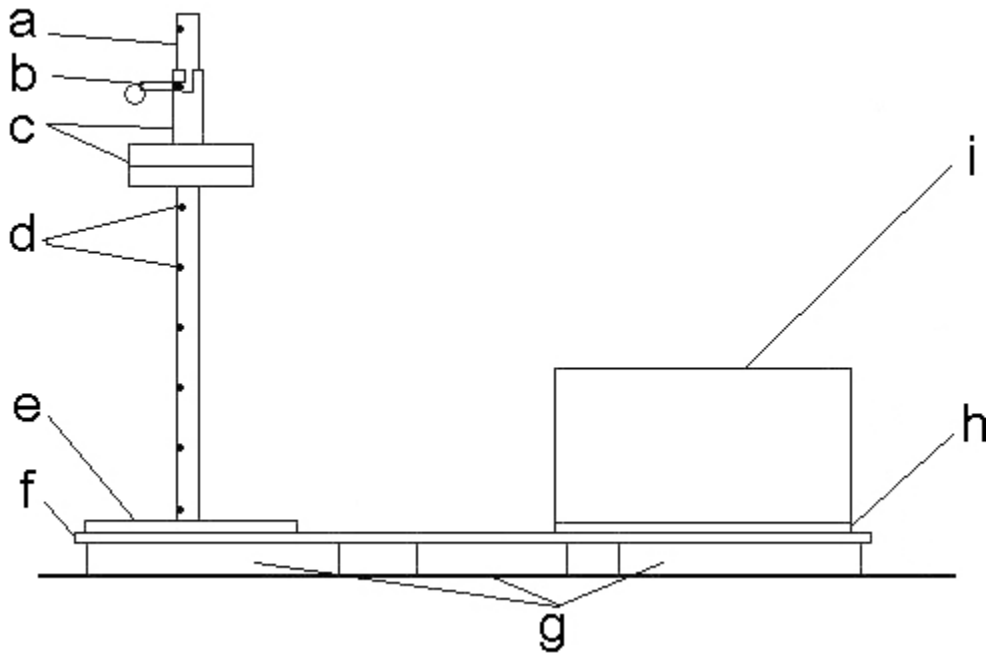

Figure 6-1) The weight-drop apparatus; a: steel pole, secured at top with straps (not shown); b: pin to release the weight apparatus; c: the weight set-up, including an aluminium sleeve and cast iron weights; d: holes drilled in the pole spaced 15 cm apart; e: 0.64 cm thick rubber mat; f: 0.64 cm thick steel base plate; g: 5 cm foam padding; h: 2.5 cm rubber mat, and i: fibreglass tank.

6.2) Results

For the third and final component of the lab study, five blasting levels were used. Figures 6-2 and 6-3 show the record for two of the levels that were used, 138 mm/s and 245 mm/s. Each level was repeated 10 times prior to actual exposures to confirm a PPV and the Standard Deviation. Note that the vertical scale is in mm/s and is set the same for each different height to show the differences in intensities.

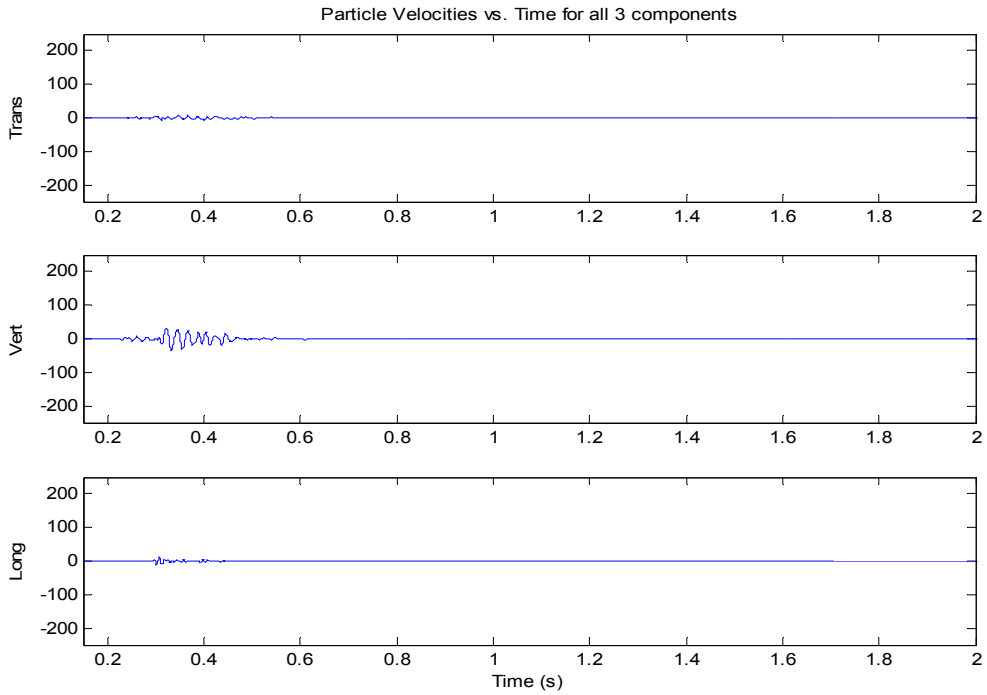

Figure 6-2) PPV = 138 mm/s Height = Standard Deviation (2.4)

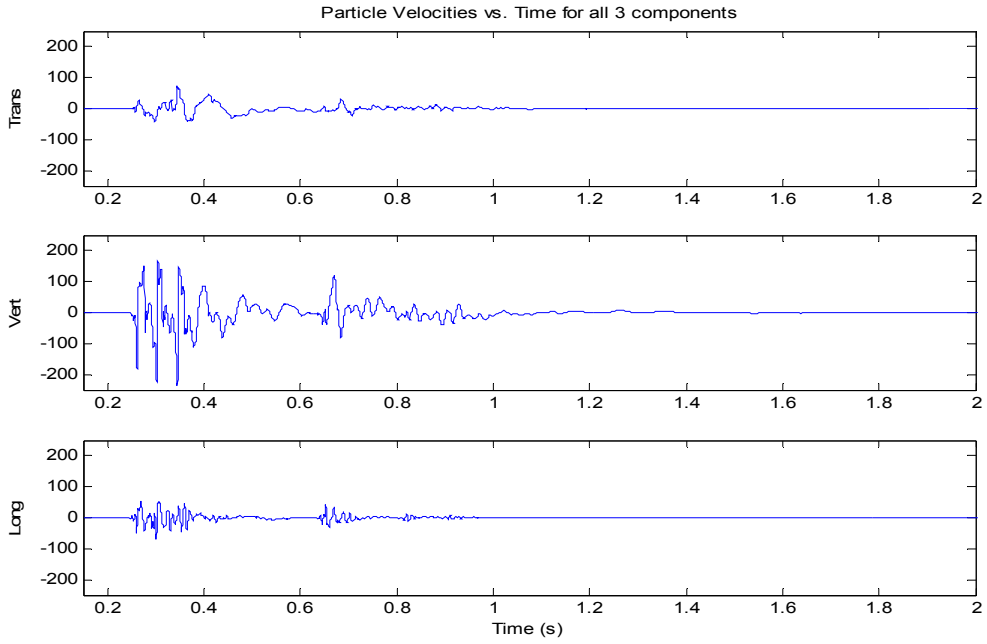

Figure 6-3) PPV = 245 mm/s Height = Standard Deviation (3.0)

6.3) Pseudo energy

Although the PPV standards have been used for a long time and are well accepted in various standards as noted in previous chapters, it must be remembered that the PPV measurement is only one simple attribute of the shaking. Indeed, one could really ask whether or not the PPV measure itself, while readily measured and easily understood, really tells us that much about the propensity of a blast to cause damage. Indeed, Dowding (1985) in his classic text makes the case that workers should not ignore the frequency of the blast vibrations. This is particularly germane to his application of building damage as most buildings will have a particular set of resonant 'modes' at given frequencies for which particle motions are amplified and can cause particular damage. It is these modal vibrations in buildings that earthquake engineers strive to dampen. The PPV value really is only one single measure or attribute extracted from the entire waveform. It contains no information about other factors that may be more important, such as the frequency content, the duration of vibration, or the total energy of vibration. While we understand the reason why field engineers prefer the simple PPV measure, we find it surprising that these other factors that may relate more to an overall vibration 'exposure' which might be more important to predicting vibration damage levels have been ignored. An implication of focusing on simpler measures might be that the legal, social, or professional criteria assigned could be overly conservative and more carefully designed and scientific assessments might even allow for greater blasting levels.

We do not expect to solve this problem as part of this study. However, it is interesting to begin the search for more informative waveform attributes. To allow for a truer comparison between blasting events an estimate for the energy, called the pseudo-energy

E_s, was developed. E_s takes into account the entire waveform, including its duration and all the particle velocities, via:

$$E_s = \sum_{t0}^{tn} [PV(t)]^2 \quad \textbf{(6-1)}$$

This stems from the formula for the instantaneous kinetic energy *KE(t)*:

$$KE(t) = \left(\frac{1}{2}\right) m \sum_{t0}^{tn} [PV(t)]^2 \quad \textbf{(6-2)}$$

where m = mass, PV = particle velocity (not wave propagation velocity), and t_0 and t_n define the beginning and end times of the waveform of duration $t_n - t_0$. Because in this application mass is constant, kinetic energy is directly proportional to PV^2. Therefore, to compare between events, this total energy was calculated. The squared particle velocities of the three geophone channels were summed and plotted over time, and the area under the curve was determined. By calculating the area under the curve, we have invariably taken into account the frequency and duration of the event. A longer event transmits and produces more energy and this is reflected in the calculation. However, it should be noted that this calculation allows for comparison between different events and is in no way a true energy calculation.

Figure 6-4 shows the 3 component waveform forms for a lab simulated event and an event recorded at Diavik. For each event the calculated pseudo energy is shown.

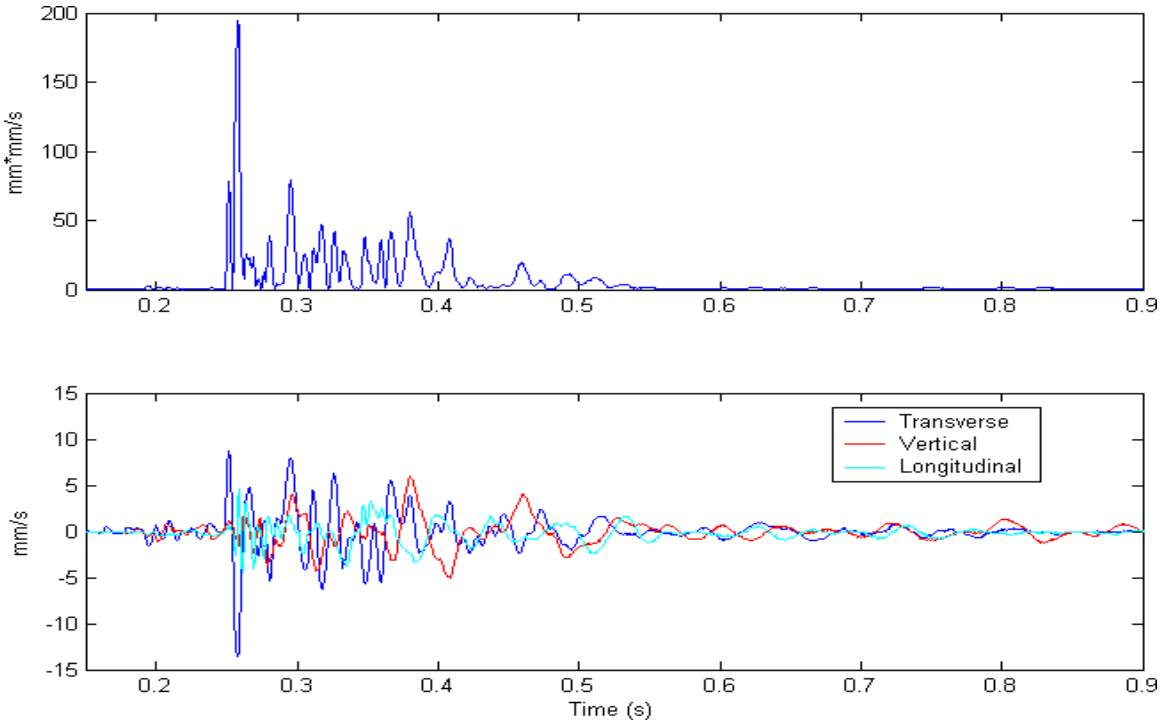

Figure 6-4a)

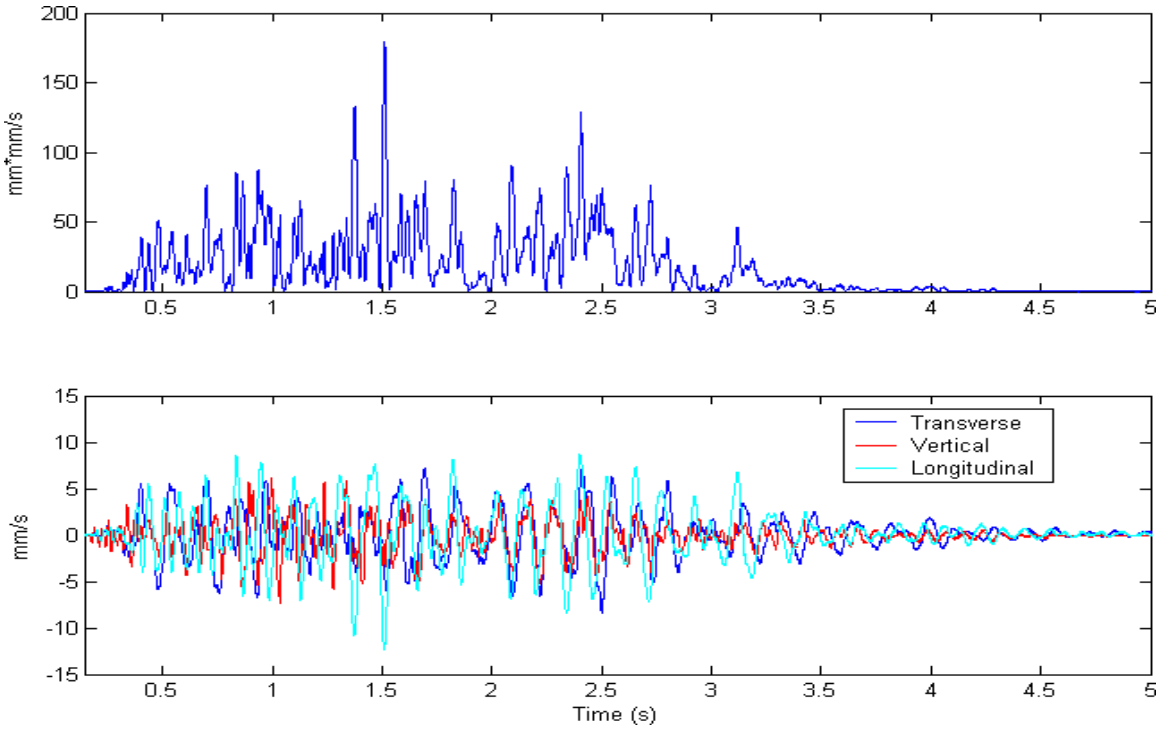

Figure 6-4) Blast records for a lab simulation event (a) and DDMI blasting event (b). The bottom panel shows the 3 component wave form and the top panel shows the pseudo energy calculated from the vector sum of the waveform. Note that the amplitude scales are the same for comparison sake but the time scales are different. The DDMI event is much longer than the lab event.

Chapter 7) *Discussion*

7.1) Field component

DFO guidelines suggest that overpressure limits within bodies of water should be limited to ± 100 kPa (about 1 atmosphere of pressure). The maximum blast water overpressure observed was 11 Pa. As noted, in most cases the water overpressure could not be reliably measured due to low intensities. This situation is not surprising and was expected at the early stages of the study. The reason for this is that the elastic impedance (the product of the materials sound velocity and mass density) for water (~ 1.5 MRayl)[1] differs substantially from that for the rock substrate (~12.5 MRayl). The contrast in these properties indicates the level of energy that can be transmitted from one medium to the next, the greater the contrast the less the transfer of energy. In this particular case the large contrast between the water and the rock substrate would suggest little energy is transferred into the water column to be detected as a pressure. Indeed the DFO relation suggests that about 20% of the pressure in the substrate will be introduced into the water column. A maximum pressure of 14.25 kPa, which is calculated based on a maximum PPV of 28.5 mm/s, in the substrate could introduce up to 2.85 kPa of pressure into the water column which is well below the DFO guideline. In fact of more concern is the Peak Particle Velocity to which the fish eggs may be exposed to.

---

[1] The Rayl is a measure of elastic impedance, 1 Rayl = $(kg/m^3)(m/s)$, 1 MRayl = 10^6 Rayl. Some care must be exercised in the use of this unit as it also exists in the cgs system as $(gm/cm^3)(cm/s)$. As this thesis employs only the MKS (Systeme International d'unites) measures, the first definition is automatically assumed. Again, the Rayl is named after our friend Lord Rayleigh.

Initially it was expected that the scaled distance function used at DDMI would fit the data at the 4 fish incubator sites. Instead, the functions for the sites display different characteristics. The 3 study sites that are closest to mining operations show a slope (exponential constant) of about -0.75 while DDMI's slope is about double, or -1.6. At reference island the slope is -0.17. The steepness of the slope is and indication of how rapidly the wave intensity decays with distance; as noted earlier this consists of a geometric component due to wavefield spreading and a material dependent wave absorption component. A third consideration depends on the stiffness, rigidity, and density of the rock substrate; the more compliant and less dense a material is the greater the expected particle motions. The decay due to simple wavefield geometric spreading is closely proportional to $r^{1/2}$ for the surface waves that cause the greatest motions here. The other factors are not so easily determined; indeed, the seismic characteristics of a given site complicate the analysis of even the highest quality seismometer data and high quality stations undergo rigorous site characterizations. Together, a steeper slope indicates higher attenuation of the blast wave as it propagates. Several possibilities exist for the difference; Dowding (1985) suggests that differences in particle velocity at a given scaled distance can be attributed to: 1) changes in geological conditions: 2) different explosive types: 3) variations in the geometry of blast patterns, and 4) errors in blast timing. He also warns that large differences in charge weight or distance will also contribute to differences in PPV. Other possible explanations for this difference include:

- Differences in sensors: The fact that the U of A study sensors are not the same as those employed by DDMI and may be calibrated slightly differently could contribute. However, this is not thought to be a major issue as the same basic

OYO geophone is used in both sensor types and all the instruments had been calibrated by Instantel. A calibration difference would be a scalar value while the U of A data shows both scalar and, more importantly, exponential differences.

- Placement of the sensors: The study sensors are all placed in water and well coupled to the hard rock. U of A sensors are located on solid granitoid substrate. In contrast, the DDMI sensors are deployed on the softer dike. The dike is made from crush and boulders and is likely to be more attenuative than the substrate to seismic waves.
- Differences in distances in relation to blast patterns: Another reason for variations in attenuation between the two data sets may be the differences in the average distance from the sensors to the centre of the blast pattern. DDMI sensors are on average placed at 344 m while U of A sensors (except Reference Island) are at 852 m. The blast pattern itself typically covers an area of 2500 m^2.
- Differences in distances in relation to attenuation. As seismic waves propagate, attenuation of the higher frequency components of these waves is much more rapid. As such, the waveforms observed by the closer sensors may include high frequency, high amplitude waves that attenuate before reaching the U of A sensor.
- Changes in blast prediction due to variations in scale function with time: attenuation value (slope of scaled distance plot) for the U of A data. Another possibility is that the DDMI scaled distance function may have changed over time. This theory is disproved by comparing data recorded prior to September 9, 2003 to data recorded after this date (figure 7-1)

- Differences in surface wave dispersion. The largest energy in these records is contained in what are referred to as *surface waves*. Although not exactly the same, one can think of the surface waves as being somewhat analogous to the slowly travelling waves that make up the bow in the water following the motion of a boat. Different components of these waves will travel at different velocities and hence the wave further from the shot points will be more spread out in time than it is closer to the blast. This must also result in a lower peak amplitude although it will extend the duration of shaking.

Our present hypothesis for the differences between the U of A and DDMI data is a combination of the placement of the sensors and the attenuation of the higher amplitude waves closer to the centre of the blast. In fact, due to preferential attenuation, the scaled distance and prediction functions are only effective over small distances in relation to actual sensor/blast pattern distance. The effects of surface wave dispersion have not to our knowledge been examined but this would be beyond the scope of the present study.

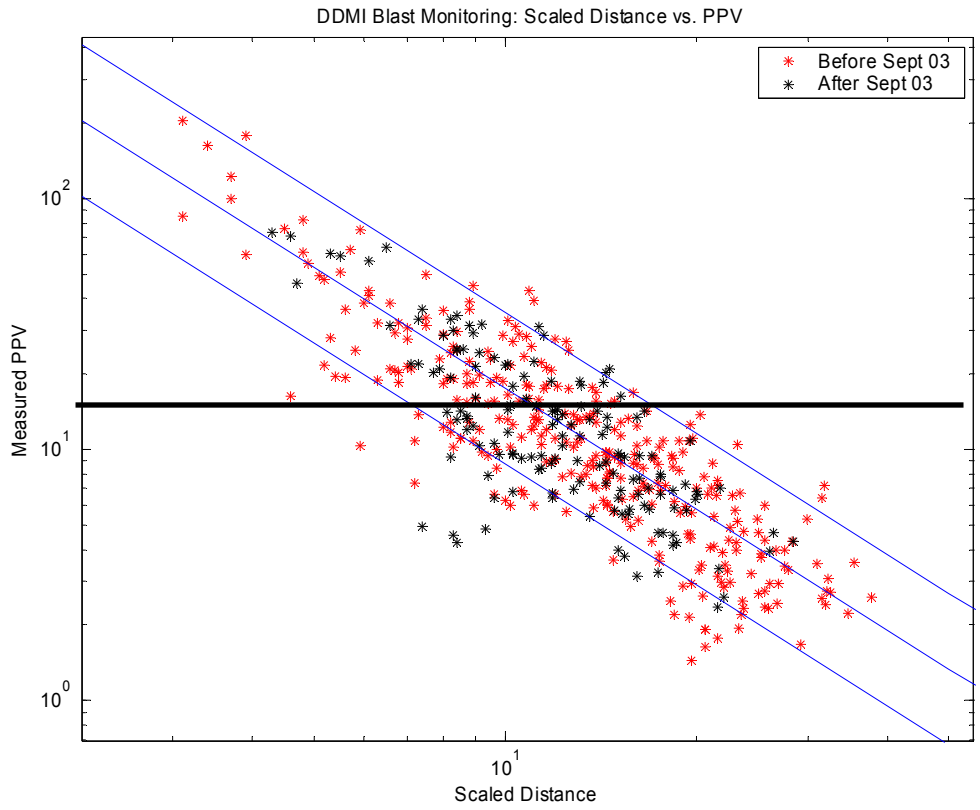

Figure 7-1) Comparison of scaled distance data over two periods shows that the distribution has stayed the same. The solid line indicates 13 mm/s.

7.2) Changes in the blasting effects

It should be expected that the blasting effects will decrease as the pit deepens. As the pit deepens the areas of concern, the dike and the nearby fish habitat are a greater distance from the blast source and as such should experience lower levels of vibration due to attenuation of the blast wave. The change in the pit depth though, is only 90 metres while the blasting area has a radius of 500 metres. The slight changes in distance attributed to the increased depth are insufficient to change the vibrations if this is the only consideration.

It has been shown (Duvall, 1972) that the level of vibration does not change for the number of blast holes as long as there is a millisecond delay between each successive blast. This argument is correct for measured PPVs but this measure does not take into account the duration of an event, which would increase with added blast holes.

Chapter 8) *Conclusions*

To satisfy the initial objectives of this study, blasting at DDMI was monitored to study its effects on fish habitat within Lac de Gras. Data collected by the U of A team within the lake were used to measure the PPVs that incubating lake trout were exposed to, predict the PPVs when instruments did not record a blast, and to redefine the 'blast zone'. Data were also analysed for changes attributed to differing conditions.

The defined blast zone is an area where PPVs up to 13 mm/s may be experienced based on many conditions, including the blast weight per delay. A better reference is a graph of safe distances based on blast weight (Figure 5-12). Over time, as the pit deepened, no changes in blasting effects could be attributed to changes in depth of the pit, which increased by only 90 metres. The geology does not change and blasting occurs over an area of radius 500 m, so the increased depth only slightly changes the distance from the blast.

Predicting the Peak Particle Velocities due to blasting can be effectively done using any of the previously discussed prediction functions that are based on data collected at DDMI. As distance from the blast increases, the rate of attenuation decreases as is seen when comparing the data collected within the pit, just outside of the pit and far away from the pit. This is because the higher frequencies attenuate faster. While all of the functions could do a sufficient job in predicting PPVs, the best function is one that is based on data that is in a similar region i.e. (similar distances and/or charge weights), as such, the data provided to the mortality study is based on data collected at the incubator sites.

Blast monitoring programmes are commonly done and recorded data are effectively used to predict safe blast charge weights for adherence to local guidelines for ground shaking and pressure in the air or water column. Simple back of the envelope type calculations can be made to safely predict initial blast weights. The success of the so called, Scaled Distance function is inherent as it is created statistically from data that it predicts. Each new data point is added and the next prediction is calculated.

Of concern is that fact that ground motions created by blasting are complex and can't be simply measured as the peak particle velocity. It is not known whether it is simply the maximum particle velocity, or if the duration and frequency of an event that will cause mortality in a fish egg. We attempted to make up for some of the deficiencies by calculating a Pseudo Energy of a blasting event. The pseudo energy calculation gives a measure of the total exposure for a blasting event.

Contributions of this work

There are two major contributions of this thesis. To some degree these contributions are more of a technical nature that allowed us to extend the range of applicability of blast monitoring and also to provide better controlled information in the laboratory.

First, this is the first blasting vibration study, to our knowledge, carried out in which both particle vibrations and overpressure are measured simultaneously at the floor of a lakebed. This work was greatly facilitated by recent technical developments in deep sea seismic exploration in the North Sea, where combined gimballed geophone and hydrophone packages were constructed and are now commercially available. Without this new equipment, the required lake floor testing would have been much more difficult and would have required that we construct our own special detectors. This would have

greatly increased the costs of the project in terms of time and funding. As noted, this technical development has opened new applications for the blast monitoring community and was consequently recognized by Instantel, a manufacturer of blast monitoring equipment.

Second, a new methodology for producing controlled and calibrated simulated blast vibrations in the laboratory has been developed. The technical aspects of this equipment is described in this thesis; the results of application of the method has been discussed in Faulkner (2006) and Faulkner et al. (2006). Prior to this, the techniques used to subject fish eggs to vibration were open to question. In this development, the new mechanism produces waveforms that are more similar to the actual blast vibrations. Further, the vibration levels were repeatable.

Recommendations for Future Work

As in many projects, this work has opened up additional questions.

First, it is not exactly clear what the actual physical basis of much of the blast monitoring prediction formula are actually based, and workers apparently simply followed the lead of the first workers. It would be useful to re-examine this problem in detail again from first principles, and while this might not be practical for a day to day application of blast monitoring it would be more comforting to have some understanding of the actual physics of the problem in order that one could better guide the development of predictive equations. Unfortunately, the problem is not as simple as we would like. There are numerous factors that will influence the blast vibrations, the most important of which are 1) coupling of the actual blast energy to the earth, 2) determination of the interference of various waves from the blast pattern on the basis of time and on the basis

of the blast geometry, and 3) the influence of the local site at which the receiver is placed. All of these problems also complicate the analysis of earthquake records, the seismic source of which consists of a complex 3-D failure plane that takes a certain time period to actually fail. This problem also plagues those who attempt to monitor large bomb blasts globally in efforts to detect nuclear events in particular. Indeed, one can essentially mask these large events by careful preparation of the blast site. For example, the coupling between the detonation and the earth is substantially reduced by carrying out the experiment within a large underground cavity. One component of future work might be additional tests of simple blasts under more controlled conditions.

To some degree the blast monitoring equipment could be improved. The current systems in place rely on taking out a recording box which still must be triggered and still have a rather limited ability to store records. The technology for recording and data storage, however, has changed very substantially in the last few years and it should not be difficult to update the equipment to record continuously. Having the full record, instead of the snippets obtained once the unit is triggered by large blasts might be useful. As well, such records might also allow, if additional dynamic range is added, the better detection of the much weaker body waves.

References

Alberta Government, 2005, Exploration Regulations, Alberta Regulation 214/98 of the Forests Act, the, Mines and Minerals Act, the Public Highways Development Act, and the Public Lands Act, http://www.srd.gov.ab.ca/land/m_geo.html, (accessed August 21, 2006)

Birch, W. J.M and M. Pegden. 2000. Improved prediction of ground vibrations from blasting at quarries. Trans. Instn Min. Metall. Sec t. A: Min. technol.), 109.

Blair, D.P., 2004, Charge weight scaling laws and the superposition of blast vibration waves, Fragblast, , 8, 221-239.

Bryan, D. and R. Bonner, 2004, The Diavik Diamond Mine, Lac de Gras, Northwest Territories, Canada, Proc. 8th Int. Kimberlite Conf. (cd-rom), Vancouver, 61-65, (Accessed http://www.diavik.ca/PDF/Diavik Field Guide 8IKC.pdf August 23, 2006).

Davis, W.J., A.G. Jones, W. Bleeker,; H. Grutter, DEC 2003, Lithosphere development in the Slave craton: a linked crustal and mantle perspective Source: LITHOS, 71 (2-4): 575- 589

DDMI. 1997b. Technical memorandum #12-2, 1997: Shoal habitat survey, Lac de Gras and Lac du Sauvage

DDMI. 1998a. Environmental effects report, Fish and water. DDMI Internal Report.

Diavik Fact Book, DDMI, July 2005.http://www.diavik.ca/PDF/Diavik_FactBook.pdf (Accessed January, 2006)

Dowding, C.H., 1985, Blast Vibration Monitoring and Control, Prentice Hall, USA.

Duvall, Wilbur, I., 1972, Chapter 7, Damage and prediction control. EM 1110-2-3800, US Bureau of Mines.

Faulkner, S.G. 2006, Blasting effects on Salmonid Eggs, M.Sc. Thesis, University of Alberta.

Faulkner, S.G. and W.N. Tonn. 2005, Effects of Explosives on Incubating Lake Trout Eggs in the Canadian Arctic. (Blasting Effects Study), DDMI Internal Report,. Biological Component. 32 pages.

Faulkner, S. G., W. M. Tonn, M. Welz, and D.R. Schmitt. 2006. Effects of Explosives on Incubating Lake Trout Eggs in the Canadian Arctic. Submitted to North American Journal of Fisheries Management. pp 31.

Faulkner, S. G., M. Welz, W. M. Tonn, and D.R. Schmitt. 2006. Effects of Simulated Blasting on Mortality of Rainbow Trout Eggs. To be published.

Goble, K.A., January 1980, Project to determine effects of seismic activity on water wells, Alberta Energy and Natural Resources.

Goble, K.A., June 1980, Project to determine effects of seismic activity on water wells, Phase II Alberta Energy and Natural Resources.

Grech, M. 1998, True Amplitude Processing in VSPs, M.Sc. Thesis, University of Alberta.

Grogan, A. and McAnuff, P., 2005, Canadian vibration and air blast regulations, presented at the Int. Soc. Explosives Eng. Conference.

Gunn, J.M. 1995. Spawning behaviour of lake trout: effects on colonization ability. Journal of Great Lakes Research 21(S1): 323-329.

Lai, C. G., G. J. Rix, et al. 2002. "Simultaneous measurement and inversion of surface wave dispersion and attenuation curves." Soil Dynamics and Earthquake Engineering 22(9-12): 923-930.

Lai, C. G., G. J. Rix, 2002. "Solution of the Rayleigh eigenproblem in viscoelastic media." Bulletin of the Seismological Society of America 92(6): 2297-2309.

Lucca, Frank, J. 2003, Tight Construction Blasting: Ground Vibration Basics, Monitoring and Prediction.

Marsden, J.E., D.L. Perkins, and C.C. Krueger. 1995a. Recognition of spawning areas by lake trout: deposition and survival of eggs on small, man-made rock piles. Journal of Great Lakes Research 21 (S1): 330-336.

McDonald, D.G., 1973, The effects of seismic explosions on fish in Sturgeon Lake, Alberta, Alberta Dept. of Lands & Forests.

Prosser, D. W., 1980, The effects of industrial seismograph operations on water wells, Alberta Environment.

Schneider, L.C., 2001, A survey of blasting vibration regulations, Fragblast, 5, 133-156.

Schmitt, D.R., J. Mwenifumbo, K. A. Pflug, and I.L. Meglis, 2003, *Geophysical logging for elastic properties in hard rock: a tutorial*, , in: Hardrock Seismic Exploration (edited by D.W. Eaton, B. Milkereit, and M.H. Salisbury), SEG Geophysical Developments 10, 20-41,

Scott, W.B. and E.J. Crossman. 1973. Freshwater fishes of Canada. Bulletin of the Fisheries Research Board of Canada 184.

Stein, S., and M. Wysession, 2003. An introduction to seismology, earthquakes, and earth structure, Blackwell Pubishing, London, pp. 498.

Telford, W. M., L. P. Geldart, and R. E. Sheriff. 1990. Applied Geophysics. Second Edition. Cambridge University Press. New York.

Welz, M. and D.R. Schmitt. 2005, Effects of Explosives on Incubating Lake Trout Eggs in the Canadian Arctic. (Blasting Effects Study), DDMI Internal Report, Geophysical Component. 40 pages.

Woods, R.S., and L.P. Jedele, 1985, Energy-Attenuation Relationships from Construction Vibrations, in Vibration Problems in Geotechnical Engineering (G. Gazetas and E.T. Selig, Eds), Special Technical Publication, ASCE, New York, pp. 187 – 202.

Wright, D.G. and G.E. Hopky. 1998. Guidelines for the use of explosives in or near Canadian Fisheries waters. Canadian Technical Report of Fisheries and Aquatic Sciences 2107.

Zywicki, D. J. and G. L. Rix 2005. "Mitigation of near-field effects for seismic surface wave velocity estimation with cylindrical beamformers." Journal of Geotechnical and Geoenvironmental Engineering 131(8): 970-977.

Appendices

Appendix 1: Response curves for the Underwater sensor

Response curve for the GS-30CT geophone element used in the 4 Component sensor.

Note that 1 in/sec = 25.4 mm/s.

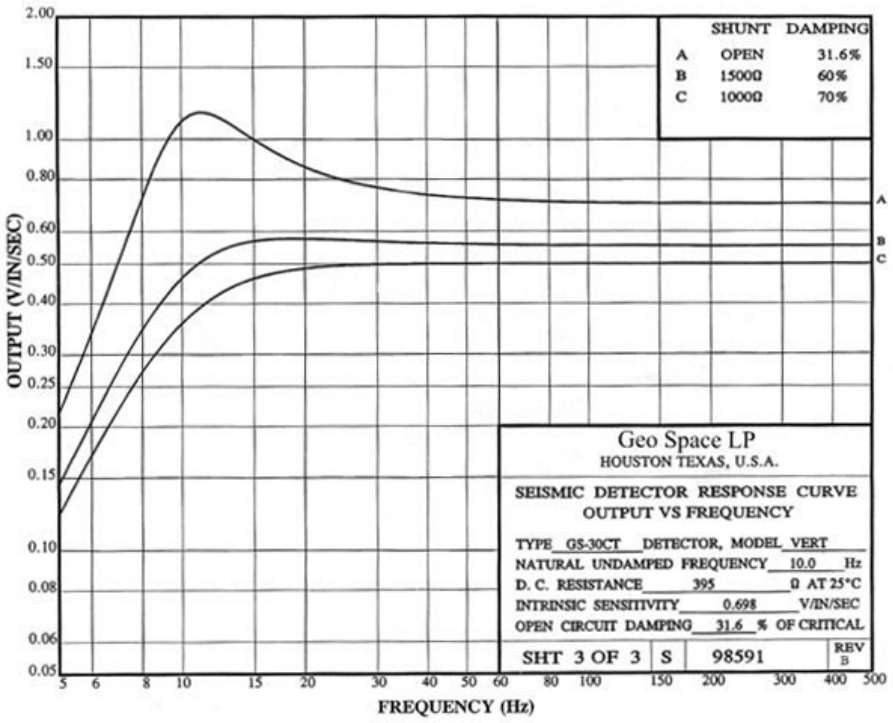

Response curve for the MP25-1200 Hydrophone element used in the 4 Component sensor. Note that 1 bar = 100 kPa.

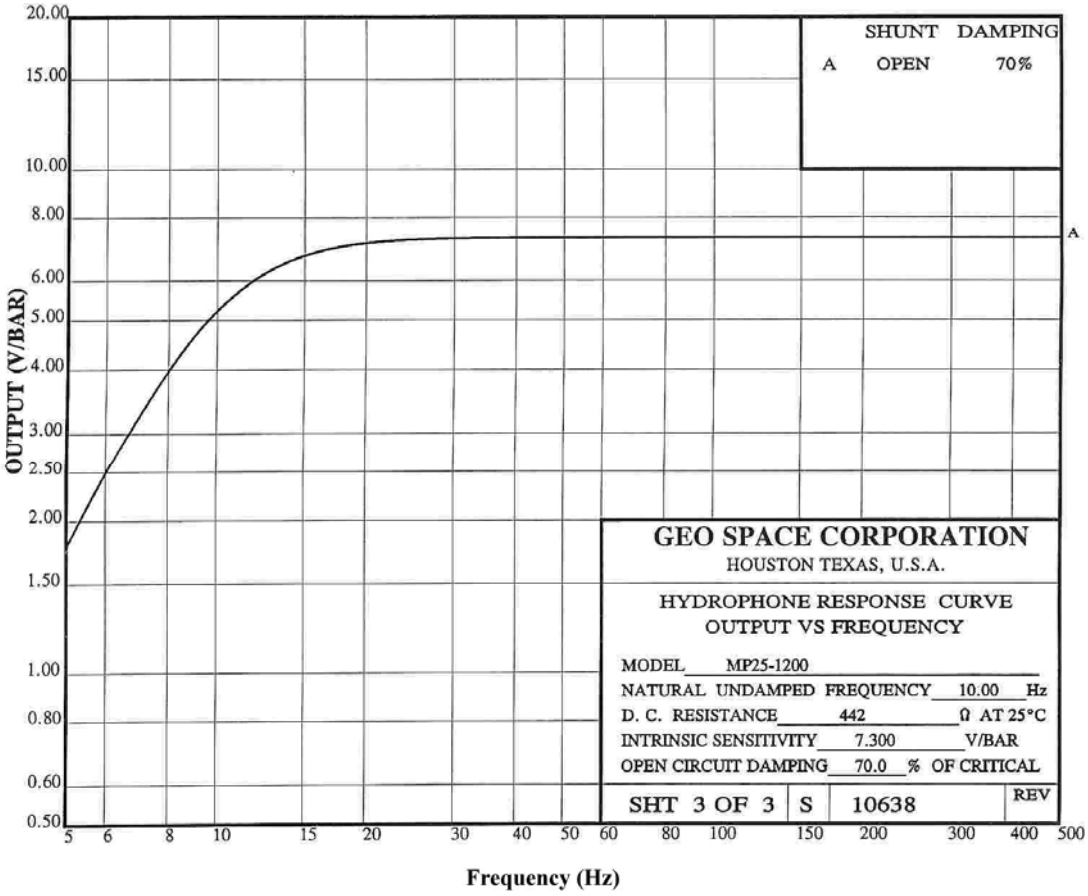

Appendix 2: Blast Mate blasting record

Typical blasting record as produced by the *Instantel MiniBlastmate*

Event Report

Date/Time	Long at 15:14:27 May 1, 2004	**Serial Number**	BE8904 V 4.37-4.35 MiniMate Plus
Trigger Source	Geo: 1.50 mm/s	**Battery Level**	6.3 Volts
Range	Geo :254 mm/s	**Calibration**	July 16, 2003 by Instantel Inc.
Record Time	10.0 sec at 4096 sps	**File Name**	J904A379.030
Job Number:	1		

Notes
Location:
Client:
User Name:
General:

Extended Notes

Post Event Notes

Microphone Linear Weighting
PSPL 4.75 pa.(L) at 0.868 sec
ZC Freq 73 Hz
Channel Test Check (Freq = 0.0 Hz Amp = 0 mv)

	Tran	Vert	Long	
PPV	14.5	6.10	8.38	mm/s
ZC Freq	8.7	7.8	8.3	Hz
Time (Rel. to Trig)	0.906	1.074	0.512	sec
Peak Acceleration	0.159	0.106	0.159	g
Peak Displacement	0.252	0.123	0.144	mm
Sensorcheck	Check	Check	Check	

Peak Vector Sum 15.6 mm/s at 0.910 sec

USBM RI8507 And OSMRE

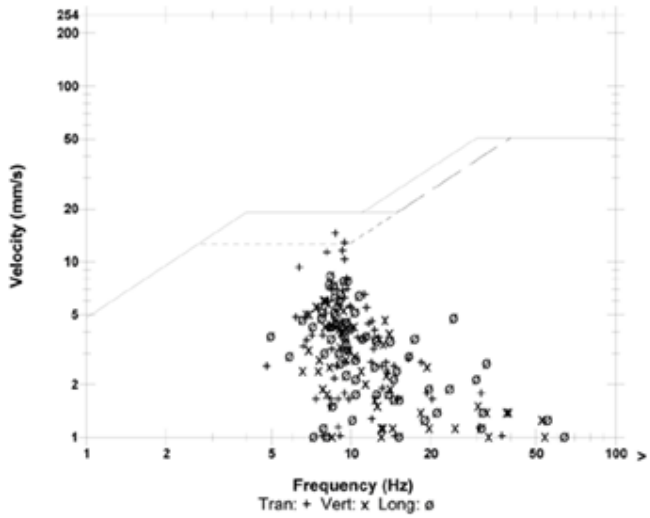

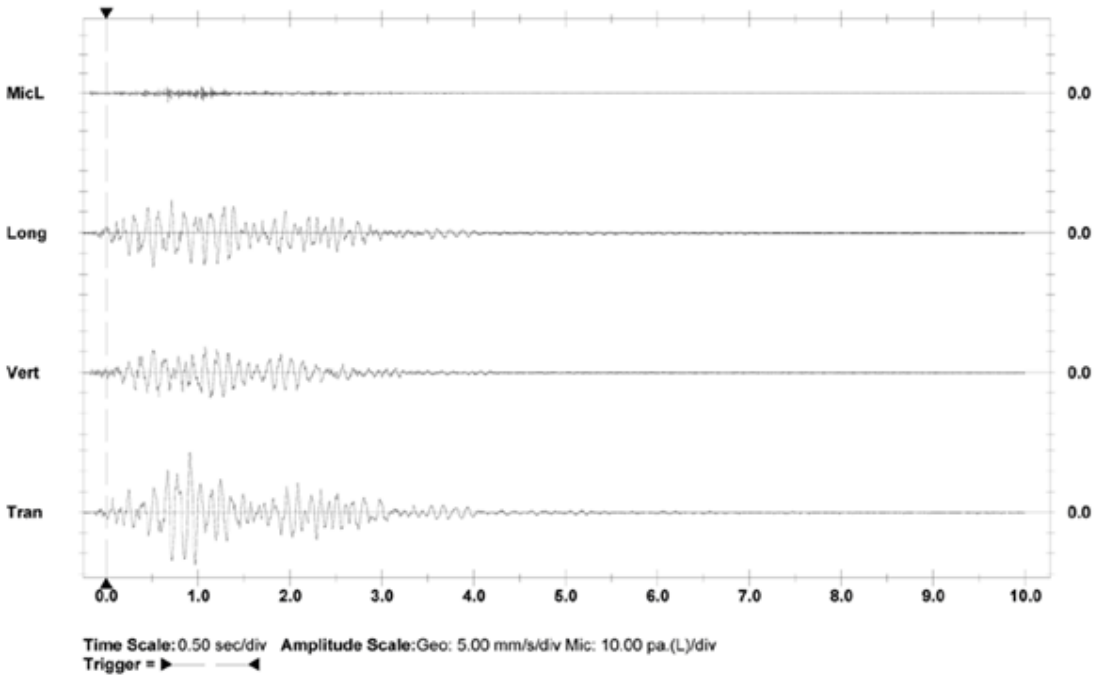

Time Scale: 0.50 sec/div **Amplitude Scale:** Geo: 5.00 mm/s/div Mic: 10.00 pa.(L)/div
Trigger = ▶ ◀

Printed: February 7, 2005 (V 4.37 - 4.37) **Format Copyrighted 1996-2003 Instantel Inc.**

Appendix 3:

Technical Specifications for the Instantel Minimate Plus Series III.

Seismic	Range	10 in/s (254 mm/s).
	Resolution	0.005 in/s (0.127 mm/s), to 0.000625 in/s (0.0159 mm/s) with built–in preamp.
	Trigger Levels	0.005 to 10 in/s (0.127 to 254 mm/s) in steps of 0.001 in/s (0.01 mm).
	Frequency Analysis	National and Local Standards for all countries (see text).
	Accuracy	3% at 15 Hz.
	Acceleration, Displacement	Calculated using entire waveform, not estimated at peak.
Air Linear	Range	88–148 dB, 7.25 x 10^{-5} psi to 0.0725 psi, 0.5 Pa to 500 Pa.
	Resolution	0.1 dB above 120 dB (0.25 Pa).
	Trigger Levels	100–148 dB in 1 dB steps.
	Accuracy	0.2 dB at 30 Hertz and 127 dB.
A weight (optional)	Range	50 to 110 dB in steps of 0.1 dB. (Impulse Response – 35 milliseconds)
Sampling Rate		Standard 1024 samples per second per channel to 16,384 (8,192 for 8 channel).
Event Storage	Full Waveform Events	300 standard and 1500 optional at standard sample rate of 1024.
	Summary Events	1750 standard and 8750 optional at standard sample rates of 1024.
Frequency Response	2 to 300 Hz	Ground and Air, Independent of record time.
Full Waveform Recording	Fixed Record Modes	Manual, single shot, continuous and programmed start/stop.
	Fixed Record Time	1 to 100, 300 or 500 sec plus 0.25 sec pre-trigger.
	Auto Record Mode	1 to 100, 300 or 500 sec plus 0.25 sec pre-trigger.
Strip Chart Recording	Record Method	Record to memory. Program interval 2, 5, 15, 60, 300 or 900 sec.
	Days Storage	2.8 or 14 days at 5 second interval. 34 or 170 days at 1 minute interval.
Histogram Combo Mode	Histogram Record Method	Record to memory and/or internal printer. Program interval 2, 5, 15, 60, 300 or 900 sec.
	Histogram Days Storage	2.4 or 12 days at 5 second interval. 29 or 147 days at 60 second interval.
	Waveform Events	Up to 13 one-second events (1024 sample rate, four channels recording).
	Waveform Record Times	1 to 13 seconds plus 0.25 sec pre-trigger.
Special Functions	Timer Operation	Programmed start/stop.
	Self Check	Programmable daily check.
	Scaled Distance	Weight and distance stored with event.
	Monitor Log	History printout programmable up to all events stored.
	Automatic download	Automatic downloading of data from a unattended monitor with Auto Call Home.
	Measurement Units	Imperial or metric, dB or linear air pressure, or in units of custom sensors.
	Location	Log GPS (Global Positioning System) data into record.
User interface	Keyboard	8 domed tactile with separate keys for common functions.
	Display	4 line by 20 character high contrast backlit display with on line help.
Battery Life		10 days continuous recording, 25 days with timer.
Dimensions		3.2" x 3.6" x 6.3" (81 mm x 91 mm x 160 mm).
Weight		3 lbs. (1.4 kg).
Warranty	2 Years Parts and Labor	Calibration and equipment check required at 1 year to maintain warranty.
Environmental	LCD	14 to 122 degrees F (–10 to 50 degrees C) operating.
	Electronics	–4 to 140 degrees F (–20 to 60 degrees C) operating.
	Humidity	5 – 90% RH non – condensing
	Storage	–4 to 160 degrees F (–20 to 70 degrees C).

Instantel reserves the right to change any specifications without notice.

Appendix 4: Blasting Data

DDMI blast data; September 17, 2003 to July 27 2004.

Date	Blast Pattern	X	Y	Z	Blast Weight (kg)
2004-07-26	370-064	36830.97	53210.99	379.6985	800
2004-07-24	410-011	36998.43	53220.88	415.5052	430
2004-07-22	370-060	36702.85	53220.42	379.5372	750
2004-07-19	410-010	37036.04	53168.81	417.5915	480
2004-07-17	410-009	37049.24	53114	416.5005	480
2004-07-12	390-100	36959.04	52700.47	401.9421	700
2004-07-09	410-005/410-006	37087.8	53091.45	417.7396	800
2004-07-04	400-041	37088.96	53002.46	412.0308	520
2004-06-25	370-057	36385.16	52873.6	380.1243	1200
2004-06-24	405-022b	36947.84	52682.3	405.2773	400
2004-06-22	360-020	36738.47	52806.28	369.72	1500
2004-06-19	380-071	36836.36	52676.96	390.0285	1500
2004-06-14	380-072	36755.22	53277.76	390.5985	520
2004-06-11	380-070	36743.36	53250.25	390.4161	560
2004-06-09	340-027	36537.97	52794.83	351.0323	1100
2004-06-07	380-069	36672.8	52600.5	390.2359	1680
2004-06-06	370-049	36753.65	53287.69	390.9025	560
2004-06-03	370-051	36682.1	52591.05	390.4147	375
2004-05-31	A380-067	36370.19	52761.7	389.9503	1500
2004-05-28	A370-052	36800.95	52783.57	380.184	1500
2004-05-23	A380-064	36387.57	52798.7	389.2335	1000
2004-05-17	A390-096	36439.94	52596.71	407.2856	840
2004-05-14	A370-046/A370-047	36796.49	52869.12	377.8843	1080
2004-05-10	A380-062	36527.94	52623.16	390.6916	1230
2004-05-08	A380-061	36496.16	52690.46	389.8793	1160
2004-05-06	A370-050	36400.76	52696.91	390.0905	375
2004-05-03	A380-060	36599.36	52646.07	390.3761	2185
2004-05-01	A370-044	36917.49	52878.81	380.3263	1700
2004-04-28	A390-095	36735.14	53295.09	401.1205	660
2004-04-27	A390-094	36853.21	53286.52	405.3811	900
2004-04-25	A340-011	36501.84	52870.94	351.342	2000
2004-04-23	A390-089	36387.74	52642.21	408.1594	1200
2004-04-22	A390-075	36869.6	53288.33	405.5253	150
2004-04-19	A380-059	36615.07	52688.04	390.0126	1010
2004-04-18	A370-041	36879.47	52986.89	380.1734	900
2004-04-13	A390-090	36434.94	52681.49	395.1259	900
2004-04-12	A380-058	36689.11	52659.57	390.1132	1030
2004-04-10	A370-040	36867.97	53067.3	380.0752	520
2004-04-07	A380-057	36696.24	52712.1	390.0146	970
2004-04-04	A395-034	36424.97	52667.6	408.1054	690
2004-03-29	A380-056	36751.52	52726.79	389.9745	2000

2004-03-25	A380-055	36783.78	52795.02	387.051	1500
2004-03-22	A390-088	36486.73	52645.02	405.7261	950
2004-03-19	A390-087	36559.93	52663.96	402.2967	765
2004-03-14	A390-086	36684.18	52717.8	397.4487	1040
2004-03-08	A380-053	36948.03	53032.78	390.7004	2500
2004-03-04	A390-085	36565.68	52588.7	400.2385	1880
2004-02-01	A380-052	36856.66	52762.05	390.8498	2000
2004-02-29	A340-004	36600.08	53047.81	351.2579	1500
2004-03-27	A390-083	36627.58	52602.31	400.196	960
2004-04-23	A340-001	36534.18	53237.2	370.2163	71
2004-05-21	A340-003	36639.94	53120.68	351.2147	600
2004-06-20	A350-023	36530.15	52787.62	360.3096	1085
2004-06-18	A340-002	36552.64	53078.2	350.6155	920
2004-02-15	390-082	36691.39	52619.27	400.2983	900
2004-02-12	380-050	36927	52859	391	660
2004-02-09	350-022	36459	52851	360	1500
2004-02-07	390-081	36744	52651	401	2000
2004-02-01	390-080	36808	52662	402	1400
2004-01-17	400-038	36575	52560	406	300
2004-01-07	390-072	36925	53219	409	580
2004-01-05	360-017	36462	52844	370	520
2004-01-01	350-014	36566	52982	361	3000
2003-12-28	350-011	36729	52959	361	1000
2003-12-26	370-038	36429	52810	387	850
2003-12-23	370-037	36422	52897	382	1300
2003-12-15	350-010	36613	52992	361	2000
2003-12-11	370-036	36802	53215	380	1800
2003-12-07	350-007	36712	53059	360	500
2003-11-30	350-006	36690	52985	361	1010
2003-11-29	370-034	36383	53073	380	490
2003-11-26	350-005	36638	53060	360	1080
2003-11-23	370-033	36488	53213	380	490
2003-11-20	350-004	36582	53118	360	1090
2003-11-19	370-035	36608	53219	380	490
2003-11-16	370-032	36510	53195	380	500
2003-11-14	350-003	36716	53117	360	800
2003-11-12	380-044	36882	53009	390	1000
2003-11-09	350-001	36628	53125	360	1500
2003-11-08	390-066	37000	53072	405	700
2003-11-06	380-043	36551	53246	390	500
2003-11-03	370-031	36402	53033	380	500
2003-11-01	370-029 PS	36539	53256	390	510
2003-10-27	360-012	36798	53061	370	1100
2003-10-25	360-013	36572	53115	371	1100
2003-10-22	360-011	36690	53119	370	1000
2003-10-19	380-042	36355	53008	390	480
2003-10-17	380-041	36488	53184	390	560
2003-10-11	370-028	36674	53167	380	510

2003-10-09	360-008	36738	53022	370	1700
2003-10-02	380-040	36355	53008	390	400
2003-09-27	360-005	36511	52928	370	1540
2003-09-25	360-006	36706	52959	370	1110
2003-09-22	390-063	36496	53254	395	280
2003-09-20	360-004	36634	53037	370	850
2003-09-17	385-039	36529	53179	390	1000
2003-09-13	370-025	36372	53092	390	1500
2003-09-07	380-038	36870	53087	390	565
2003-09-06	370-024	36760	52915	380	1875
2003-09-03	370-023	36699	52848	380	1000

U of A blast data; September 17, 2003 to July 27 2004.

	South Dike (8902)			Ref. Island (8903)			Tern Island (8904)			East Dike (8905)		
Date	**Dist.**	**SD**	**PPV**	**Dist.**	**SD**	**PPV**	**Dist.**	**SD**	**PPV**	**Dist.**	**SD**	**PPV**
26-Jul-04	871.2	30.8	1.98	2804.7	99.2		956.1	33.8		711.0	25.1	5.83
24-Jul-04	844.7	40.7		2637.2	127.2		865.1	41.7		554.8	26.8	
22-Jul-04	927.0	33.8	1.89	2930.8	107.0	0.635	1050.2	38.3		837.1	30.6	3.65
19-Jul-04	789.2	36.0	1.77	2607.2	119.0		801.1	36.6		501.8	22.9	6.52
17-Jul-04	733.6	33.5	4.49	2602.9	118.8		747.5	34.1		475.0	21.7	6.51
12-Jul-04	347.2	13.1		2790.0	105.5		537.0	20.3		638.4	24.1	11.5
9-Jul-04	709.5	25.1	2.6	2568.9	90.8		708.1	25.0		432.9	15.3	9.15
4-Jul-04	620.5	27.2	2.14	2585.4	113.4		632.6	27.7		425.3	18.6	6.14
25-Jun-04	865.6	25.0	6.33	3300.7	95.3		1134.6	32.8		1138.2	32.9	3.25
24-Jun-04	335.3	16.8		2806.3	140.3		540.3	27.0		657.2	32.9	
22-Jun-04	556.9	14.4		2972.4	76.7		782.6	20.2		804.4	20.8	
19-Jun-04	394.1	10.2	12.9	2914.1	75.2		643.9	16.6		758.0	19.6	8.7
14-Jun-04	958.9	42.1	9.05	2872.5	126.0		1055.8	46.3		802.9	35.2	
11-Jun-04	937.7	39.6	8.5	2887.2	122.0		1043.3	44.1		805.7	34.0	
9-Jun-04	697.4	21.0	7.39	3169.8	95.6		965.7	29.1		1002.5	30.2	3.21
7-Jun-04	477.6	11.7	9.87	3093.2	75.5		786.3	19.2		938.4	22.9	4.72
6-Jun-04	968.8	40.9	4.47	2873.2	121.4		1064.3	45.0		807.7	34.1	7.83
3-Jun-04	465.0	24.0	10.9	3087.3	159.4		775.7	40.1		934.4	48.2	7.98
31-May-04	820.3	21.2	6.16	3340.2	86.2		1115.4	28.8		1171.9	30.3	
28-May-04	499.8	12.9		2917.9	75.3		715.9	18.5	7.98	750.6	19.4	
23-May-04	823.0	26.0	9.42	3314.6	104.8		1108.5	35.1	3.53	1147.4	36.3	
17-May-04	691.3	23.9	5.81	3316.4	114.4		1016.4	35.1	2.38	1153.0	39.8	1.95
14-May-04	573.3	17.4		2900.7	88.3		759.7	23.1	5.79	733.1	22.3	9.57
10-May-04	618.4	17.6	4.95	3224.6	91.9		932.8	26.6	2.5	1061.6	30.3	2.11
8-May-04	675.7	19.8	4.47	3236.4	95.0		976.4	28.7	2.79	1068.8	31.4	
6-May-04	764.4	39.5		3326.7	171.8		1071.0	55.3		1158.2	59.8	
3-May-04	563.7	12.1	10.5	3149.6	67.4		866.3	18.5		986.8	21.1	5.77
1-May-04	529.1	12.8	13.4	2780.9	67.4		664.2	16.1	15.6	612.8	14.9	12.6
28-Apr-04	982.2	38.2		2890.9	112.5		1081.9	42.1		827.4	32.2	
27-Apr-04	936.8	31.2	12.2	2774.1	92.5		1000.9	33.4		714.0	23.8	12.2
25-Apr-04	772.5	17.3		3187.6	71.3		1026.1	22.9	10.3	1024.2	22.9	7.31

23-Apr-04	755.5	21.8		3353.7	96.8		1074.1	31.0	7.48	1186.7	34.3	
22-Apr-04	934.4	76.3	6.61	2757.6	225.2		992.7	81.1	5.31	699.6	57.1	6.81
19-Apr-04	571.2	18.0	7.03	3122.6	98.3		860.0	27.1	5.23	957.1	30.1	4.14
18-Apr-04	643.5	21.5	8.26	2793.7	93.1		761.8	25.4		635.9	21.2	7.67
13-Apr-04	726.8	24.2	5.41	3297.7	109.9		1034.4	34.5		1129.8	37.7	2.74
12-Apr-04	493.8	15.4		3059.8	95.3		781.4	24.3		898.8	28.0	
10-Apr-04	723.2	31.7	7.7	2789.7	122.3		825.3	36.2	8.14	648.8	28.4	9.11
7-Apr-04	519.6	16.7		3038.0	97.5		788.1	25.3		872.6	28.0	4.63
4-Apr-04	730.2	27.8		3311.0	126.0		1041.5	39.7		1143.4	43.5	4.04
29-Mar-04	488.5	10.9	24.9	2980.8	66.7	0.508	740.1	16.5	17.4	815.7	18.2	11.2
25-Mar-04	518.9	13.4	8.16	2931.3	75.7		736.0	19.0		763.3	19.7	4.64
22-Mar-04	664.5	21.6	9.9	3257.8	105.7		976.8	31.7	3.5	1092.2	35.4	3.78
19-Mar-04	606.6	21.9	5.27	3182.2	115.1	0.508	908.3	32.8	9.63	1017.0	36.8	4.44
14-Mar-04	532.3	16.5	7.44	3047.9	94.5		801.1	24.8	4.71	881.9	27.3	5.39
8-Mar-04	667.9	13.4	15.6	2717.3	54.3		744.7	14.9		566.5	11.3	19.2
4-Mar-04	570.2	13.2		3198.7	73.8		890.7	20.5		1040.2	24.0	
1-Feb-04	450.1	10.1		2870.0	64.2		656.0	14.7		704.9	15.8	
29-Feb-04	832.9	21.5		3057.4	78.9		1022.2	26.4		916.4	23.7	
27-Mar-04	518.6	16.7	1.57	3135.6	101.2		831.1	26.8		978.3	31.6	3.95
23-Apr-04	1024.6	121.6	3.3	3096.7	367.5		1187.1	140.9		1005.3	119.3	9.56
21-May-04	870.6	35.5	7.21	3006.6	122.7		1032.6	42.2		882.3	36.0	3.14
20-Jun-04	698.8	21.2	2.88	3179.0	96.5		970.3	29.5		1011.2	30.7	
18-Jun-04	885.8	29.2	5.36	3099.3	102.2		1078.4	35.6		965.2	31.8	5.05
15-Feb-04	470.0	15.7		3069.7	102.3		770.8	25.7		913.3	30.4	5.69
12-Feb-04	506.7	19.7	8.32	2776.5	108.1		644.4	25.1		607.9	23.7	7.61
9-Feb-04	793.4	20.5	6.21	3233.6	83.5		1058.3	27.3		1069.0	27.6	3.43
7-Feb-04	443.9	9.9	14.6	3009.9	67.3		725.8	16.2		852.2	19.1	10.9
1-Feb-04	402.5	10.8	19.5	2945.6	78.7		666.5	17.8	12.7	789.8	21.1	12.1
17-Jan-04	551.5	31.8	4.69	3198.7	184.7	0.582	878.4	50.7	10.7	1043.9	60.3	6.13
7-Jan-04	854.5	35.5	6.62	2710.3	112.5		904.1	37.5	5.3	623.0	25.9	8.52
5-Jan-04	786.3	34.5	6.29	3232.1	141.7		1052.6	46.2	3.41	1066.7	46.8	2.95
1-Jan-04	802.7	14.7	0	3102.3	56.6		1016.3	18.6	5.55	949.9	17.3	
28-Dec-03	686.1	21.7	7.36	2946.9	93.2	0.696	865.3	27.4	6.18	788.6	24.9	5.55
26-Dec-03	793.7	27.2	3.99	3271.7	112.2		1072.3	36.8		1104.6	37.9	
23-Dec-03	849.5	23.6	6.56	3259.8	90.4		1108.6	30.7		1098.8	30.5	7.48
15-Dec-03	780.2	17.4	4.49	3054.3	68.3		980.8	21.9		902.7	20.2	4.79
11-Dec-03	884.2	20.8	12.5	2833.0	66.8		978.1	23.1		739.9	17.4	28.5
7-Dec-03	780.4	34.9	4.6	2945.0	131.7		937.5	41.9		804.7	36.0	5.21
30-Nov-03	729.1	22.9	4.67	2980.0	93.8		912.1	28.7		826.0	26.0	5.18
29-Nov-03	994.1	44.9	0	3267.3	147.6		1219.6	55.1		1132.8	51.2	
26-Nov-03	820.3	25.0	6.51	3017.8	91.8		997.4	30.3		878.5	26.7	4.12
23-Nov-03	1030.7	46.6	2.42	3145.1	142.1		1208.0	54.6		1045.2	47.2	2.29
20-Nov-03	899.7	27.3	3.77	3064.2	92.8		1076.6	32.6		938.9	28.4	4.38
19-Nov-03	969.8	43.8	1.99	3025.2	136.7		1118.7	50.5		928.9	42.0	2.98
16-Nov-03	1003.2	44.9	0	3125.3	139.8		1179.6	52.8		1020.3	45.6	
14-Nov-03	829.4	29.3	0	2931.8	103.7		971.2	34.3		805.9	28.5	
12-Nov-03	663.1	21.0	0	2786.7	88.1		774.4	24.5		632.4	20.0	
9-Nov-03	880.1	22.7	2.54	3017.6	77.9		1044.2	27.0		894.1	23.1	4.25

8-Nov-03	696.8	26.3	2.5	2658.8	100.5		741.2	28.0		517.1	19.5	10.8
6-Nov-03	1022.3	45.7	2.09	3078.9	137.7		1179.3	52.7		990.3	44.3	2.17
3-Nov-03	952.7	42.6	0	3254.8	145.6		1183.9	52.9		1112.5	49.8	
1-Nov-03	1037.1	45.9	4.88	3089.9	136.8		1194.9	52.9		1004.3	44.5	2.79
27-Oct-03	743.0	22.4	3.11	2859.8	86.2		872.2	26.3		718.5	21.7	5.65
25-Oct-03	902.5	27.2	1.82	3074.3	92.7		1082.5	32.6		948.0	28.6	2.1
22-Oct-03	842.9	26.7	2.58	2957.0	93.5		991.8	31.4	4	831.4	26.3	4.15
19-Oct-03	971.0	44.3	2.08	3305.1	150.9		1214.5	55.4		1159.2	52.9	1.86
17-Oct-03	1007.2	42.6	4.42	3148.4	133.0		1190.5	50.3		1039.9	43.9	
11-Oct-03	892.2	39.5	1.84	2966.0	131.3		1034.9	45.8		854.0	37.8	2.9
9-Oct-03	734.9	17.8	0	2925.8	71.0		893.9	21.7		777.1	18.8	
2-Oct-03	971.0	48.5	0	3305.1	165.3		1214.5	60.7	1.25	1159.2	58.0	
27-Sep-03	801.9	20.4	3.87	3166.6	80.7	0.582	1039.9	26.5	4.37	1007.6	25.7	3.1
25-Sep-03	698.1	21.0	0	2969.3	89.1		884.1	26.5		811.0	24.3	
22-Sep-03	1059.2	63.3	0	3132.8	187.2		1226.7	73.3		1045.6	62.5	
20-Sep-03	803.1	27.5	3.44	3025.5	103.8		987.1	33.9		881.2	30.2	
17-Sep-03	978.9	31.0	0	3108.3	98.3		1154.6	36.5		998.6	31.6	
13-Sep-03	1015.0	26.2	0	3275.4	84.6		1238.3	32.0		1144.7	29.6	
7-Sep-03	740.9	31.2	3.27	2784.2	117.1	0.582	837.6	35.2	5.43	648.2	27.3	5.71
6-Sep-03	631.3	14.6	7.51	2925.7	67.6	0.907	814.6	18.8	10.3	761.3	17.6	8.64
3-Sep-03	613.6	19.4	5.42	3000.4	94.9	0.582	835.5	26.4	6.03	832.7	26.3	4.01